Quantum state storage in a rare-earth doped crystal, which sits inside a cavity

Samuel Tornibue Kometa

March 31, 2011

ACKNOWLEDGEMENTS

I owe a great deal of thanks to Professor Stefan Kröll and Dr. Lars Rippe for all the discussions I had with them during this project. By accepting me into your research group and giving me access to your time and knowledge, you both put me on the path to success and for that I will always be indebted to you both.

The strength of a research group lies in the staff and students. Therefore without the staffs and fellow students of the quantum information research group here at Lund University, this work would never have been possible. I therefore express my special thanks to the members of the group, that is, Mahmood Sabooni for always been a listening ear and you were a good lab partner, Yan Ying, Jenney Karlsson, Axel Thuresson and Adam Wiman for your helps and in creating a friendly environment to work-in. Also, I wish to thanks my office mate Esben Witting Larsen for the helps and helpful discussions we had together.

I also want to acknowledge Dr. and Mrs. Yessi for their moral support, Serge Nzoke, Stella Ayuk, Stella Wule, Herbert Mbufong, Tebi Magnus, Elvis Zelefac for their support and friendships.

Also, a special thanks goes to the Atomic Physics division, Professor Anne LHuillier for accepting me into the Photonics program, the Erasmus Mundus Lot10 for the financial support, Professor Pilesjo for coordination of the Lot10 window.

To my parents, my brothers and sisters for all their prayers and love, I say thank you.

ABSTRACT

Quantum memories with efficiencies above 90 % are required in the implementation of quantum repeaters for long distance quantum communication. Quantum memories with high effeciencies requires the memory materials to have high absorption. This is such that, the quantum state to be stored should be completely absorbed within the memory material. We consider using a resonant optical cavity to enhance the absorption of a quantum memory material with low absorption [24]. The memory consist of a praseodymium doped crystal with mirrors coated directly to its surface. The incoupling and the back mirror have reflectivity of R=0.8 and R≈1 respectively. One of the crystal surfaces is slightly tilthed, so that the cavity resonance frequency can be changed by moving the cavity. The crystal then functions both as a passive optical cavity and the memory material. We showed that on creation of a spectral pit in the crystal cavity, we get very strong frequency pulling effects on the cavity resonance frequencies. Also, the frequency pulling effects are greater with the inclusion of absorption peaks within the spectral pit. We can thus create from our crystal cavity, an equivalent of a "cold" cavity with length in the order of hundreds of meters.

POPULAR SCIENCE

The secure transfer of information, e.g. private information, secret codes or messages, from one location to another is very important. These messages are meant for an authorized party only and should be unintelligible to any eavesdroppers. Quantum cryptography using quantum states (EPR pairs), offers such a secure system. Quantum states are mathematical variables describing systems at the microscopic level and the EPR pair is one such states. The security of a quantum cryptography system is ensured by the no-cloning theorem, which states that, an unknown quantum state can not be copied perfectly. The quantum states are implemented using photons (quanta of light). For quantum cryptography to be very effective, it will need to work over long distances. Long distance propagation of photons in optical fibre, suffers greatly from losses within the fibre. Quantum repeaters can be used along the quantum network to over-come the problem of photon losses. Their operational principle is similar to that of the classical repeaters. The quantum repeaters uses entanglement (EPR pair) generation, entanglement purification and entanglement swapping, which are all probabilistic in nature, as such; a memory is therefore needed to store the entangled state. These processes are quantum mechanical, as such the memory should be able to store both the amplitude and phase of a single photon and we call this a quantum memory.

For a quantum memory to be effective in the quantum repeater protocol, the memory efficiency must be above 90% [6]. Most of the existing quantum memory protocols operational principle is based on the absorption of the quantum state to be stored in the memory material and the readout of this state at a later time. The memory efficiency is the ratio between the readout quantum state amplitude and the stored quantum state amplitude. Therefore, high efficiency quantum memory will require the memory material to have high absorption also. Quantum memory using Atomic Frequency Combs protocol faces difficulties with high absorbing memory materials, for there is a trade-off between the comb's height and the comb's finesses. This posses a problem as increasing the memory material absorption does not automatically increases the comb's height.

An optical cavity can be used to overcome the material absorption problem in the atomic frequency comb protocol. The optical cavity is made up of 2 mirrors with a medium (in our case, the memory material) in between them. If the cavity mirrors have the same reflectivity, and there is no losses within the cavity, we say the cavity is impedance matched, and the reflected power from the cavity is almost zero and the transmitted power is almost equal to the input power (no losses in the medium). Replacing the transmission of the second mirror by an equal round trip absorption losses in the cavity medium, will lead to almost complete absorption of the input light power within the cavity. Therefore, using an optical cavity together with any of the quantum memory protocol, we can achieve almost complete absorption of the input quantum state, without the material necessarily having a high absorption.

The crystal will be cooled down to liquid helium temperature, due to the fact that, at this temperature, the crystal has very nice optical properties, like long coherence time of its excited state and its absorption profile is more confined. At this temperature, the crystal will shrink. One of the cavity surface was tilted, such that, even after the shrinking of the crystal cavity, the ion absorption profile can always be matched to the cavity resonance. The tilting of the surface, introduces extra losses in the cavity, explaining why the input state could not be completely absorbed within the cavity. Clearly for this idea to work, the cavity

resonance peak must be large enough to cover fully the part of the crystal absorption profile that will be used in the storage.

Our crystal is made from a Pr^{3+}:Y_2SiO_5 with a dopant concentration of 0.05%. The Pr^{3+} ions absorbed light at a wavelength of 605.9 nm. On absorption of this light, the ions are excited. While at the excited state, they can either fall down to their original state or to another state in the ground level. If they fall down to their original state, they re-absorbe and are excited again, until they fall down to a different ground state. When this happens, the intensity of the light absorbed by the absorption profile of the ions decreases at that particular frequency thus creating a spectral hole like structure there. This can be repeated until there are no absorbing ions left at that particular frequency. By scanning the frequencis, a spectral pit can be created with no absorbing ions present within that frequency range. The spectral pit is the name given to a pit in the frequency domain, that is, a range of frequencies within which, there are no absorbing ions present, therefore, outside this frequency range, there are plenty of absorbing ions. On creation of a spectral pit in the crystal cavity, frequency pulling effect pulls the cavity resonance frequency closer. Due to these changes in the atomic spectral distribution of the ions, they will now contribute to the imparted round trip phase shift of the light wave. This contribution is the sole cause of the frequency pulling effects. The inclusion of an absorption peak within the spectral pit will cause further frequency pulling effects, due to the same reason above. The Pr^{3+} ions are absorbing thus the present of this ions within a certain frequency range in the spectral pit will causing some absorption within that frequency range and no absorption outside that frequency range. These ions form what we called an absorption peak. Thus, the presence of a spectral pit and absorbing peaks in the crystal cavity, pulls the cavity resonance frequency from GHz to MHz, depending on the number of peaks present and the separation between the peaks. Thus with the help of a spectral pit plus peaks, we can turn our crystal cavity to an equivalent of a "cold" cavity (refering to a normal cavity without any spectral pit or absorption peaks) with length of the order of hundreds of meter.

Quantum state storage in a rare-earth doped crystal, which sits inside a cavity

Samuel Tornibue Kometa

March 31, 2011

Contents

List of Figures

Chapter 1

Introduction

" We are currently in the midst of a second quantum revolution. The first quantum revolution gave us new rules that govern physical reality. The second quantum revolution will take these rules and use them to develop new technologies."
Dowling and Milburn [1]

Quantum information is the study of information processing task accomplished using quantum mechanical systems [2]. The informations are encoded into quantum bits (qubits) which are then either stored or transmitted using a communication channel. Quantum information involved static resources like qubits, dynamical processes like the ability to store the quantum state as well as tradeoffs during performance of the dynamical processes [2]. Quantum computation, deals with the manipulation of these qubits, in order to solve complex as well as simple problems. The existence of information or the processing of information, can not take place without the presence of a physical medium, thus leading to the merging of computer science and physics in field of quantum computation [3]. The quantum bits (qubits) are the quantum mechanical analogy to the classical bits. The classical bits have one of two states label 0 or 1. The qubits also have states $|0>$ and $|1>$ ($|>$ is called the Dirac notation, used to represent a quantum state), corresponding to the classical bit states 0 or 1. The qubits can also be in a superposition state, that is, a linear combination of the states $|0>$ and $|1>$, for example

$$|\Psi>= \alpha|0> +\beta|1>, \tag{1.1}$$

Where $|\Psi>$ is the superposition state and α and β are complex numbers [2]. The state $|0>$ and $|1>$ are called the computational basis states, since any other state in the system can be expressed as a linear combination of them. The superposition states are the main difference between a classical bit and a quantum bit. Also, in a composite quantum system, the state of the system can be entangled, that is (it can't be expressed as a product of the individual state) for example the EPR pair [2]. This entangled states plays a central role in quantum information and quantum computation for example in quantum cryptography, quantum teleportation as well as in the violation of Bell's inequalities [2]. This leads to new and interesting methods in the processing and manipulation of information [3]. Though a qubit can exist as a superposition state, any measurement on it, collapse the state to its basis states (either $|0>$ or $|1>$).

Most of the quantum information and quantum omputation systems derive so far, requires a means of storing the quantum state within or at the end of an operation. The

quantum memory therefore plays a very important role in these applications. Consider for example, quantum cryptography using the Ekert scheme (that is, E91 protocol) [2–4] with the Einstein−Podolsky −Rosen (EPR) entanglement been shared between two parties, say Alice and Bob. The EPR pair is used to ensure that quantum cryptography is secure. For quantum cryptography protocol to be use fully for transmitting information securely, they must be able to do so over large distances, say $\approx 10^3$ km and above. This has prove to be very difficult to achieve due to the exponential scaling with distance of the photon losses in the communication channel as well as noise in the detector [2, 5, 6].

To overcome this problem, quantum repeaters [5, 6] can be used, allowing for long distance quantum communication. Quantum teleportation [7, 8], quantum memories [9–11], entanglement purification [12, 13] are all combined in a quantum repeater, in order to allow for entanglement distribution over large distances. For this purpose, the quantum memory needs to have a long coherence time (on demand readout), good quantum efficiency and the possibility for quantum swapping [14] using teleportation.

Quantum memories importance in long distance quantum communication systems and building blocks for quantum computers need not to be over emphasised. Different European Union projects (e.g. Qubit application (QAP) [11], and quantum repeaters for long distance fibre−based quantum communication (QuRep) [15]), as well as many research groups, are all working on different methods to realize quantum memories and to improvement the efficiency. The efficiency and fidelity of a quantum memory are closely related, and in an atomic ensemble system, the system decoherence affects the efficiency but not the fidelity of the quantum memory [11]. This explains why many research groups working with atomic ensembles are involved with the improvement of the efficiency.

There have been many quantum memory protocols [16–20], with theoretical calculations predicting a 100% recall efficiency. As of date, quantum memories with high efficiencies [21–23] have been realized. The recall efficiency of the quantum memory, irrespective of the protocol used for the realization, depends on the attainable optical depth in the memory material. Therefore, very high absorbing material (high optical depth, since the state to be stored needs to be completely absorbed in the memory material) [10, 11], is required in order to get very high efficiency in the quantum memory. This is a problem because first, achieving very high optical depth is difficult and if achieved, it will lead to re−absorption of the emitted stored quantum state, thus reducing the recall efficiency.

Many attempts have been made to solve this problem, the Gradient echo memory protocol [20, 21] is one such attempts and a recall efficiency of 87% has been achieved using it. Another such attempt, is using a resonance optical cavity [24, 25], which this diploma work is based on. With the aid of a resonant optical cavity, a low absorbing material (used for a quantum memory), can be tend into a very high absorbing material. This overcomes the problem associated with very high absorbing materials that is, no re-absorption of the recall quantum state. Theoretical calculation shows that, recall efficiency as high as 90% and above [24, 25] can be achieved with a low absorbing material.

In this diploma project, both theoretical and experimental work will be done to verify and test this cavity idea. The project is divided into 2 parts:

(i) The first part, which is covered in chapter 3 and 4, involves the theoretical verification,

that a low absorbing material can absorbed completely the storage pulse with the aid of a cavity, which has been done in reference [24, 25]. Our aim is to evaluate how well our geometry with tilted sides works. The cavity together with a low absorbing material is design and built.

(ii) The second part, which is covered in chapter 5, is the experimental part, were the cavity is tested.

The main idea is to have a quantum memory with recall efficiency above the no−cloning limit (for above this limit, it is impossible to perfectly copy a quantum state [2]), that can be used in a quantum repeater as well as a building block for a quantum computer. This diploma project originally started with the main theme being quantum memory with high efficiency. A phenomenon that we never though about, called cavity resonance frequency pulling was observed during the experiments for the first time to my knowledge in this material. This phenomenon is well know in literatures with regards to lasers [26, 27]. Therefore, the quantum memory experiments were suspended, such that, we can investigate this phenomenon in this crystal further. This thesis is divided into 4 chapters:

In chapter 2, an overview of quantum memories is given. This will includes various aspects to asset the performance of the memory, types as well as experimental realization of a quantum memory and their applications.

In chapter 3, an overview of the coherence interaction of light and matter is presented together with resonance cavities and Atomic Frequency Comb (AFC) in them.

Ray tracing of a resonance cavity with tilted sides, together with optimization of the cavity parameters in FRED are presented in chapter 4. How to write, edit and run scripts in FRED will also be described. The optimize cavity design and cavity properties will also be presented here.

In chapter 5, an overview of the optical properties of the memory material, experimental techniques for measuring cavity surface flatness, preliminary testing of the crystal cavity and results from the test will be presented.

Chapter 2

Optical quantum memories

Long distance quantum communication using optical fibres, suffers greatly from photons losses in the fibres. This problem can be overcome by the use of quantum repeaters. Quantum repeaters divide the quantum network length into segments and utilize the quantum memory to store and distribute entanglement between two nodes in the network [28]. Entanglement purification [12, 13], and swapping [14] are used to propagate the entanglement along each network segment. Entanglement purification and swapping are all quantum processing requiring the present of more than one entanglement mode, therefore, the quantum memory used for a quantum repeater should have multimode storage capabilities. Multimode quantum memories [18, 29] have been realized with very high modes numbers. For the quantum repeater to be used in practical situations, it will not only required the quantum memories to have multimode capabilities but also, it should have very high fidelity and efficiency as well as scalability (that is, long storage time as this will lead to an on-demand readout) [11, 17]. The quantum repeaters are to be used with optical fibres, thus the quantum memories, should be able to operate using the optical fibre wavelength [30, 31]. It has been shown that, it is possible to have quantum memories operating in the optical fibre wavelength [31] as well as converting the stored entanglement to optical wavelength [30].

Several different protocols have been proposed for the implementation of a quantum memory. In this chapter, criteria for assessing the performance and quality of a good quantum memory is presented, together with some of the protocols (emphasis will be place on the one, relevant for this project, that is AFC), as well as applications of a quantum memory.

2.1 Definition of an optical quantum memory

An optical quantum memory is a device that faithfully maps a quantum state (it can be a qubits strings or part of it [10]) onto the memory material (using the optical transition in the material), which is able to store the quantum state with an on demand released of it [9, 32]. A quantum memory should be able to store both the phase and the amplitude of a quantum state simultaneously.

To describe an optical quantum memory using quantum mechanics, we consider the memory to be a close system, whose state evolution can be described using unitary operators. Suppose at some time, t_1, the system is in state $|\Psi(t_1)>$. At some later time, t_2 say, the system has evolve to $|\Psi(t_2)>= U|\Psi(t_1)>$. To recalled the original state of the system, at

some later time, t_3 , an inverse of the unitary operator can be applied to the system, that is, $|\Psi(t_3) >= U^{-1}|\Psi(t_2) >= |\Psi(t_1) >$, thus a recall of the original quantum state [33].

2.2 Performance criteria for assesing an optical quantum memory

Different quantum information applications have different requirements for the quantum memory (that is, the stored quantum state). For example, for quantum logic gates operations, as long as the stored quantum states can be recalled above a certain fidelity, the states can be used as they are together with quantum error correction schemes [2] for the logic operation. Thus, such a system does not require a quantum memory with perfect recall capabilities. Below, an evaluation of the various criteria for assessing the performance of a quantum memory is presented.

2.2.1 Fidelity

In a quantum memory, a quantum state to be stored, should be written onto the memory material and after some time, t, the quantum state should be readout. The stored quantum state can be expressed as a density matrix, ρ, the read out state can also be expressed as a density matrix $\acute{\rho}$ [2, 10]. Therefore, the storage fidelity of the state ρ is defined as [10],

$$\mathcal{F}(\rho) = Tr\sqrt{\sqrt{\acute{\rho}}\rho\sqrt{\acute{\rho}}}. \tag{2.1}$$

From equation(2.1), there is a threshold value $\mathcal{F}_{thrs}(\rho)$, such that when $\mathcal{F}(\rho) > \mathcal{F}_{thrs}(\rho)$, the quantum error correction scheme can be apply to the read out quantum state to correct its imperfection [2].

The fidelity can also be defined as the square root of the overlap between the stored quantum state and the read out state. Suppose the stored quantum state is a pure state ($|\Psi >$ or$\rho = |\Psi >< \Psi|$ in density matrix notation), and the read out state is $\acute{\rho}$, then using equation (2.1), the fidelity of the quantum memory is

$$\mathcal{F}(\rho) = Tr\sqrt{< \Psi|\acute{\rho}|\Psi > |\Psi >< \Psi|} = \sqrt{< \Psi|\acute{\rho}|\Psi >}. \tag{2.2}$$

There are other definitions of fidelity used in experimental works. For example, conditional fidelity used in the previous paragraph or unconditional fidelities, when the memory is used to store any state of light or quantum state [10, 11].

2.2.2 Efficiency

The efficiency of a quantum memory can be defined as how well a quantum memory can preserved stored information or stored quantum state [11]. Simply stated, the efficiency of a quantum memory is the ratio of the energies of the stored quantum states to that of the read out quantum states [10, 34]. The fidelity and the efficiency are closely related [2], the higher the fidelity, the higher the chance to get a high efficiency and vice versa (but this is not always the case). Quantum memories with high efficiencies have been realized in atomic ensembles, due to a collective constructive interferences effects of all the atoms (emiiters) in the ensembles [39].

This diploma work is mainly concerned with the improvement of the quantum memory efficiency, using atomic ensembles with the aid of a cavity to increase the light matter coupling, that is material absorption [24].

2.2.3 Storage time

The storage time is how long the quantum memory can keep the coherent quantum state, before it losses its coherence, that is, become de-coherent. A quantum repeater divides the quantum network into segments. The length of each segment set a lower bound to the storage time of the quantum memory [28]. Also for entanglement swapping and purification between nodes in a quantum repeater to be very effective, there must be the present of entanglements in both nodes. As such, the quantum memory should be able to store an entanglement for as long as it takes for the other entanglement to get to the other node. Studies shows that, storage time of the order of second is very important for efficiency operation of a quantum repeater [11].

Not all quantum application using quantum memory requires long storage time. For example, single photon sources using quantum memory and parametric down conversion sources [11], does not required quantum memory with long storage time. In general, the quantum memory should be able to store the photon state for as long as the state is needed.

2.2.4 Bandwidth

The possibility for multiplexing a quantum memory [11] to matching sources and to obtain high repetition rate, will all depends on the memory bandwidth. Therefore, the usefulness of the quantum memory depends on the operational bandwidth of the quantum memory [11].

2.2.5 Wavelength

As of date, most of the long distance communications (classical), uses optical fibres, except for free space communication. Long distance quantum communication will obviously need to use optical fibres. Since photons will be used to transmit the information, the wavelength of the photons should be in the region where there are very little losses optical fibres. This limits the wavelength of the photons to around 1.3 to 1.5 μm [30, 31]. For quantum memories to be used along the network, it should be able to store photons with the prescribe wavelength. Recent studies shows that, it is possible to store photons within this wavelength band in a quantum memory as well as store the photons using a different wavelength and converting it to the required wavelength after retrieval before transmission [30, 31]. This will relax the condition on the operational wavelength of the quantum memory.

2.2.6 Multi−mode storage capacity and dimensionality

The total number of optical modes that can be stored in a quantum memory determines the applicability of the quantum memory. Most quantum application using quantum memory needs multi-mode storage capacity of the memory [6, 35]. The multi-mode capability of a quantum memory depends greatly on the protocol used to realize the memory, some protocols have an inherent multi-mode capability while others don't [18, 29].

2.3 Types of optical quantum memory

Quantum memories can be classified based on their different applications. Different applications requires different performance characteristics of the memories. There are 3 main types of quantum memories, that is, quantum memories for storing a single photon, quantum memories for storing a general quantum state of light and lastly quantum memories charged by the emission of a photon. Below, we give a brief overview of these 3 types of quantum memories.

2.3.1 Single photons optical quantum memory

These are quantum memories whose output is a single photon state. They are very essential components in the implementation of single photon sources [11] or in quantum repeaters [6]. In a quantum repeater protocol, the quantum memories used should be able to absorb a photon, stored the photon and re-emit the store photon [6]. In this type of memories, the efficiency and the fidelity are the two parameters used to characterize the memory. This is because the memory can fail to emit the stored photon (efficiency) or it can emit a photon whose quantum state overlap with that of the stored photon (fidelity). For this protocol to be efficient, the memory efficiency as well as its fidelity should be very high [11].

This diploma work is aimed toward quantum memories for quantum repeaters. As such, improving the efficiency is of paramount important because the memory is implemented based on an ensemble of atoms; whose de-coherence affects the efficiency but not the fidelity [11].

2.3.2 General state of light optical quantum memory

In some application, the state of the light to be stored is not know (third party production) before the storage process [11]. For example, in linear optics quantum computation involving a quantum memory, at some point in the computation, the state of the light maybe unknown. In such memory the re-emitted general state can be measured in some basis and can be a coherence state, or a squeezed state or a fock state (single photon state) [11]. The performance of the memory, can be asset using quantum tomography [36, 37] as well as the fidelity of the quantum memory [2].

2.3.3 Optical quantum memories for emitted photons whose state can be measured directly or through a retrieval process

In a single trapped atom quantum memory, the trapped atom emits photons which are entangled to trapped atoms (the memory). The state of the emitted photons can be detected or measured directly [11]. As such, to characterize the memory performance, the fidelity (unconditional) is the main parameter. This is due to the fact that, the detection process of the state is a deterministic process leading to no distinction between the efficiency and the fidelity [11].

Duan-Lukin-Cirac-Zoller (DLCZ) type memory is another type of memory [28]. This type of memory is excited by the absorption of a photon and read out is done by converting this excitation into a single photon. The fidelity and efficiency are the two parameters used to characterize the performance of such memories [11].

2.4 System requirements for optical quantum memories

Optical quantum memories requires a medium for storing the light state. For the storing to be possible, the medium must have certain properties. The necessary properties of the medium are mainly determined by the quantum memory performance criteria. Since the fidelity, efficiency and storage time are the three main performance criteria, the requirement on the medium must be such that these three parameters can be optimized. For good memory fidelity and efficiency, the medium must possess good coupling to the light state and for long storage time, the medium needs to have long optical coherence time or the stored state has to be transfered to some other state with long coherence time.

2.4.1 Light−matter coupling

For quantum memories operating through the absorption and re-emission of the light state, good light matter coupling is necessary. The probability of an incident light state to be absorbed is determined by the coupling between the light state and the medium. This can be measured through the optical depth of the material in solid and gases, therefore, good coupling will required very high optical depth. The high optical depth, can also lead to re-absorption of the re-emitted light state, a major problem encountered by simply increasing the optical depth of the material. There have been different proposal to over-come this difficulty, and one such proposal is placing the memory material within an optical cavity. At the optical cavity resonance, the optical depth of the material should be very large (even if the material optical depth without the cavity is small) [24]. This then leads to good coupling between the light and the memory material.

2.4.2 Coherence/decoherence

Most quantum memory protocols implemented so far, uses a Dicke state (collective atomic coherence) [16–18, 38, 39], to store the light state. Therefore, de-coherence in the atomic ensemble, limits the storage time in the quantum memory [38].

De-coherence have different effect on the different memory protocols. For example, in the CRIB (Controlled Reversible Inhomogeneous Broadening) and AFC (Atomic Frequency Combs) protocols using atomic ensembles, the efficiency of the memory is greatly affect by de-coherence in the optical transition used for the storage but the fidelity (conditional) is not affected [16–18, 38, 39].

The memory material coherence properties can be greatly improved upon, and for a full discussion of this, see reference [40] and the references therein.

2.5 Experimental realisation of an optical quantum memory

There are different schemes to realize an optical quantum memory, e.g. using a trapped single atom but this has some drawbacks, that is, to achieved high efficiency strong light matter coupling is required which is very difficult to achieve in such systems. High Q-cavities

are used nowadays to over-come the coupling problem but the atoms (trapped atoms) suffers greatly from losses as a result of dissipation [34].

NV-centers are also good candidates for quantum state storage. They also have low dipole moments, thus low coupling strength. This has however been over-come by placing them inside waveguides or micro-cavities but the difficulties associated with processing the NV-centers still remains [34].

Atomic ensembles [41] are another candidate for the realization of a quantum memories. They have the advantage that high light matter coupling can be achieved with ease, using memory materials with high optical depth. The main problem with them is the control of the light matter interaction and elimination of any dissipative processes present [34]. Atomics ensembles in gaseous form, were the first to be used for quantum state storage, due to the ease with which they can achieve a high number density, thus strong light matter coupling [34]. They had some problems, due to the random motion of individual atoms, leading to Doppler broadening. To over-come the Doppler broadening, the atoms had to be cooled down. The process of cooling down the atoms uses the evaporative cooling technique [42] thus reducing the number of atoms (number density) as well as the light matter coupling (since there are less atoms presence now).

Rare-earth-ions doped materials [40, 43–45], are ideal solid state system for quantum state storage. There are two main quantum memory protocols based on these materials, that is, photon-echo quantum memories (which includes CRIB and AFC [16–18, 38, 39], the latter being the protocol used for this work) and electromagnetically induced transparency (EIT) [46–48]. These are the 3 experimental protocols that will be presented below.

2.5.1 Photon−echo optical quantum memory

Photon-echo optical quantum memories, grows from the corresponding classical optical data pulse storage technique [49]. The classical optical data storage technique is a four wave mixing technique. In this technique, 3 input waves separated in time, are mixed to produce the fourth wave called the echo. The fourth wave can be expressed mathematically as [49]:

$$E_{echo}(t) \propto \int E_1^*(\omega)E_2(\omega)E_3(\omega)e^{i\omega t}d\omega, \tag{2.3}$$

where E_{echo} is the fourth wave or the echo, $E_{1,2,3}$ are the three input waves or the write, data and read pulses respectively. Under certain special conditions, or circumstances, for example, if $E_1(\omega)$ and $E_3(\omega)$ are constants, equation (2.3) reduces to

$$E_{echo}(t) \propto \int E_2(\omega)e^{i\omega t}d\omega. \tag{2.4}$$

The main operating principle behind the photon-echo optical quantum memory is the transfer of the light state to be stored to an ensemble of atomic coherence excitation [39]. This coherence excitation can either be an optical (optical transition) or spin (hyperfine transition) coherence excitation. Photon-echo optical quantum memories, uses the inhomogeneous broadening of the memory materials and thus have the operational possibility of a large bandwidth [16–18, 38, 39]. The memory protocol is based on the absorption and re-emission of the absorbed quantum state using a photon-echo effect.

Consider an atomic ensemble, made up of two level atoms, as the memory material, having an inhomogeneous broadening larger than the homogeneous line-width of the atoms. Assume that initially, all the atoms are in the state $|\Psi_1>$, at some time, t. At a later time, t_2, the ensemble absorbed a single photon and the new state of the system (un-normalized) is a Dicke state, that is [17, 18, 39]:

$$|\Psi_2>=\sum_j \psi_j e^{-i\delta_j t} e^{ikz_j} |g_1 \cdots e_j \cdots g_N>, \tag{2.5}$$

where N is the total number of atoms in the ensemble, k the wave vector of the photon (signal field), δ_j the detuning of the signal field with respect to atoms j transition, ψ_j is a function of the frequency and position of atoms j, $|g_j>$ and $|e_j>$ the ground state and excited state of atom j, z_j the position of atom j. Note that for simplicity, only the forward propagating mode of the input light field has been consider.

Due to the large inhomogeneous broadening, there will be de-phasing of the Dicke state due to the present of the term $e^{-i\delta_j t}$, which is different for different individual atoms. This de-phasing can be corrected, thus forcing a collective atomic coherence excitation [39].

The photon-echo optical memories operates by re-phasing the atomic dipole moments of the atomic ensemble (Dicke state) at some later time, thus creating an atomic coherence excitation [17, 18, 39]. There are two main categories of photon-echo optical quantum memories, that is Controlled Reversible Inhomogeneous Broadening (CRIB) and the Atomic Frequency Combs (AFC). They are differentiated base on the spectral detuning δ_j of the initial distribution [10].

(i) ***Controlled reversible inhomogeneous broadening (CRIB)***: If the initial spectral detuning distribution δ_j is continuous, then each atom in the ensemble will not have an independent phase evolution. For each atom to have an independent phase evolution, that is, $\int_0^{t_e} \delta_j(t)dt$, it should be possible to change all atoms resonance frequencies from δ_{j1} to δ_{j2}, after some time, t$'$, after the absorption of the storage pulse. This changes should be such that, at all time, $\delta_{j1}t' + \delta_{j2}(t_e - t')$ should be a constant [10].

The Maxwell-Bloch equations (see chapter 3) describing the light matter interaction possess hidden time reversal symmetry [17, 38]. In the Maxwell-Bloch equation describing the evolution of the forward propagating wave (the wave to be absorbed in the medium), changing the signs of the detuning and the wave, the equations then describes the evolution of the backward propagating wave from the medium [17]. The CRIB protocol exploit this hidden symmetry property of the Maxwell-Bloch equations [17, 38]. For detail mathematical description, see reference [17] and references therein. The CRIB protocol can be implemented experimental [16, 38] in 5 steps, using a memory material with large natural inhomogeneous broadening and permanent electric dipole moment. The inhomogeneous broadening must be larger than the homogeneous line-width of the material for the protocol to be very effective, since the inhomogeneous absorption profile will be reshaped using optical pumping.

step 1: In the first step, a spectral pit is created in the inhomogeneous broadening profile by spectral hole burning technique [40, 44, 51]. This is done by frequency scanning of the laser, for detail see reference [44]. See figure (2.1) a.

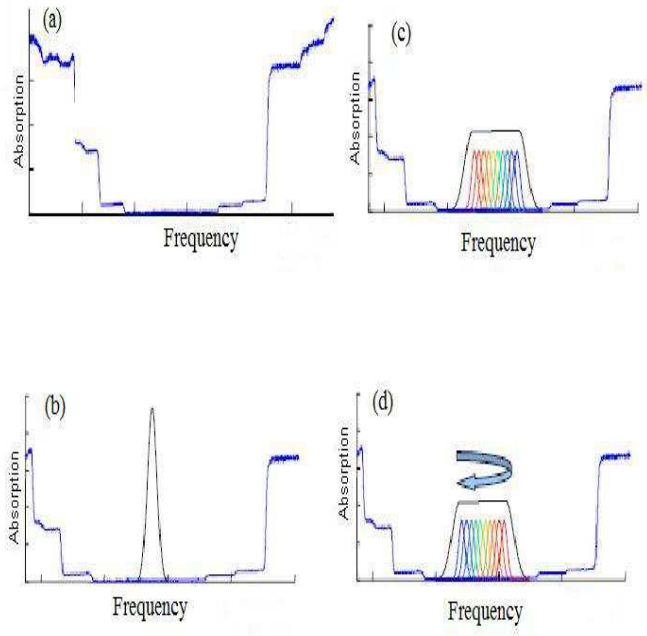

Figure 2.1: Steps in the implementation of the CRIB protocol. (a) An empty pit is created by scanning the laser frequency. (b) Optical pumping is used to create a narrow absorption line. (c) A linear electric field causes broadening of the narrow absorption line in a control manner. (d) Re-emission of the stored pulse by a reversal of the linear electric field. Figure adopted from reference [50]

step 2: After the pit is created, the next step is creating a narrow absorption line or a peak within the spectral pit. This is done by optical pumping of ions with a selected frequency range back into the pit [51]. See figure (2.1) b.

step 3: Next, the absorption line or peak is broaden with the aid of an electric field gradient. The electric field will produce a linear stark shift in the ions as such ion at different positions in the absorption line, will acquire different resonance frequency and hence a broaden absorption line with reduce optical depth. This step is completely reversible, as such the name of the protocol [16, 38], see figure (2.1) c.

step 4: A weak light field or quantum state is now send into the medium for storage in the broaden absorption line.

step 5: The re-emission process can be done in two ways:

- Reversing the sign of the electric field thus inverting the linear stark shift and thus triggering the echo or the re-emission of the stored state.
- Reversing the detuning on each atom through the application of a position dependent phase shift 2kz. This is to ensure mode or phase matching and reversal of the inhomogeneous broadening. This will lead to re-emission in the backward direction, that is, directional emission.

The advantages in this method is that, the rephrasing is controlled, by controlling the artificially broaden peak or absorption line, along-side, inhibiting the natural

inhomogeneous broadening. The broadening of the peak can be controlled as well as, it can be reversed, these are not true with the natural inhomogeneous broadening [16, 17, 38].

Due to the reduction of the optical depth of the broaden peak, the medium must have sufficiently large optical depth to guarantee complete absorption of the storage pulse. Also, the memory bandwidth is limited by the width of the broaden peak [10].

The efficiency of this protocol (using transverse broadening of the peak) in the backward direction, has been found to be [17] $\eta = (1 - e^{-\alpha L})^2$ and $\eta = (\alpha L)^2 e^{-\alpha L}$ in the forward direction. αL is the absorption depth of the broaden peak. Clearly, an efficiency of 100% can be achieved in the backward direction but that will required an additional phase shift to constraint the system to propagate the echo in the backward direction. If the phase shift is not applied, the emitted echo will propagate in the forward direction and will be partly absorbed, as such the maximum efficiency that can be achieved is 54%. Recent progress in this technique, shows that, the re-absorption of the forward propagating pulse can be reduced or even removed by the application of a gradient electric field thus giving a possibility of a 100% efficiency in the forward direction [19].

(ii) ***Atomic frequency comb (AFC)***: Here the spectral detuning distribution has a periodic comb like structure. The structure has discrete absorption lines (or comb like structure) with spacing Δ apart, thus each atom can have an independent phase evolution [10]. Re-phasing of the atoms occurs every time $t = (\frac{2\pi}{\Delta})$.

The AFC protocol uses the inhomogeneous broadening of the storage material, same as the CRIB protocol. The use of this protocol for quantum state storage, has mainly been implemented in solid state materials, made up of an ensemble of atoms, whose excited state $|e>$ is connected to the ground state $|g>$ optically. This protocol has also been used for time domain holography as well as in photon echo using accumulated frequency grating [10]. In the AFC protocol, the quantum state to be stored create an entanglement between the excited and ground state of the system, used mainly for the (initially) storage. If need be for long storage time, the entanglement is transfered to between the hyperfine ground state $|s>$ and the ground state $|g>$ using a π pulse. Thus the entanglement can be shuzzle between the excited and hyperfine states using a π pulse. Note also that, this applies to the CRIB protocol as well.

To make maximum use of the inhomogeneous broadening Γ_{inh}, the homogeneous line width Γ_{hom} must be far less than Γ_{inh}, in the optical transition $|g> \rightarrow |e>$. For a full mathematical description of the AFC protocol, see reference [18] and the references therein.

The AFC protocol is implemented experimentally in 3 steps:

step 1: First a spectral pit is created in the ground state, $|g>$ of the material. This is done using spectral hole burning techniques [40, 44, 51]. In order for this to be possible, the storage material must have a shelving state ($|aux>$) (population storage reservoir [39]) which is another ground meta-stable state with a long life time. The pit is created by scanning the laser frequency over a certain frequency

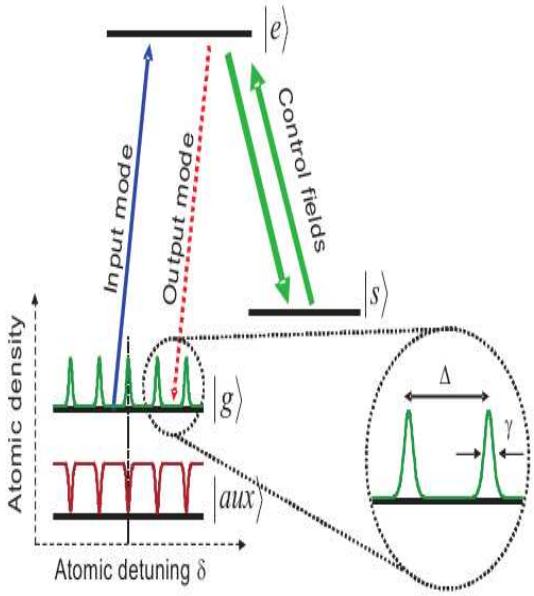

Figure 2.2: Implementation of a complete AFC protocol including spin storage protocol. The inhomogeneous broaden absorption profile is shape into a comb like structure by selectice frequency pumping to the aux state. The peaks have width γ, seperation Δ and finesse F. Figure adopted from reference [18]

range, back and fore several times, such that, all ions within that frequency range are selectively transfer from the ground state $|g>$, to the meta-stable state $|aux>$ see figure (2.1) a.

step2: Next, narrow absorption peaks or lines are created within the pit, through a coherent burning back of selected ions or frequencies. The only absorber present within the pit, are the peak ions, thus forming absorption peaks spectrally. To increase the number of peaks, more burn back pulses (coherent pulses) are applied with each one having an appropriate frequency off set, Δ, see figure (3.2), [18]. The peaks features can be changed, simply by changing the burn back pulses. For example, to change the shape of the peaks, the shape of the burn back pulses should be changed and to increase the peaks height, the power of the burn back pulse should be increased (this will increase the height of the peak, if the sample has more ions present at that frequency else the increase in power will cause peak saturation) or decrease [22, 52].

step 3: The light field to be stored is then send into the pit, and will be absorbed uniformly by the peaks. It will be stored in the medium as a collective coherent excitation of the optical transition [39]. The condition for uniform absorption of the storage pulse is that, the FWHM of the storage pulse must be large than the peak spacing (Δ) but less than the AFC bandwidth [18, 39]. If nothing is done after the absorption of the storage pulse, it will be re-emitted as an echo after a pre-define time of $t = \frac{2\pi}{\Delta}$. At this time, all the dipole moment of all the atoms in the peaks re-phases and emits a coherent echo, which is the stored pulse [18, 39]. The re-emission is due entirely to the periodic structure of the absorption profile

or peaks. To increase the storage time above the optical coherence time T_2, the optical coherent excitation amplitude is transferred to a long live spin hyperfine coherent excitation [53]. While the excitation is in the spin hyperfine ground state, the phase evolution is stoppped. Read-out is then done by transferring back the spin hyperfine coherent excitation to the optical coherent excitation, using π pulses and the echo comes out after the pre-defined time $t = \frac{2\pi}{\Delta}$.

The efficiency of the AFC memory protocol in the forward direction given by [39]

$$\eta \approx \tilde{d}^2 e^{-\tilde{d}} e^{-\frac{\pi^2}{F^2 2ln2}}, \tag{2.6}$$

Where $\tilde{d} \approx d/F$ called the effective optical depth, d is the AFC optical depth and $F = \frac{\Delta}{\gamma}$ the AFC finesse and γ is the FWHM of the AFC peaks. The first term $\tilde{d}^2$ describes the coherent response of the system to the stored light pulse, the second term, $e^{-\tilde{d}}$ describe the re-absorption of the emitted echo and finally $e^{-\frac{\pi^2}{F^2 2ln2}}$ the de-phasing factor which is due entirely to the finite width of the AFC peaks.

In the backward direction, the AFC memory protocol efficiency is [18]

$$\eta \approx \left(1 - e^{-\frac{\alpha L}{F}}\right)^2 e^{-\frac{\pi^2}{F^2 2ln2}}, \tag{2.7}$$

and an efficiency of 100% can be achieved in the backward direction as long as the optical depth is large enough. In an AFC protocol, there is always a possibility to chose between high absorption and small AFC finesse or large finesse (de-phasing) and small absorption [18, 39].

2.5.2 Electromagnetically induced transparency

Electromagnetically induced transparency is a phenomenon that is common in atoms whose states can be in the Λ configuration, see figure (2.3). The Λ configuration is a 3 level system, $|a>, |b>$ and$|c>$, where the two lower levels $|b>$ and $|c>$ are both couple to the same upper state $|a>$. EIT is a quantum interference effect introduced by 2 coherent fields, driving the two transitions $|b> \rightarrow |a>$ and $|c> \rightarrow |a>$. The medium will experience zero absorption (dark state) for one of the coherent fields if the conditions are right [33].

When EIT is used for quantum information processing, the two coherent fields are a weak signal fields (carrying the quantum information and coupling the states $|b> \rightarrow |a>$) and a strong control field (for controlling the atomic system and coupling the states $|c> \rightarrow |a>$). The main effect of this two fields, is to put the system in a superposition state between state $|b>$ and $|c>$. Since EIT is a quantum interference effect, then with the appropriate conditions, the absorption due to the transition $|b> \rightarrow |a>$ will be out of phase with the absorption due to the transition $|c> \rightarrow |a>$ and they will cancelled each other (dark state) [33]. If only one field is present, say the signal field resonant with the optical transition $|b> \rightarrow |a>$, it will be absorbed by the medium or atoms. When both fields are present, the absorption of the signal field is greatly reduced as long as the Raman transition frequency between the ground states ($|b>, |c>$) is closed to the frequency difference between the two fields.

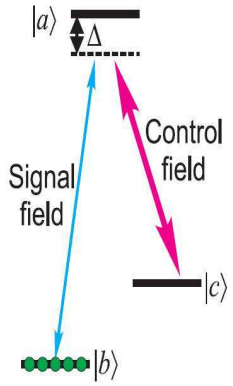

Figure 2.3: The Λ shape used for EIT memory protocol. Figure adopted from reference [10]

The EIT memory protocol uses the slow light effect created due to the transparency of the medium. The slow light effect can be understood using the Kramers-Kronig relation [27], that is:

$$\chi^{'}(\nu) = \frac{2}{\pi}\int_0^{+\infty} \frac{s\chi^{''}(s)}{s^2-\nu^2}ds \tag{2.8}$$

$$\chi^{''}(\nu) = \frac{2}{\pi}\int_0^{+\infty} \frac{\nu\chi^{''}(s)}{\nu^2-s^2}ds. \tag{2.9}$$

This relation links the absorption and the dispersion of a medium. The signal field is slowed down (group velocity deceleration), due to the fact that, in the present of the control field, the signal field experiences a large normal dispersion (large changes in the slope of the refractive index) and this is inversely proportional to the control field amplitude. The slowing down of the signal field is the basis of the EIT memory protocol and operates as follows: first a transparency window is created (EIT window). Once this is created, the signal field resonance with the window, is send in, the signal field is slowed down inside the medium by spatial compression of the pulse, until it fits entirely inside the medium. At this point, the control field is adiabatically decrease, collapsing the EIT window until the signal field group velocity is zero. At this point, the pulse is stored within the medium [47].

For retrieval of the pulse, the control field is turn on and the compressed pulse resumes its propagation out of the medium. Its stretches to its original shape as its leaves the medium [47].

2.6 Applications of optical quantum memories

Below, a brief over-view of some of the application of an optical quantum memory is presented.

2.6.1 Deterministic single photon sources

Deterministic single photon sources are essential elements for secure quantum cryptography applications requiring deterministic single photon sources [6, 35]. Non-deterministic photon

sources are problematic since you cannot be sure, if a photon is present or not. With the help of a quantum memory, a non-deterministic photon source can be converted to a deterministic photon source. For example, a parametric down conversion photon pair source can be change to a deterministic singe photon source. This can be done by connecting a quantum memory to one of the output channel and a photon detector in the other. When a photon is detected in the detector, this will imply that the memory is charged, thus a click in the detector, implies the memory is ready to send out a single photon [11].

2.6.2 Quantum repeaters

As mentioned earlier, long distance quantum communication network suffers greatly from photon losses. To overcome this, quantum repeaters can be inserted at regular interval within the network.

Basically, a quantum repeater is some sort of a cascade of entanglement purification and swapping [6, 28]. The long distance quantum network is divided into segment, each having a length comparable to the attenuation length of a photon in a photonic channel [28]. Three main processes take place in each quantum repeater, that is:

(i) The entanglement to be transmitted is generated. Here a single photon source can be very useful depending on the type of repeater.

(ii) The generated entanglement is purified [12, 13] and stored in a quantum memory.

(iii) Two adjacent segment of the network are then connected through entanglement swapping [14]. Entanglement swapping then uses quantum teleportation to exchange the states between the memories, thus increasing the propagation distance of the entanglement. After each entanglement swapping, the amount of entanglement reduces and as such entanglement purification should be performed again. The process of entanglement swapping and purification is a continuous process, until a perfect entanglement state is created at the two ends of the network [28].

Quantum memories are very essential elements of the quantum repeaters, since the entanglement purification is probabilistic. The memory stores the entangled state if the purification is successful or else the purification process is repeated until it does succeed. Also since the entangled states will not reach the nodes at the same time, the one that get there first, will be stored in the quantum memory, while waiting the arrival of the other entangled state. The process of entanglement swapping can only take place if both nodes have an entangled state present [14].

2.6.3 Precision measurement

Sensing and precision metrology using entangled state can be greatly improved upon with the aid of a quantum memory, with the capability of storing long live entanglement state. With the quantum memory present, the precision will be quantum mechanically limited not classical [11].

This is done using quantum interference effects of the atomic ensemble, by transferring the optical quantum state properties to the atomic ensemble, thus reducing the quantum noise level greatly. This has led to improved spectroscopy precision-measurement and improved atomic clocks [11].

2.6.4 The uncertainty principle in the presence of quantum memory

Recent studies (theoretical) have shown that, with the aid of a quantum memory, the lower bound of the Heisenberg uncertainty relation can be reduces to zero. Thus we can be able to measure both the position and the momentum of an atom with equal precision. Mario Berta et al. [54], in their paper wrote, I quote "if the particle is prepared entangled with a quantum memory, a device that might be available in the not to distance future, it is possible to predict the outcomes for both measurement choices precisely".

2.7 Summary

- An optical quantum memory is a device that is capable of storing both the amplitude and phase of a quantum state faithfully.
- The fidelity, efficiency, storage time, memory bandwidth, the memory wavelength and multimode capabilities are different criteria for accessing the performance of a quantum memory.
- Quantum memories has been realized using atomic ensembles with CRIB, AFC and EIT protocols.
- Detreministic single photon sources, quantum repeaters and precision measurements are different application using quantum memories.

Chapter 3

Theoretical treatment of cavity assisted optical quantum memory

In this chapter, an over view of resonance cavities and some of their peculiar properties will be presented. The response of the atoms in the present of a coherent field of radiation will be treated and finally, the light matter interaction within a cavity and the application to AFC protocol. The simulation of the Bloch equations in a simple cavity will be given.

3.1 Resonance cavity

In this section, key ideas with regards to passive optical cavity (no gain), will be presented. The plane-wave or transmission line model applied to a standing wave will be used for the discussions. An example of a resonance optical cavity is the Fabry-Perot interferometer or the Fabry-Perot etalon. Here the cavity is made up of 2 flat highly reflecting mirrors placed closed to each other.

In this work, the optical cavity we will be working with is a low losses optical cavity. The cavity is made from a Pr^{3+}:Y_2SiO_5 crystal (solid state material) with a dopant concentration of 0.05%. Two faces of the crystal is polished to optical quality and coated with high reflectivity (99.7%) and partially transmitting (20%) mirrors respectively. The two mirrors are deliberately made none parallel; this will introduce additional losses in the cavity. We hope to optimize the cavity and make the loss as small as possible, using the raytracing software FRED. This will be described in the next chapter. In the rest of this chapter, we consider an ideal cavity with parallel mirrors.

Our resonance optical cavity is a standing wave cavity since we have forward and backward travelling waves in it, due to reflections from the end mirrors. These standing waves will form an optical standing wave pattern within the cavity, with periodic spatial variation along the cavity axis. The period of this standing wave pattern is equal to one half the cavity optical wavelengths [26]. Note: the analyses below closely follow that of reference [26].

3.1.1 The circulating E-field amplitude

Let the reflection coefficient for the elctric field of the two mirrors of the cavity be r_1 and r_2 respectively (note also that $r_1 = \sqrt{R_1}$ and $r_2 = \sqrt{R_2}$ where R_1 and R_2 are the electric

field reflectance of the two mirrors). Let the input wave be a sinusoidal optical field, with complex amplitude denoted E_{inc}, the circulating complex amplitude field within the cavity E_{circ}, a transmitted complex amplitude field E_{trans}, and a reflected complex amplitude field E_{ref}. The circulating field measure just after mirror M_1 is made up of two part, that is, the transmitted field from mirror M_1 and the field that has made one round trip within the cavity. The transmitted field amplitude through mirror M_1 is the product of the transmission coefficient of mirror M_1 and the input field amplitude, that is, jt_1E_{inc} and the round trip field is $\tilde{g}_{rt}(\omega)E_{circ}$, where $\tilde{g}_{rt}(\omega)$ is the complex round trip gain of the field. The material of our cavity has a round trip absorption coefficient of α_0, such that, the field amplitude is attenuated by a factor of $exp(-2d\alpha_0)$ after one round trip, where d is the cavity length. The input field acquires a phase shift of $exp(-j2\omega d/c_m)$, after one round trip, where $c_m = c_0/n$ light spend in the crystal, n the crystal refractive index, c_0 the velocity of light in a vacuum, ω the cavity axial mode frequency and d is the cavity length. The round trip gain within the cavity becomes $\tilde{g}_{rt}(\omega) = r_1r_2exp(-2d\alpha_0)exp(-j2d\omega/c_m)$ and the circulating E-field complex amplitude becomes

$$E_{circ} = \frac{jt_1E_{inc}}{1 - r_1r_2exp(-2d\alpha_0)exp(-j2d\omega/c_m)}. \tag{3.1}$$

The circulating field, equation (3.1), has a maximum each time the phase shift acquired by the field is an integer multiple of 2π, that is, $\nu_q = q\frac{c_0}{2nd}$ and $E_{circ} = \frac{jt_1E_{inc}}{1-r_1r_2exp(-2d\alpha_0)}$ with q an integer. ν_q are called cavity axial modes and the spacing between them is called axial mode spacing or cavity free spectral range. The magnitude of the complex round trip gain $\tilde{g}_{rt}(\omega)$, is less than unity, as such, at position of resonance the circulating E-field is greater than the incident E-field on the cavity.

3.1.2 Transmitted Cavity E-field amplitude

The transmitted cavity E-field amplitude is that portion of the circulating E-field amplitude that is transmitted through the mirror M_2. This is on the assumption that, there is no field leakage in the cavity or beam walk in the cavity.

$$E_{trans} = \frac{-t_1t_2exp(-d\alpha_0)exp(-jd\omega/c_m)E_{inc}}{1 - r_1r_2exp(-2d\alpha_0)exp(-j2d\omega/c_m)}. \tag{3.2}$$

At resonance, equation (3.2) becomes $E_{trans} = \frac{t_1t_2exp(-d\alpha_0)E_{inc}}{1-r_1r_2exp(-2d\alpha_0)}$. Since $\tilde{g}_{rt}(\omega)$ is less than 1, the transmitted field at resonance should have the highest value.

3.1.3 The reflected cavity E-field amplitude

The reflected field amplitude is a sum of two fields amplitudes, that is, a direct reflection from mirror M_1 with value r_1E_{inc} and a transmitted part of the circulating field amplitude from the same mirror with value $jt_1\left(\tilde{g}_{rt}(\omega)/r_1\right)E_{circ}$. Notice that the complex amplitude gain is divided by this mirror reflectance, since its goes through the mirror. Hence, with lossless mirrors, the reflected amplitude becomes:

$$E_{ref} = \left[r_1 - \frac{t_1^2r_2exp(-2d\alpha_0)exp(-j2d\omega/c_m)}{1 - r_1r_2exp(-2d\alpha_0)exp(-j2d\omega/c_m)}\right]E_{inc}. \tag{3.3}$$

At resonance, the reflected field becomes

$$E_{ref} = \left[r_1 - \frac{t_1^2 r_2 exp(-2d\alpha_0)}{1 - r_1 r_2 exp(-2d\alpha_0)} \right] E_{inc}. \tag{3.4}$$

Clearly from equation (3.4), it is possible to make the reflected amplitude to be zero. For that to happen, the reflectivity r_1 of the first mirror (input mirror) must be matched to the losses in the cavity, that is, material losses and the second mirror losses, that is, $r_2 exp(-2d\alpha_0)$. This can also be interpreted as the reflected wave from the first mirror is out of phase with the transmitted circulating wave in the cavity and thus interfere destructively. When this happen, we say the cavity is impedance matched. In a losses passive resonance optical cavity, we can impedance match the cavity by setting the round trip absorption coefficient of the cavity to be:

$$\alpha_0 = \frac{1}{2d} ln\left(\frac{R_2}{R_1}\right), \tag{3.5}$$

if the two mirrors reflectance are known and cavity thickness are know. Equation (3.5) will be used to calculate the starting absorption coefficient in chapter 4, for the FRED simulation.

3.1.4 Cavity parameters

The cavity free spectral range (see figure (3.1))

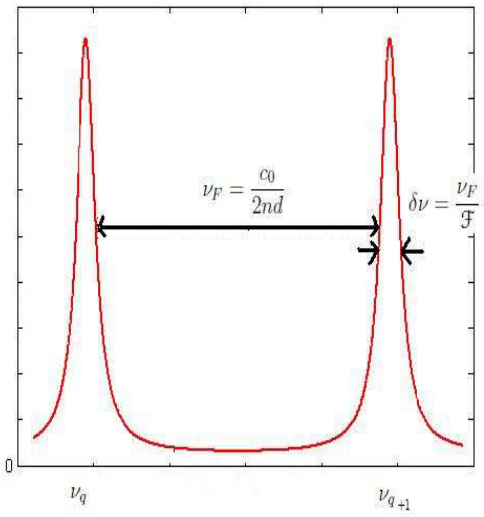

Figure 3.1: Transmission intensity of a lossy cavity. The losses in the cavity leads to broadening of the resonance peaks thus sustaining other frequencies apart from its resonance frequency. The free spectral range ν_F and the spectral width $\delta\nu$ together with the cavity finesse $\mathcal{F}$ are all shown in the figure.

$$\nu_F = \frac{c_0}{2nd}. \tag{3.6}$$

Cavity finesses

$$\mathcal{F} = \pi \frac{\sqrt{r_1 r_2 e^{-2d\alpha_0}}}{1 - r_1 r_2 e^{-2d\alpha_0}}. \tag{3.7}$$

The cavity spectral width of individual modes

$$\delta\nu = \frac{\nu_F}{\mathcal{F}}. \tag{3.8}$$

The cavity quality factor $Q = \frac{\nu_0 \mathcal{F}}{\nu_F}$ where ν_0 is the cavity resonance frequency.

3.2 Light−matter interaction

In this section, the equations governing the coherent interaction of light and atoms will be presented. We start with the description of light as an electromagnetic wave using Maxwells equations. This is followed by the optical Bloch (Maxwell-Bloch) equations and the interaction of specific pulse type with atoms.

3.2.1 Maxwell's equations

The 4 Maxwell's equations are the four basis equation used in the description of light field as an electromagnetic wave. The equations are [27, 34, 42]:

$$\begin{cases} \vec{\nabla} \times \vec{E} &= -\frac{\partial \vec{B}}{\partial t}, \\ \vec{\nabla} \times \vec{H} &= \vec{J} + \frac{\partial \vec{D}}{\partial t}, \\ \vec{\nabla} \cdot \vec{D} &= \rho, \\ \vec{\nabla} \cdot \vec{B} &= 0, \end{cases} \tag{3.9}$$

where $\vec{J}$ is the current density due to free charges, $\vec{D}$ is the electric displacement field, $\vec{E}$ the electric field, $\vec{H}$ the magnetic field, $\vec{B}$ the magnetic flux and ρ the charge density of free charges.

These equations are used to describe how a material with susceptibility χ and magnetization M, react in the present of an electric field and or magnetic field. In the present of an electric field and or magnetic field, the material displacement field and magnetic flux are modified as shown belown [27]:

$$\begin{cases} \vec{D} &= \epsilon_0 \vec{E} + \vec{P}, \\ \vec{B} &= \mu_0 \vec{H} + \mu_0 M, \end{cases} \tag{3.10}$$

where $\vec{P} = \epsilon_0 \chi \vec{E}$ is the induced polarization due to the present of the E-field in the material. This induced polarization will cause a small displacement of the positive (nucleus) and the negative (electrons) charge centers. The displacement results in the material having a dipole

moment, equal to the sum of the product of the charges and their respective displacement [55].

Assuming that our light field propagates in an isotropic homogeneous media, the four Maxwell's equations can be combined to give the electromagnetic wave equation, that is,

$$\left(\nabla^2 - \frac{1}{c_0^2}\frac{\partial^2}{\partial t^2}\right)\vec{E} = \mu_0 \frac{\partial^2}{\partial t^2}\vec{P}, \tag{3.11}$$

where $c_0 = \sqrt{\frac{1}{\mu_0 \epsilon_0}}$ called the vacuum velocity of light. The polarization (dipole moment) is the driving factor in this wave equation.

3.2.2 The Bloch equations

In the present of a light field atoms emit spectral lines. If the frequency of the light field is such that, it corresponse to the frequency difference between two energy levels in the atom, the atom emits a spectral line that corresponse specifically to this transition. Thus, the atom can be approximated as a two level atom, where only the two allowed energy levels, that is, $|g>$ and $|e>$ are present. This approximation is generally not valid but for simplicity, we assume it is so in our case. The Hamiltonian describing the interaction of a two level atom with a light field can be describe by the Schrödinger time-dependent equation [42]:

$$i\hbar\frac{\partial \Psi}{\partial t} = H\Psi. \tag{3.12}$$

The Hamiltonian, H has two parts, that is, $H = H_0 + H_1$, where H_0 is the atomic energy levels Hamiltonian or the Hamiltonian of the atom in the absence of the light field, H_1 is a small perturbation of the energy level due to the present of the light field. The dipole moment, μ, of the atoms in the present of the light field (E-field), determines the susceptibility of exciting different transition in the atom. The Rabi-frequency (angular) Ω, is used to describe the oscillation of the population in the two level atom at a given atomic transition and can be defined using the dipole moment of the transition as [55]:

$$\Omega(t) = \frac{\mu\varepsilon(t)}{\hbar}(rad/s). \tag{3.13}$$

$\varepsilon(t)$ is a complex E-field with the dipole moment, μ directed along it. The Rabi frequency is in general a complex quantity, which can be written as $\Omega = \Omega_{re} + i\Omega_{im}$. The optical Bloch equation (for detail derivation see reference [42]) can be written as [55]:

$$\begin{cases} \frac{\partial u}{\partial t} &= -\frac{1}{T_2}u - \Delta v + \Omega_{im} w \\ \frac{\partial v}{\partial t} &= \Delta u - \frac{1}{T_2}v + \Omega_{re} w \\ \frac{\partial u}{\partial t} &= -\Omega_{im} u - \Omega_{re} v - \frac{1}{T_1}(w - w_0), \end{cases} \tag{3.14}$$

where w measured the population difference between the excited state and ground state of the atom due to the presence of the light field with Rabi frequency Ω. When the atom is fully excited, that is, the is no atoms left in the ground state, $w = 1$, and when no atom is excited, all the atoms are in the ground state, $w = -1$. The phase and polarization of the state is describe by the vector $u + iv$. w_0 is the equilibrium state of the system, which in this case is the

ground state ($w_o = -1$). $\Delta(rad/s)$ is called the detuning, which is the difference in frequency between the targeted atomic transition (resonance frequency of the atom) and the light field. T_1 is the decay time of the excited state and T_2 is the coherence time of the excited state. Therefore, if the atom is initially in the excited state, the rate at which the population will decay to the ground state (equilibrium state) is $1/T_1$. Also, while in a superposition state, the phase of the light field can be kept for a duration T_2 before its de-phases. Further, discussion of T_1 and T_2 will be defered to chapter 5, where the memory material properties are discussed.

The pulse area [55]

$$\Theta = \int_0^t \Omega_{re}(\grave{t})d\grave{t}, \tag{3.15}$$

determines the net effect of the pulse on the state, over the duration, t at resonance. When $\Theta = \pi$, the pulse is called a π (pi) pulse, and the net effect of the pulse on a state is total population transfer (population inversion) from one state to the other [42]. When $\Theta = \pi/2$, the pulse is called a $\pi/2$ pulse, and it puts the population in a $50-50$ superposition state [42].

3.2.3 Maxwell−Bloch equation

To take into account, the modification of the light field by the radiation from the atoms, the Maxwells wave equation, equation (3.11), can be re-written in-terms of the Bloch vectors (u, v, w) as [55]:

$$\left(\frac{\partial}{\partial z} + \frac{n}{c}\frac{\partial}{\partial t}\right)\Omega = \frac{i\alpha_0}{2\pi}\int_{-\infty}^{+\infty} g(\Delta)(u - iv)d\Delta, \tag{3.16}$$

Where $g(\Delta)$ is the atomic distribution of the atoms as a function of the detuning and normalized such that it is equal to 1 at α_0. Equation (3.16) is called the Maxwell-Bloch equation in complex form. The Bloch equations, equation (3.14) together with the Maxwell-Bloch equation, equation (3.16) completely describes light-matter interaction and the propagation of the light field through the media. These are the starting point of any quantum memory protocol using atomic ensembles [16–18, 38, 39] .

3.2.4 Sample pulse types and their interaction with atoms

In this section, we consider briefly, 3 sample pulse types mostly used in the experimental investigation of the interaction of light and matter in this work. They are square pulse, Gaussian pulse and secant pulse.

(i) ***Square pulse***: The square pulse is a pulse with a constant amplitude over a given duration, τ, and zero otherwise. It is the simplest of the pulse types. The present of the sharp edges in the square pulse produces undesirable effects when its interact with the atoms. These sharp edges will give rise to high frequencies in the Fourier transform of the pulse. These high frequencies are responsible for the undesirable effects, when the pulse interacts with atoms. Therefore, the square pulse is not an efficient pulse type, when the pulse needs to interact with only atoms of a certain frequencies range. This pulse has a pulse area of $\Theta = \tau\Omega_{re}$ [34].

(ii) ***Gaussian pulse***: A Gaussian pulse is a far better pulse type than the square pulse. This is due to the fact that, the Fourier transform of a Gaussian pulse is another Gaussian. Thus, there are no unwanted frequencies appearing in the Fourier transform. The Gaussian pulse intensity profile is given by [55]:

$$I(t) = I_0 exp(-t^2/\sigma^2). \tag{3.17}$$

I_0 is the peak intensity, t is the time and $\sigma^2 = t^2_{FWHM}/(4ln2)$ and t_{FWHM} is the pulse length measured at the full width half maximum intensity. The Rabi frequency $\Omega(t) \propto E \propto \sqrt{I}$, thus $\Omega(t) = \Omega_0 exp(-t^2/2\sigma^2)$, which is still a Gaussian. The pulse area is then $\Theta = \Omega_0\sqrt{\pi/2ln2}t_{FWHM}$.

The Gaussian pulse can be used efficiently to interact with atoms of a certain frequency range. The wings of the Gaussian pulse does not drop directly to zero, thus still posing a problem, as they might be some energy stored in them. As such, atoms interacting with the pulse center might see a different Rabi frequency and those at the wings, a different Rabi frequency, thus different atoms might interacting differently with the pulse [55].

Also, if the atomic ensemble has an inhomogeneous broadened profile, during the interaction period, different atoms might acquire different phases (de-phasing) and this will be a problem, since the Gaussian pulse has no control over the de-phasing [55].

(iii) ***The sechyp pulse***: The complex hyperbolic secant pulse is defined as [55]

$$\Omega(t) = \Omega_0 \text{sech}[\beta(t-t_0)]e^{i\mu ln[\text{sech}(\beta(t-t_0))]}, \tag{3.18}$$

Where β is linked to the pulse width, μ is a real constant and Ω_0 the Rabi frequency at the pulse center. The pulse envelope is given by the real part of the equation (3.18), that is, $\Omega_{re}(t) = \Omega_0 \text{sech}[\beta(t-t_0)]$. The instantaneous angular frequency of the pulse is given by the time derivative of the pulse phase, that is, $\frac{d}{dt}(\mu ln[\text{sech}(\beta(t-t_0))]) = \mu\beta \tanh[\beta(t-t_0)]$. The parameters β and the dipole moment μ, can be link to the pulse length measured at the full width half maximum of the intensity and the frequency width as $t_{FWHM} = 1.76/\beta$ and $\nu_{width} = \mu\beta/\pi$.

The secant pulses have the same effect on atoms with different detuning in an inhomogeneous broaden media. The wings of the pulse drop sharply to zero; as such its energy is confine within a small frequency range. It is a very efficient pulse to use, when you need to interact with atoms inside a certain frequency range, while those outside that frequency range should be left un-affected. In an inhomogeneously broaden media, they can transfer an ensemble of atoms between two states efficiently, thus this is the pulse that will be used in the experimental part of this project.

3.3 The dynamical equation of cavity quantum memories

High efficiency quantum memories relies heavily on the input quantum state to be completely absorbed by the memory material. Below, we present the basic dynamical equations governing the complete absorption of the input quantum state due to the help of an impedance matched

cavity. The memory material is an inhomogeneously broaden atomic ensemble placed within a one-side cavity. The evolution of the cavity modes (E-field), the atomic polarization at a detuning δ and the output field mode are [24, 56]

$$\begin{cases} \dot{\epsilon} & = & -\kappa\epsilon + \sqrt{2\kappa}\epsilon_{in} + i\tilde{\wp}\int d\delta n(\delta)\sigma_\delta \\ \dot{\sigma}_\delta & = & -i\delta\sigma_\delta - \gamma_h\sigma_\delta + i\mathcal{P}\epsilon \\ \epsilon_{out} & = & -\epsilon_{in} + \sqrt{2\kappa}\epsilon, \end{cases} \tag{3.19}$$

Where 2κ is the cavity decay rate or the rate at which the cavity losses its stored energy, $\tilde{\wp} = g_0^2\mathcal{P}$, with $g_0 = \sqrt{\omega_0/(2V\epsilon_0)}$ is the photon-atom coupling constant, $\mathcal{P}$ is the dipole moment of the optical transition, ω_0 is the photon frequency, V is the quantization volume, δ the detuning, $n(\delta)$ the inhomogeneous broadened atomic spectral distribution with $\int d\delta n(\delta) = N$, N the total number of atoms, σ_δ the atomic polarization at the detuning δ, γ_h the homogeneous line-width of the atoms. We make the assumption that the initial cavity atomic distribution has no atomic polarization, that is, all the atoms are initially in the ground state, $\sigma_\delta = 0$.

Since the atomic ensemble inhomogeneous broadening line width (γ_i) is larger than the homogeneous line width, the atomic distribution can be approximated as a delta function. Under steady state conditions, that is, adiabatically reducing $\dot{\epsilon}$ to zero, the output field becomes

$$\epsilon_{out} = \frac{\kappa - \Gamma}{\kappa + \Gamma}\epsilon_{in}, \tag{3.20}$$

where $\Gamma = \frac{N\tilde{\wp}\mathcal{P}}{\gamma_i}$ is the rate at which the atomic ensemble is absorbing the input cavity field.

When the cavity is impedance matched, as describe above (section 3.1.3), the reflected output field intensity is zero. Thus this occurs when $\kappa = \Gamma$ in equation (3.20). When this occurs, the input field is totally absorbed within the cavity, no other losses present in the cavity.

3.3.1 Application using AFC protocol

Above, we showed that, it is possible to completely absorb the input signal field with the help of a cavity. For the purpose of a quantum memory, it is also important that, the absorbed input field be read out efficiently.

We thus assumed that the complete absorption of the input field took place over the AFC peaks (see section 2.5.1). In the presence of the absorption peaks, the output field becomes [24]

$$\epsilon_{out}(t) = -\sqrt{\eta_F}\epsilon_{in}(t - \frac{2\pi}{\Delta}), \tag{3.21}$$

where $\eta_F = e^{-7/F_A^2}$ for the Gaussian peaks. The AFC finesse is now the only limiting factor and the $t - 2\pi/\Delta$ argument is to take care of the fact that at $t = 2\pi/\Delta$ there is no input

field.

The efficiency of the cavity assisted quantum memory is [24]:

$$\eta = \left[\frac{2\tilde{d}e^{-\tilde{d}}T_1\sqrt{R_2}\sqrt{\eta_F}}{(1-\sqrt{R_1R_2}e^{-\tilde{d}})^2}\right]^2 . \tag{3.22}$$

For this readout to work, the AFC bandwidth must be smaller than the cavity resonance spectral width $\delta\nu$ and also, the absorption probability must be higher than any other losses in the cavity.

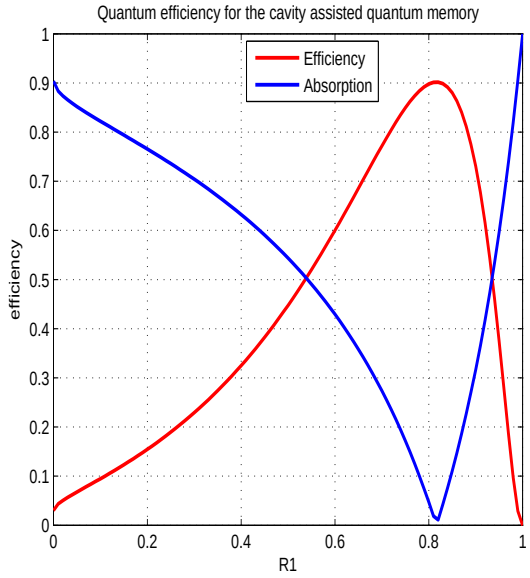

Figure 3.2: The AFC cavity assisted quantum memory efficiency and the absorption within the cavity as a function of the input mirror reflectivity $R1$ using equations (3.22) and (3.4). The finesse of the AFC structure is assume to be 10 and the optical depth 1 given an effective optical depth of 0.1 [24].

Using the cavity design in section 4.5, with $R_2 = 0.997$, figure (3.2) shows the variation of the memory efficiency with respect to the input mirror reflectivity R_1. The absorption (equation (3.4)) of the input field is also included, showing the enhancement of the memory efficiency by the cavity. At $R_1 = 0.8$, the memory efficiency is 0.9 while the absorption is almost zero. Since $R_2 \neq 1$, the pulse will never be completely absorbed as shown in figure (3.2).

3.3.2 Simulation of the Bloch equation in a simple cavity

In a travelling wave cavity, at steady state, the cavity has standing waves within it. Due to the standing wave pattern, there will be a position dependent intensity built-up within the cavity. If there are atoms within the cavity, different atoms at different position within the cavity, will see different field intensity (Rabi frequency). Atoms at the nodes will see little or no intensity at all, while atoms at the anti-nodes will see very high intensity (Rabi frequency).

For simplicity, we assume that the cavity has a length equal to $\lambda_m/2$, that is just one standing mode within the cavity. Due to the standing wave, the circulating electric field now have spatial dependent, which is

$$E_{circ} = \frac{j2t_1 \sin((2\pi/\lambda_m)x)E_{inc}}{1 - r_1 r_2 exp(-2d\alpha_0)}. \tag{3.23}$$

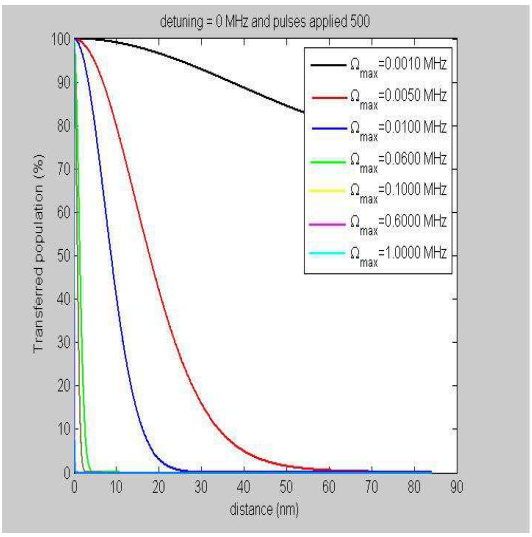

(a)

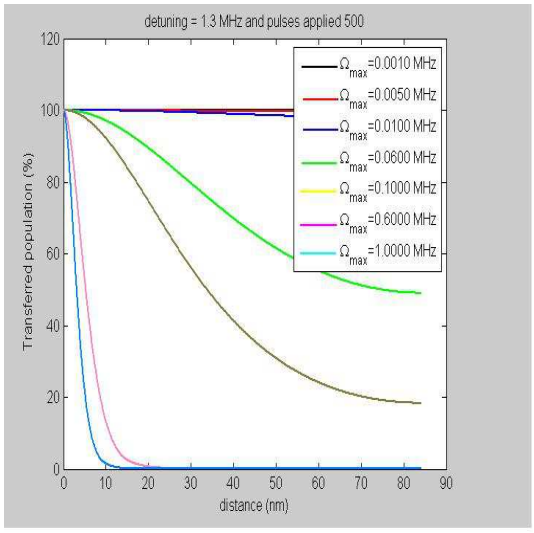

(b)

Figure 3.3: Simulation of the Bloch's equation, equation (3.14) in the presence of a standing wave pattern, equation (3.23) within a cavity. The pulses are applied repeatedly, 500 times. The E-field now have a spatial dependent and as such, at different positions within the cavity, the Rabi frequency will be differents using equation (3.13). (a) The case in which the light field frequency and the atomic transition frequency are equal, that is zero detuning. Even for a light field with very low Rabi frequency, 5kHz, after 500 application, all the atoms are completely transfer from one state to the other. The pulse type is a sechyp pulse, optimized for efficeincy popultion transfer. (b) Same as a but with a detuning of 1.3 MHz between the light field frequency and the atomic transition frequency. This shows that, in the present of a standing wave, the pit created with the sechyp pulses will not have straight edges as we would want them to be. If a light field of Rabi frequency of 5 kHz is used, we can get a pit with fairly staright edges.

Figure (3.3) show that, in the presence of a standing wave patter, the shape of the spectral pit will not be a staright one, except the input light field into the cavity has a very small Rabi frequency, say below 5kHz. For all input Rabi frequency higher than this value, the pit will have wings, which will stretched depending on the number of times the pulse is applied. Due to this standing wave pattern within the cavity, they will be nodes with zero Rabi frequency and all atoms present at those nodes will not be affected by the light field. Therefore, it is possible to create an absorption grating where the only absorber present will be atoms at the nodes.

3.4 Summary

- An impedance matched optical cavity has zero or close to zero reflected intensity from the cavity.

- The Maxwell-Bloch equations completely describe the interaction of light with atoms.
- The sechyp pulse is a very efficient pulse for interaction of light with atoms over a certain frequency range.
- With the aid of an impedance matched resonance optical cavity, an input quantum state can be completely absorbed. With no other losses present in the cavity, a quantum memory with efficiency as high as 90% can be achieved.
- Due to the standing wave within a cavity, different atoms at different position within the cavity will interact differently with the input light field. This can be used to create an absorption grating.

Chapter 4

Raytracing of cavity assisted optical quantum memory using FRED

The optical engineering software FRED, is a ray tracing software, used to simulate how light (treated as rays), propagate through systems or materials. Design of optical systems can be done in FRED or imported from some other design software like CAD. Thus FRED can be used virtually for prototyping optical systems before it is design [57].

The application of FRED is vast due to [57]:

(i) The ease with which optical properties of various systems can be assigned and thus it is not limited to a certain problem class.

(ii) It can propagate both coherent and incoherent light sources through optical elements, thus making it applicable to diverse fields of studies.

Here we intend to design a cavity made up of an absorbing crystal (Pr^{3+}:Y_2SiO_5), with both cavity mirrors directly coated on to the crystal. The crystal is to function both as a resonance matched optical cavity as well as a storage medium for quantum states. The cavity will be used at liquid helium temperatures ($\approx 2.2K$), as such, to ensure that the absorption profile of the crystal matches at all time one of the cavity modes, one of the surfaces of the cavity or crystal is tilted, that is a wedge cavity. The mirrors reflectance, the wedge angle, the absorption in the cavity and the wedge length are different parameters to be optimized, and to do that, the ray tracing software FRED is used.

In this chapter, an overview of the cavity design in FRED is given. The light source, the cavity and detection system is presented. Simulation and results obtain in FRED and how its talks to Microsoft excel program will be presented also. The last part of the chapter present the optimized optical cavity together with its properties.

4.1 The setup in FRED

The setup in FRED is as shown in figure (4.1). Its consist of a coherent optical source generating a laser beam, a wedge optical cavity with absorptive material inside the cavity and two detectors, which measures the reflection and transmission beam intensity from the cavity. The design in FRED of the various components will be described in the next section.

In the lower left corner of figure (4.1), is the in-build coordinate system in FRED, the three colors green, red and blue represents the Y-axis, the X-axis and the Z-axis respectively. Below the virtualization window is the output window, which is used for outputting the ray tracing summary and any desired output.

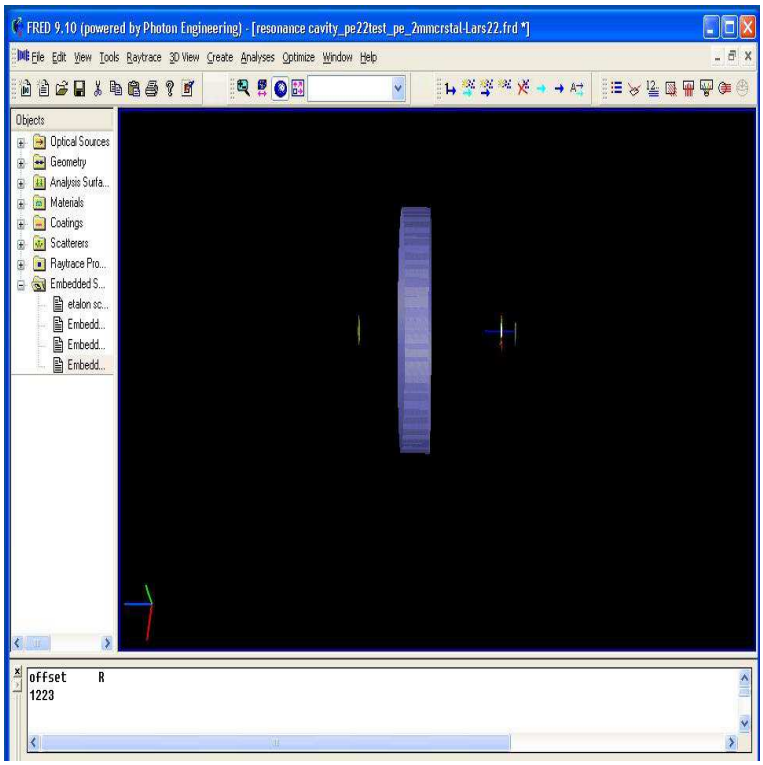

Figure 4.1: The setup in FRED

4.2 Components design in FRED

Designing of optical components in FRED has been made really easy with the help of a visualization output window, which outputs the designed optical system in real time as well as changes made to it. Optical components can either be designed here in FRED or imported from other software programs. Importation of designed optical systems from other design software is done using the import command, found under the file dropdown menu. FRED can also export its design to other design software, and this can be done using the export command found under the file dropdown menu. In this project, all the optical components used will be design in FRED and none will be imported or exported to other software directly. Below we describe the design of the three main components we will be using, that is, the optical source, the cavity and the detectors. Designs of optical components in FRED are done with the help of the menu in the left of figure (4.1).

4.2.1 Optical source

Design of the light source in FRED is done with the help of the optical source tab. To do that, we right click on optical source and select "create simplified optical source". A new popup window will open in the virtualization window, see figure (4.2) a. In it, we have the

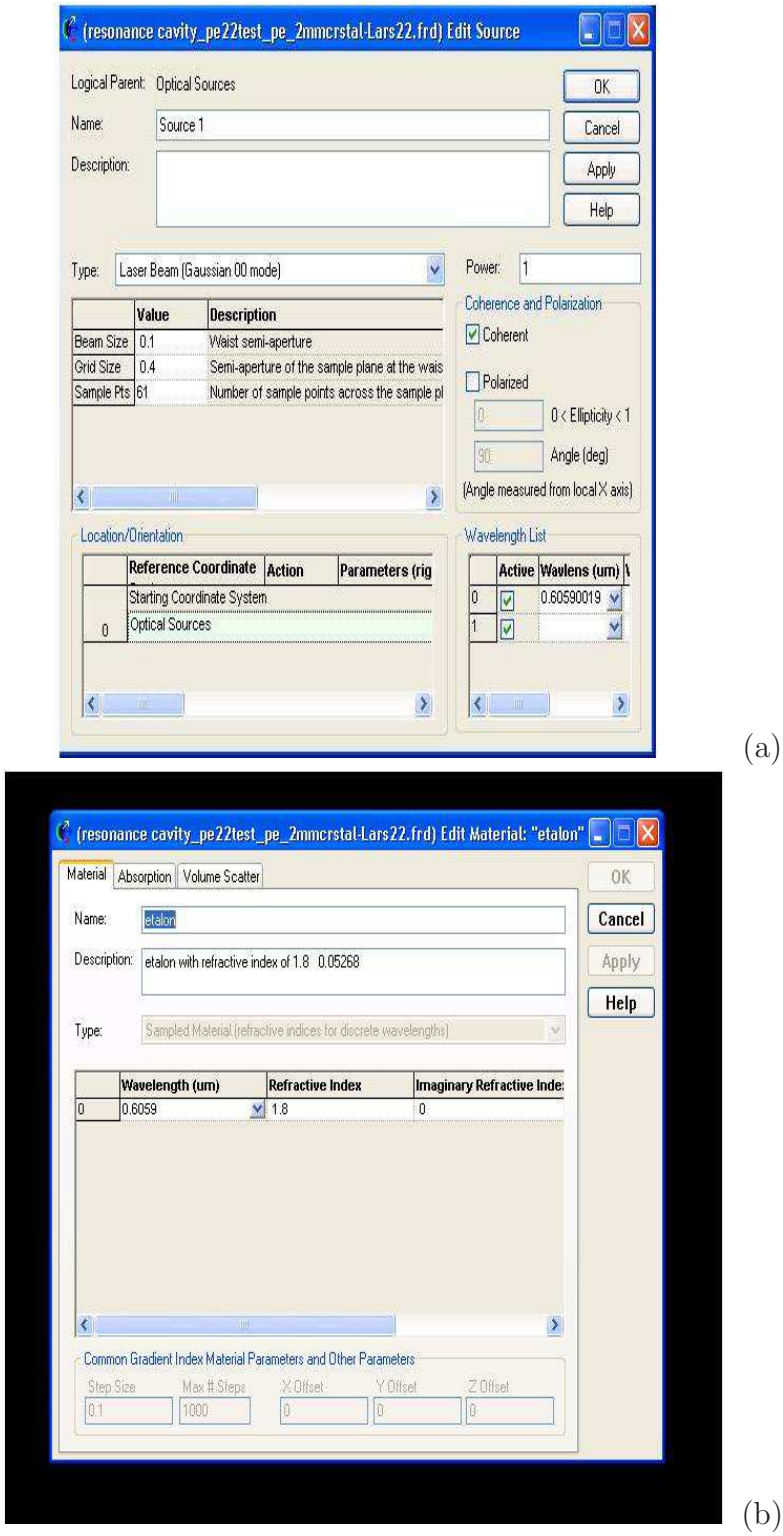

(a)

(b)

Figure 4.2: Optical designs in FRED. (a) Optical source design popup window. (b) Material design in FRED popup window.

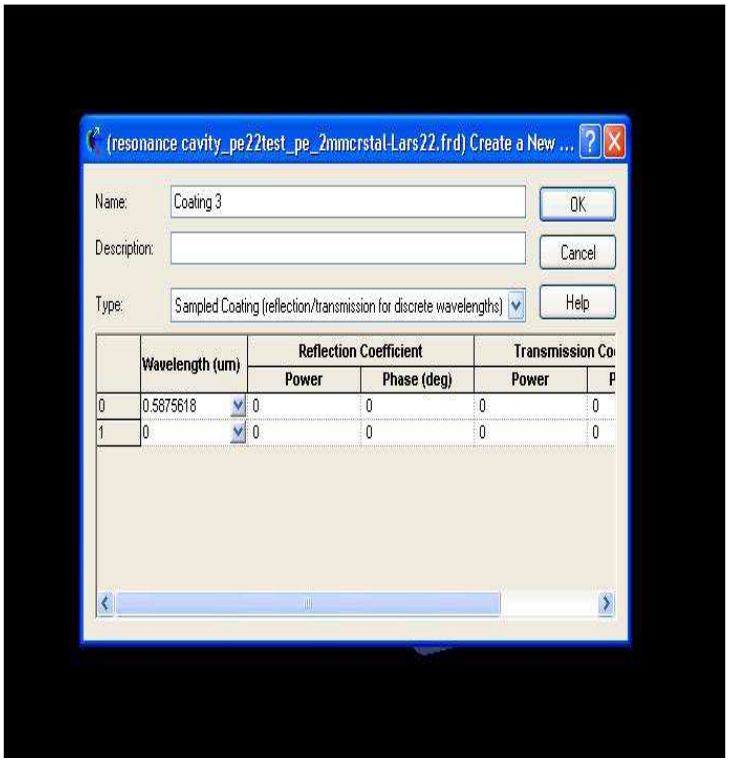

(a)

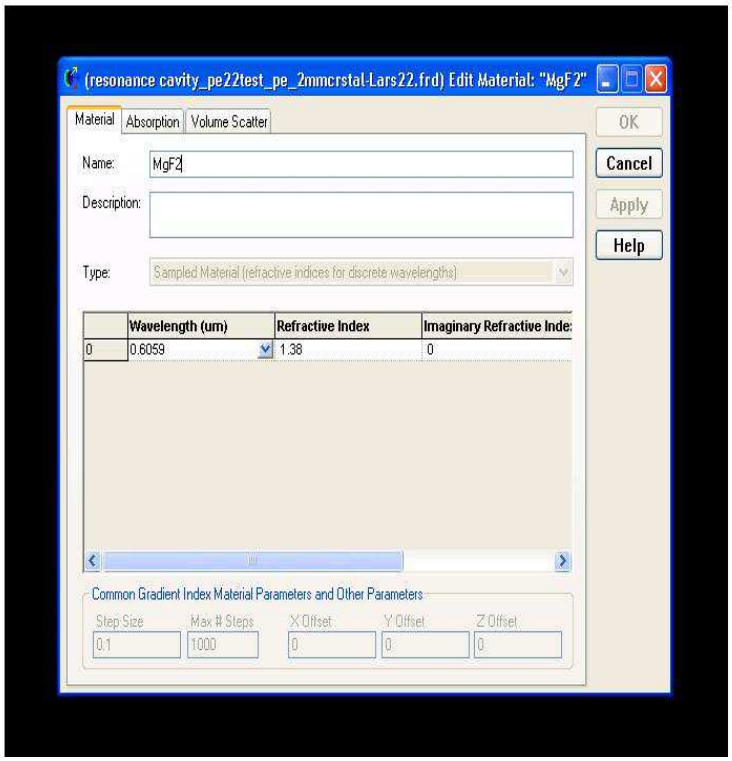

(b)

Figure 4.3: Optical designs in FRED. (a) Sample coating design, this coating can not handle phase changes due to reflection. It is too idealize for use in any coherent process, where phase changes due to reflections are important. (b) Design of materials for use in thin film coatings. Thin film coatings can handle phase changes due to reflection and therefore are good for usage in coherent processes where phase changes are important.

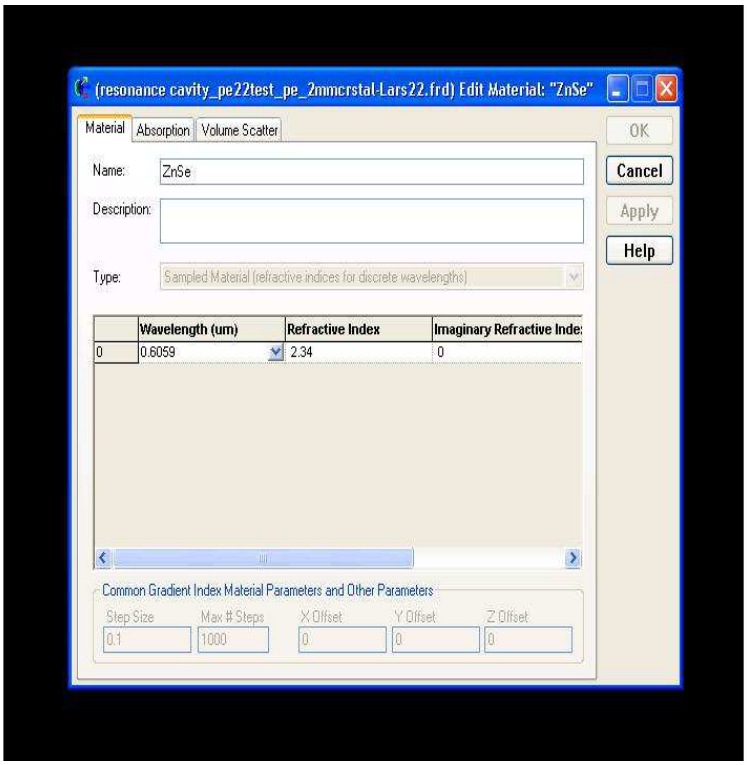

(a)

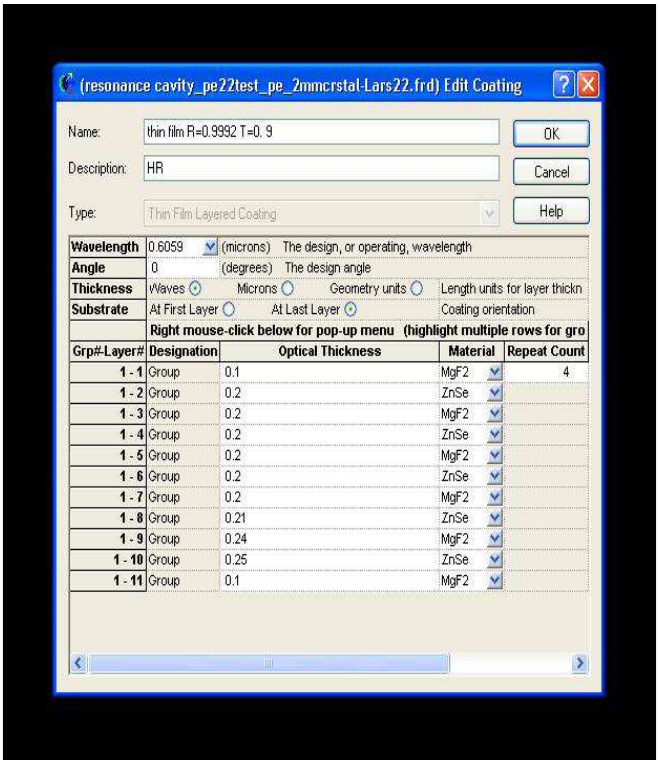

(b)

Figure 4.4: Optical designs in FRED. (a) Popup window for the design of a thin film material. A thin film material is a material used for thin film coating. Thin films are layers of materials with thickness ranges from nanometers (mono-layer) to several micrometers, used for coating to form reflective interface in a substrate. (b) Coating design 2, using thin films. Sample popup window when creating a coating using thin films.

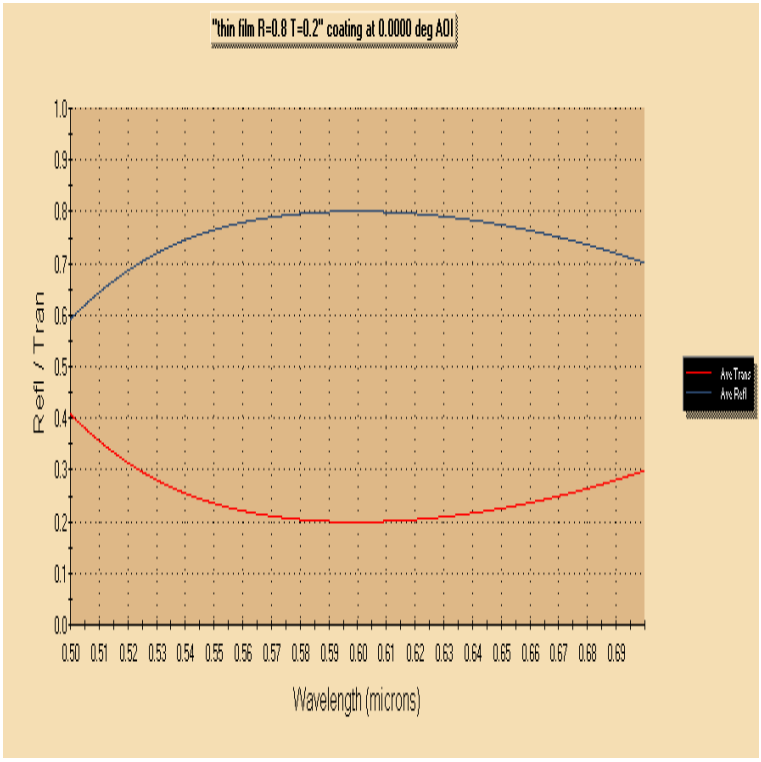

(a)

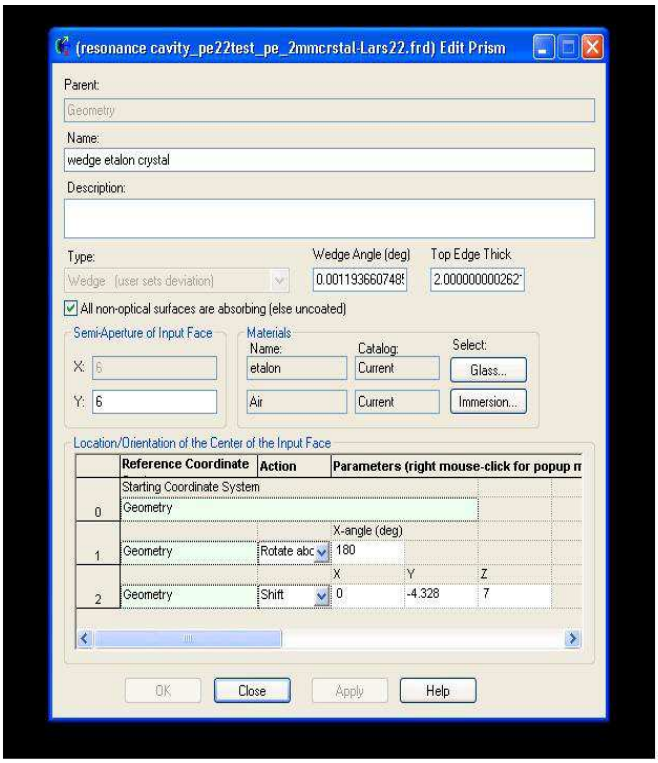

(b)

Figure 4.5: Optical designs in FRED. (a) A plot of the reflection and transmission coefficients of a thin film coating. (b) Design of a wedge cavity using a wedge prism.

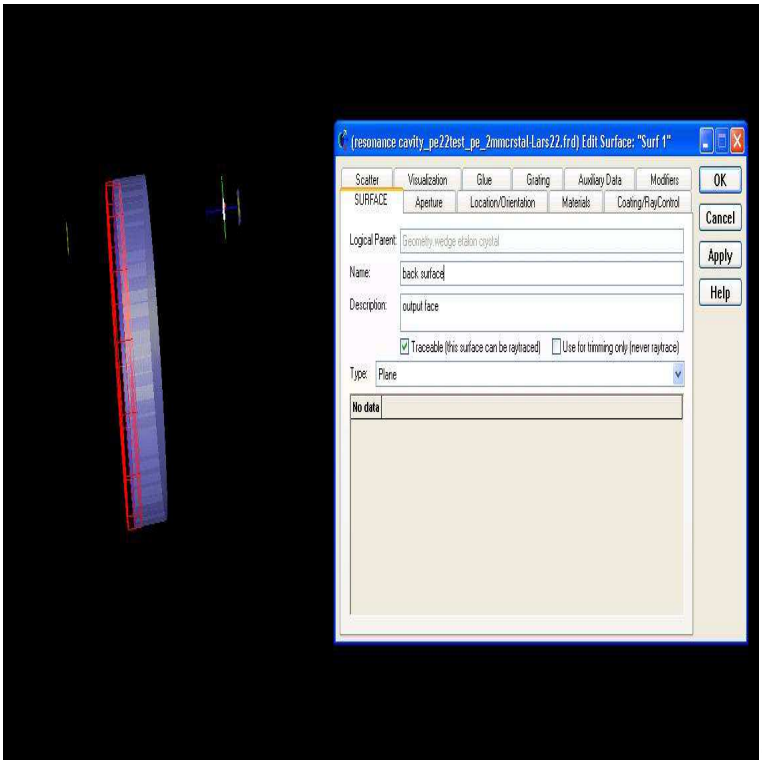

(a)

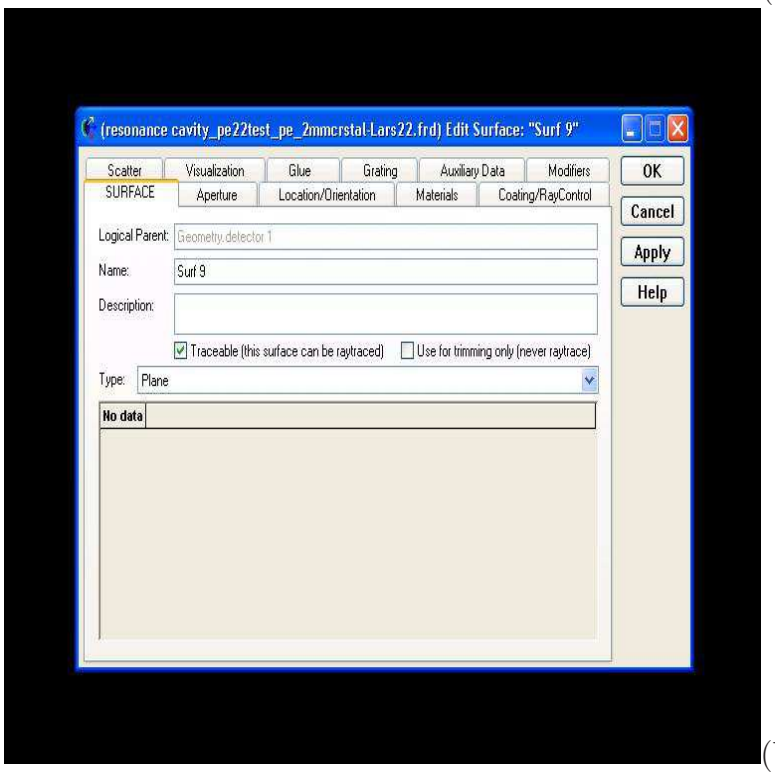

(b)

Figure 4.6: Optical designs in FRED. (a) Adding coating to the cavity. (b) A popup window used for the design of a detector.

option of naming our source, defining the source type as well as its properties. Also, we can do the following for our source:

(i) Define the power of the source,

(ii) Make it coherent or not,

(iii) Make it polarized or not and decide the polarization type,

(iv) Define the source wavelength (or wavelengths, if the source is not a coherent source),

(v) We can also define the source location/orientation.

The first 4 things can be done directly but the fifth that is, defining the source location/orientation, needs some extra steps. In order to change the source location/orientation, first we locate the location/orientation tab and right click on the optical source in it and select "Append". A new column will be added below the optical source column, and there we have the freedom of changing the source location as well as its orientation with respect to whatever axis we choose to carry the action with. In figure (4.2) a, our optical source is a coherent laser beam with beam waist of $100\mu m$ and wavelength of 605.9 nm, position at the origin of the coordinate system. The sample points are useful during the simulation and determine how fast FRED does the simulation. At the end of the design process, we click ok or apply to save the design or changes made to it. To see/edit the source, at a later time, we click on the plus sign close to the optical source and the source we want to edit will appear below it, for editing, we double click on it and the popup window, see figure (4.2) a, open.

4.2.2 The cavity

The cavity is made of three parts, that is, the cavity material (the crystal), the cavity coating (mirrors) and the wedge cavity structure.

(i) ***The cavity material***: FRED has in-built material types but it also has possibility for users define materials. In this project, we will use a user define material and below I describe how to define a material in FRED.

To design a new material in FRED, we right click on "material", a popup window opens, see figure (4.2) b, there we name the material, the refractive index (real and imaginary) and the wavelength which has that refractive index, the material absorption (if the material has any absorption and the imaginary refractive index has not been specified, see equation (**??**)), as well as any scattering present in the material. The complex refractive index can be written as [27]

$$\tilde{n} = n - i\alpha = \sqrt{1+\chi} \tag{4.1}$$

where n is the real refractive index of the material, $\alpha = \frac{1}{2}\frac{\alpha_0}{k_0}$ the absorption coefficient of the material and χ the electric susceptibility, which is in general complex. Figure (4.2) b, is our material design for a real refractive index of 1.8 at a wavelength of 605.9 nm, with an absorption of $0.05mm^{-}1$ (the absorption is not shown in figure (4.2 b)). We click on ok or apply at the end of the design and to see or edit the material, we click on the plus sign close to the material tab. Our design material is called etalon, with properties as shown in figure (4.2) b.

(ii) ***The coatings or mirrors***: FRED also has a set of in-built coating but users define coatings can be made, just like for the materials, will be using a user define coating for the project. To design a coating in FRED, we right click on coating and select "create a new coating". A popup window opens, see figure (4.3) a, were we can name our coating, define the transmission as well as reflection coefficients. We click on ok or apply to save the new coating and it can be view later or edited later by clicking on the plus sign close to coating.

The design above has one major flaw for our purpose ; it is too idealized and does not represent any physical coating. Its takes care of the input field amplitude but not the phase, for a coherent input field has both amplitude and a phase and both must be accounted for by the coating. When an input field (E-field) is reflected from a mirror, its acquired a phase shift of π or when it travels from a less dense media to a more dense media, some part of it is reflected and acquires a phase shift of π, while the other part goes through without any phase shift. Our coating as defined above, will not impart this phase shifts to the reflected beam and as such, cannot be used for our simulation.

To correct this defect in our coating, we define two new materials and call them thin films, see figure (4.3) b and figure (4.4) a, resembling materials used in real coating. This two materials are define exactly as explain above but they have no absorption nor scattering in them. The new coatings now use these thin film materials, and place them in a layered structure. The coating is designed exactly as explained above but the coating type is change to thin film layered coating under the type tab. Here, the wavelength, angle, thickness as well as the substrate to which the coating will be attached to, can be specified. Note that, it is important to specify the right substrate material, since this effects the properties of the coating. Stacking the thin films in layers, creates certain reflection/transmission coefficients, see figure (4.4) b. We click on ok to save the coating. The reflection or the transmission coefficients of the coatings cannot be read off directly. To see the reflection and or transmission coefficients, we click on the plus sign and right click on the coating. We select plot on the dropdown menu and a popup window opens, in it we select the input material (from which the input field will come from, in this case air), the substrate (etalon in this case), the wavelength range we wish to plot (605.9 nm should be within the range), the number of steps and what we wish to see. Figure (4.5) a is an example plot of one of the coating we used in the simulation, its has reflection coefficient of 0.8 (80%) and a transmission coefficient of 0.2 (20%). The second coating has a higher reflectivity of 0.997.

(iii) ***The wedge cavity structure***: With the cavity material and cavity coating both designed and ready to be used, we are now ready to start designing the cavity itself. FRED has in-built geometrical structures but a user defined structures can also be built. Here we will use an built-in geometrical structure, due to the ease of its design and close resemblance to our cavity.

We intend to build a cavity with one of its surfaces slightly tilted (a wedged cavity, with the wedge of the order of 250 nm). Figure (4.7) shown the wedged cavity, with the dimensions exaggerated to show clearly the cavity wedge length, the cavity wedge angle and the cavity base length. The wedge prism is an in-built structure that closely

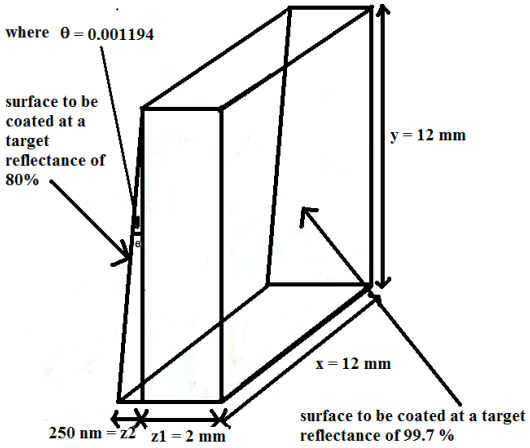

Figure 4.7: The wedged cavity with an exaggerated wedge length. The cavity wedge length (250 nm) is measured from the cavity base length (2mm). Both the cavity wedge length and the cavity base length have been exaggerated for clarity purpose only.

resembles the wedge cavity, and as such, we will use it for our geometrical design. To do so, we right click on geometry and select "create new prism", a popup window open. We give a name to the design, etalon, under the type tab, we select "wedge (user sets deviation)", we give the wedge angle, the top thickness of the etalon, the size of the etalon, the material of the etalon (we also called etalon), and the location/orientation of the etalon, see figure (4.5) b. We click on ok to save the design and notice that we called it etalon crystal not a cavity because its doesnt have the mirrors yet. To apply the coating and make it a full cavity, we click on the plus sign close to geometry and click on the plus sign close to etalon crystal. A list of the etalon surfaces will be shown below it, and we wish to apply the coating to the front (surface facing the source) and back surfaces of the etalon. We want to make the front surface 80% reflective and the back surface 99.7% reflective, as such we need to apply the right coating to them from the coatings we designed above. Doubling clicking on a surface, opens a popup window and the corresponding surface will be highlighted in the virtualization window (see figure (4.6) a). This makes it easier to edit the structure and avoid making erroneous changes to it. The popup window has several tabs and in this case, we are interested in just two of them, which are "Materials" and "Coating/Raycontrol" tabs. We first select the material tab and make sure that the material etalon is assigned to material 2 (our desired material) and we click apply. Next we select the coating/Raycontrol tab, select the desired coating and click on "assign", to assign it to the surface, next, we select "allow all" in the Raytrace control and assign it. Colors can also be assigned to the reflected as well as the transmitted rays from a surface. We click on ok, to save the changes made to the surface and open the next surface, until all the surfaces function exactly as we needed them to. Now we have design the cavity and the light source and what is left is the detectors.

4.2.3 Detectors

To design the detector, first we need to design an analysis surface over which the measurement will be done. To design an analysis surface, we right click on Analysis Surface and select "new analysis surface". We name the surface and click on ok. The new analysis surface will appear below the analysis surface tab and needs to be placed on the detector. To design the detector, we right click on the Geometry tab and select "create new custom element". We give a name to the element and click on ok. In order to attach or place the analysis surface on the detector, we need to define a surface on the detector, on which the analysis surface will be placed. To define the detector surface, we click on the plus sign close to the geometry tab then right click on the custom element (the detector) and select "create a new surface". A popup window appears (see figure (4.6) b), on which, we can name the surface and its location /orientation. After saving the surface, we can attach the analysis surface to it, using the drag and drop method. To do that, we click on the Analysis surface tab and select the analysis surface that we need to attach. Holding the left mouse bottom down, we drag the surface to the detector surface we want to attach it to and let go. At this point, the detector is complete and ready for use. The other detector can be design in the same way.

Now we have designed all the optical components needed for the simulation and are ready for the simulation.

4.3 Simulation in FRED

The main idea here is that for an impedance matched cavity with high parallelism, the reflected power of the cavity is close to zero [26]. As such, when the cavity is impedance matched, the laser input power is either totally transmitted (no absorption in the cavity and no gain) or totally absorbed (if the back mirror has 100% reflectivity and the cavity material has some absorption). The latter is used in the simulations and any reflected and/or transmitted power is/are considered as losses of the cavity due to the non-parallelism of the cavity mirrors with one minus the losses given us the material absorption in the cavity.

To impedance match the cavity, we use equation (3.5). The aim of the FRED simulation is to see the effect on the cavity when the parallelism between both mirrors are not too good and how to optimize it. The cavity will be placed in liquid helium and this will cause shrinking of the cavity length as such the cavity must not be made with high parallelism. At liquid helium temperature, the Pr^{3+}:Y_2SiO_5 crystal has good optical properties useful for the quantum memory. The simulation results are mostly using the wedge cavity with a base length of 2 mm and wedge length of 250 nm, see figure (4.7). The 1mm base length crystal cavity was rejected base on the fact that the simulation showed less absorption in the cavity less than 20% at the cavity resonance. The 3mm base length on another hand, gave a larger beam walk off than we wanted and higher absorption than we required. Therefore the 2mm crystal was the better choice and the reflectivity of the mirrors chosen to be 0.8 and 0.997, giving a good round trip losses (absorption) in the cavity of about 0.2. Using equation (3.5), we calculated α_0 to be 0.05. Most of the simulation were done using this α_0, except that where we were changing the α_0 itself.

Two different simulations methods were used, that is direct simulation in FRED and simulation with the help of a script.

4.3.1 Direct simulation in FRED

Direct simulation in FRED can be done in several ways depending on the optical effect you are interested in. You can use the Trace and Render function found under the Raytrace tab, to see the light ray and how they propagate in any optical component of choice. In our case, this is not interesting as we are interested in the absorption (power or intensity) in the cavity, while the detectors measured the reflected and transmitted intensity.

To see the intensity spread on the detectors, we right click on the analysis tab and select either intensity spread function or the energy density. A popup window opens and we can choose which detector (Analysis surface) we want to do the measurement on. Figure (4.8) a, b and Figure (4.9) a, (normalized to 1) shows the input intensity, reflected intensity as well as the transmitted intensity at the point of resonance in the cavity. This is done at a wedge angle of 0.0012^0, base length of 2 mm and wedge length of 250 nm. This shows that, we have absorption in the cavity above 90% at the cavity resonance.

4.3.2 Simulation with the help of a script in FRED

In FRED just like in many other simulation program, you can write a simple script to automate the simulation process. The advantages of using scripts in FRED are numerous, but for our case, it gives us a wide option of controlling the parameters to be optimized. Below, I present a brief introduction into this vast field of studies and for further details see the help menu in FRED software and scripting help.

(i) ***Script setup***: Scripts in FRED have the same programming format like most programming languages. It is made up of 3 parts that is, the definition part, the simulation part and the output part.

- In the definition part, all the variables as well as optical components that will be change/used during the simulations are define. Names of variable and assigning them to optical components are done in this part also. For example, "Dim id As string" (see appendix A) says that the variable id hold values of type strings. Another example is "$ida\& = FindName(\text{"}Analysis3\text{"})$" which find the optical component with name Analysis 3 and assign it to ida. Any changes made to "ida" affects Analysis 3 directly and this is true for the other assignment statements as well. Files for temporary storage of data during a calculation are also defined in this part.
- Changes to optical components, calculations as well as looping are all done in the simulation part. For example "SetMaterialAbsorb idm,wv,testv" sets the material "idm" absorption to "testv" and the wavelength to "wv". The statement "$Fori = 0tonstep$. Next i" loops over all the statements within nstep times. Also, the type of calculation you want to do at the detector can also be determined. For example "$cnt\& = IrradianceToFileAs(ida, fname)$" tells the program to do an irradiance measurement at the detector with analysis surface 3, which was assign to "ida" above and save the result to file "fname". This is done for each cell in analysis surface 3 and sum over all the cells. The final result is assign to "ptot".
- The final result can either be output directly to the output window using the write statement, "Print chr(9) ptot". This tells the program to print the value in "ptot" to the output window using 9 characters. The values in "ptot" can also be send to

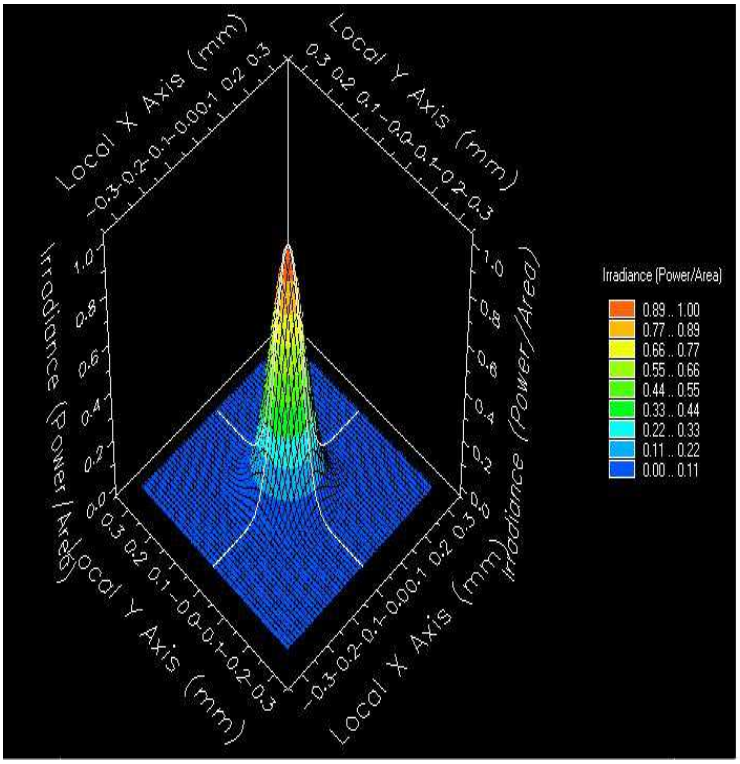

(a)

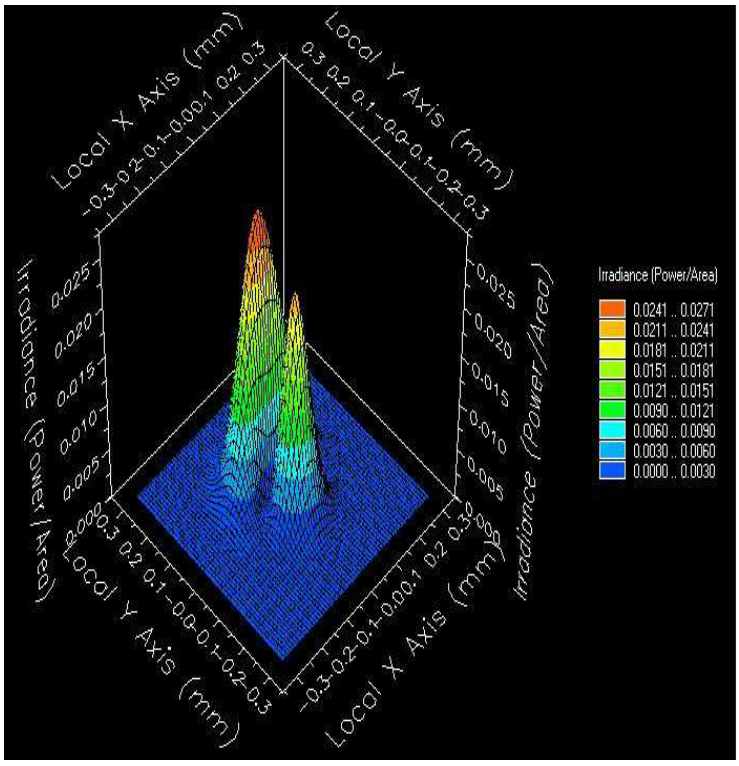

(b)

Figure 4.8: Irradiance plots normalized. (a) Input intensity of Gaussian beam, (b) Reflceted intensity from cavity.

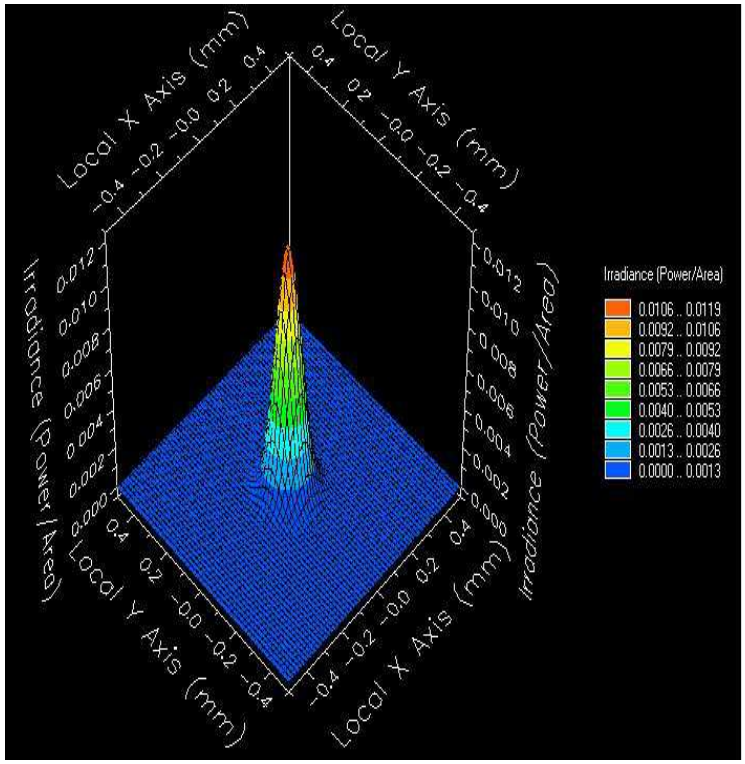

(a)

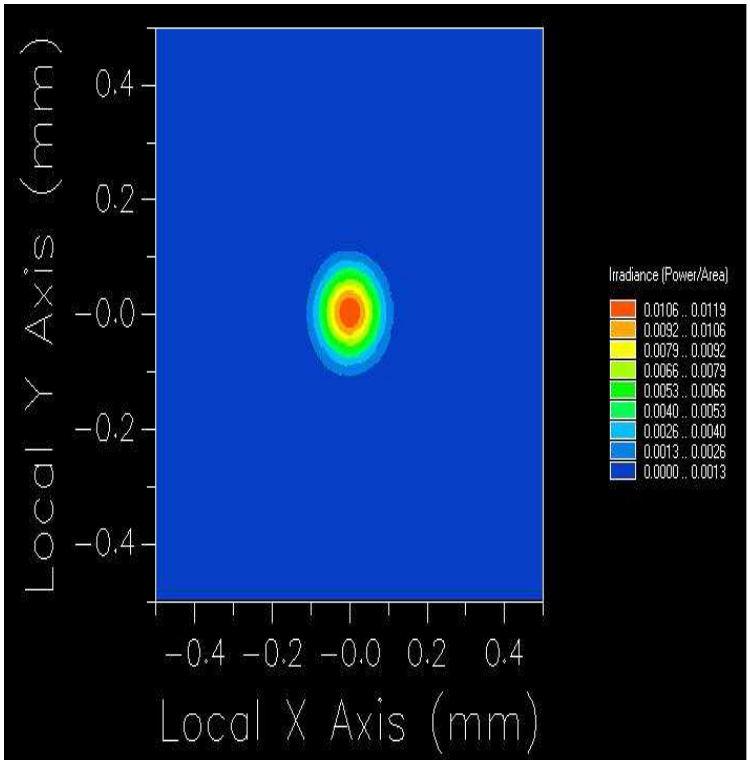

(b)

Figure 4.9: Irradiance plots normalized. (a) Transmitted intensity through cavity, (b) Interferences fringes.

other software (e.g. Microsoft Excel) for further calculation or for plotting of the data.

(ii) ***Editing the script***: For ease of understanding the script, comments can be included in it. If a statement is preceded by a quotation mark, it is a comment statement. For example " 'print results to output window" is a comment statement in FRED scripts saying that the next set or next statement prints the result to the output window. These statements are for ease of understanding the scripts as well as for ease of editing the scripts.

If we now wish to set the material absorption to a constant value, and move the cavity instead, all we need to do is comment the statements that changes the material absorption and change the absorption in the material tab to the desire value. After, commenting the statement, we can write a new statement that changes the cavity position, for example, "SetOperation idl, 2, op update". This statement sets the cavity (which is assign to "idl") to a new y position given by the value in "op". The "update" command, update the position of the cavity after the changes has been made.

The above are just few commands in FRED scripting. The scripts in FRED can be used to do nearly everything you wish to do in FRED. Below I present one more uses of FRED scripting, that is, using it to talk to other software, for example Microsoft excel software.

(iii) FRED can talk to other software, in particular we take the example of it talking to Microsoft Excel software for outputting data.

The output window in FRED can handle only a limited amount of data, after which its starts to delete old data. To over-come this, we make FRED constantly talk to Excel, outputting data to it as it runs. For FRED to do this, we need to tell it that it will be talking to this program and this is done in the definition part of the scripting. The statement "SetexcelApp = CreateObject("Excel Application")" and "excelApp.Visible=True" tells FRED that it will be talking to excel and that excel needs to be visible. The column in the excel document can be assign names for easy understanding of the data later. For example, "excelRange.Cells(RowCount,1).Value=xname" assign the name "xname" to column 1. FRED must be instructed to output the data to excel after each simulation, this is done using the statement "excelRange.cells($Rowcount + i$,2).value=ptot". The value in "ptot" is assign to column 2 and row "$Rowcount + i$". The "$Rowcount + i$" command ensure that, new output data are output to new rows in the same column not over-writing existing values.

(iv) ***Running FRED scripts***: The script is ready now to be used in the simulation and to do that, the script must first be saved. It is saved as a .frs file and imported into FRED as an embedded script. To import the script, we right click on embedded script and select "import a script file" and choose the script we wish to import. Once the script is imported, it can be run and to do this, we right click on the embedded script to be run and select "run an embedded script" in the drop down menu. This will start the simulation, (only after it has compiled correctly) and the output will be send to the desire output, in our case excel.

4.4 Results and discussion from FRED script simulations

Below, we present the optimization results from the simulation in FRED.

4.4.1 Cavity resonance peaks

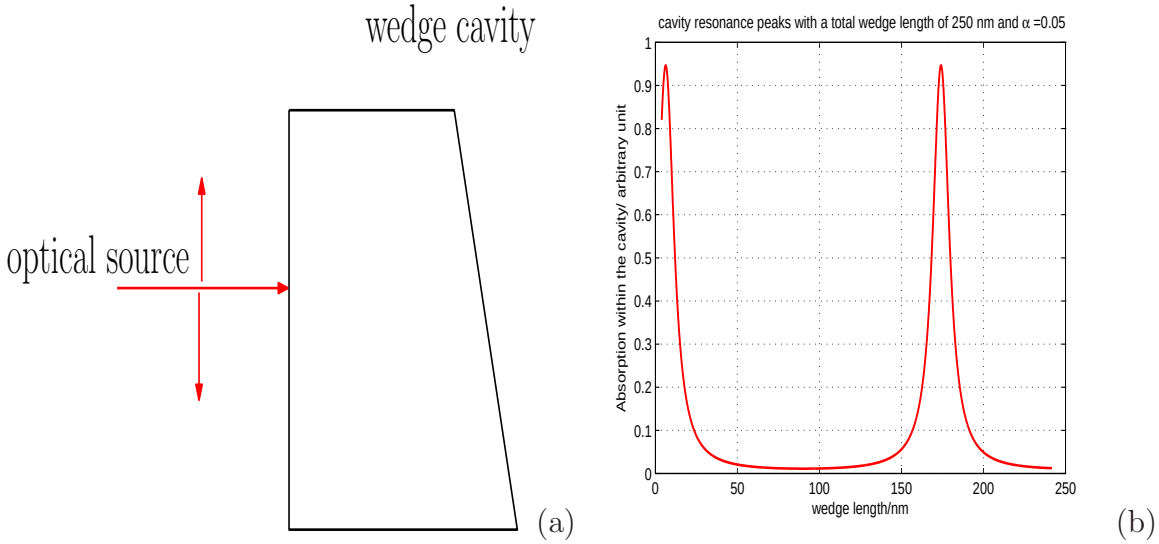

Figure 4.10: (a) Direction of movemnet of the optical source (b) Resonance peaks of the cavity with a wedge of 250 nm. The total thickness of the cavity is the base length 2mm (omitted in the plot above) plus the wedge length of the cavity. The scale on the x-axis is therefore, 2 (mm) + x (nm) and that in the y-axis is in percentage with 1 corresponding to 100%. One minus the total reflected and transmitted intensity from the cavity at different positions of the cavity gives us the absorption in the cavity.

The resonance of a cavity for a fixed resonance frequency ν_q and cavity mode, q, will occur at a fixed cavity length, $d = q\frac{c_0}{2n\nu_q}$. Therefore, changing the cavity length while keeping the wedge angle constant, we will get to a cavity length for which the cavity is on resonance. The cavity length can be changed by moving across the cavity diameter either along the x or y axes. This is acomplished in FRED by changing the position of the optical source while keeping the cavity position fixed. The cavity thickness or length is along the z axis, therefore, moving the optical source along the y-axis, from left to right (assuming that the left position has the less cavity thickness), we get figure (4.10). Figure (4.10) shows a plot of the total cavity absorption against the cavity length (which is shown in the plot by the wedge length). From figure (4.10), we can see that, if we have a flat cavity (by setting the wedge angle to 0) with a thickness of 2 mm, the cavity will not be resonant for this length with the wavelength 605.9 nm since there is no resonance peak at the wedge length of 0. Also, with a wedge of 250 nm, we see that we have at most 2 resonance peaks, separated a distance of 168 nm which correspond to the mode spacing ($\lambda_0/2n$) in the cavity. On cooling the crystal to cryogenic temperatures, the crystal shrinks and the resonance peaks shift to the right. The shrinking of the crystal causes both the base length and the wedge length of the cavity to shrink equally. The base length becomes less than 2mm, and as such the first resonance peak in figure (4.10) (at a wedge length of 0) will be completed and will not be at the edge of the cavity any longer.

The second peak is far from the right edge of the cavity, as such will move toward the right edge due to the shrinking of the wedge length, thus we will have the presence of atleast one peak at all time within the cavity. Also, the total absorption in the cavity at the resonance position are more than 90%, which is very good for our memory protocol.

4.4.2 Effect of the wedge angle

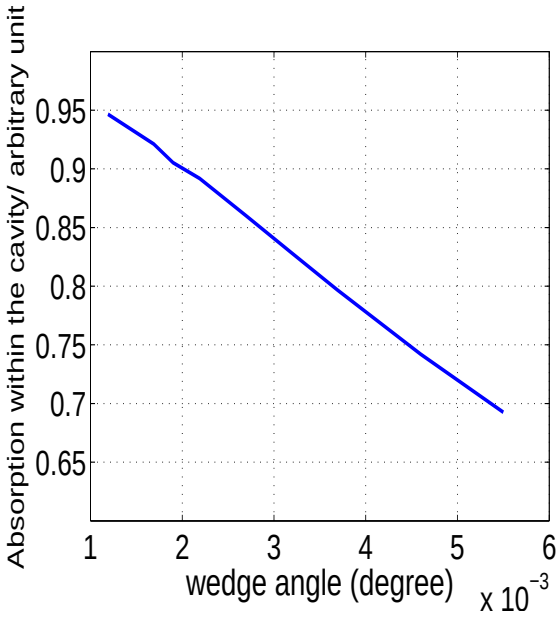

Figure 4.11: Effect of the wedge angle on the cavity absorption.

The wedge angle is very important, for it defines the level of parallelism we have in the cavity. In order to change it, we can either change the cavity diameter or the wedge length of the cavity. Changing the crystal cavity diameter is problematic as this might lead to increase manufacturing cost of the crystal as well as the cavity being too large to fit well in the cryostat. We are now left with just one choice to change the cavity wedge angle, the wedge length of the crystal. Since we need at least 2 resonance peaks in the cavity, this also puts a lower limit to the wedge length. In figure (4.11), we see that changing the wedge angle, reduces the absorption of the input pulse in the cavity. This can be seem as, increasing the wedge angle, we can no-longer neglect beam walking, which results in less absorption as the angle increases.

4.4.3 Changing the material absorption in the cavity

Equation (3.5) was used to calculate the starting absorption of the cavity material. To see how good that value was, we change the material absorption and calculate the corresponding absorption in the cavity. Figure (4.12 b), shows that the absorption in the cavity with an absorption of $\alpha_0 = 0.06$ is slightly higher than that at $\alpha_0 = 0.05$ but both are still below 10%.

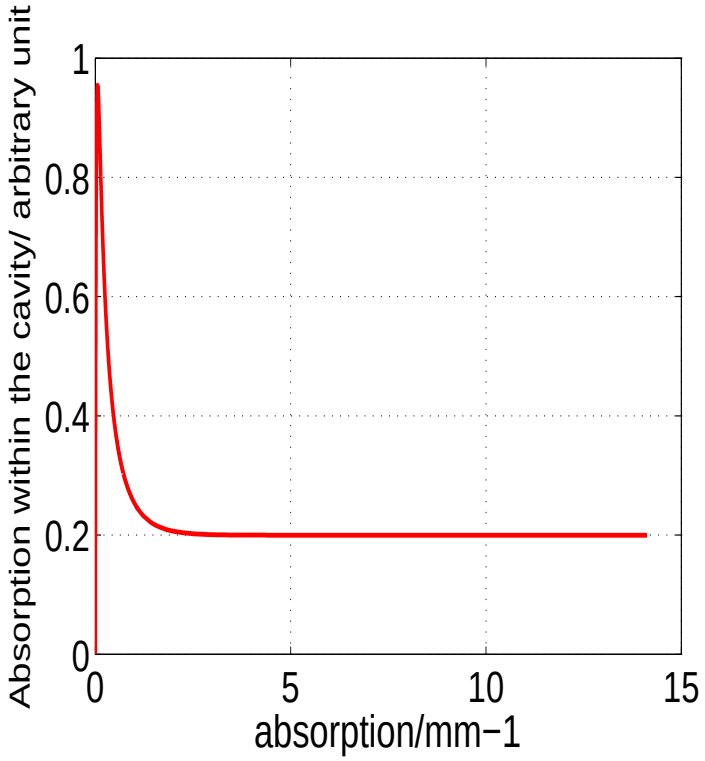

(a)

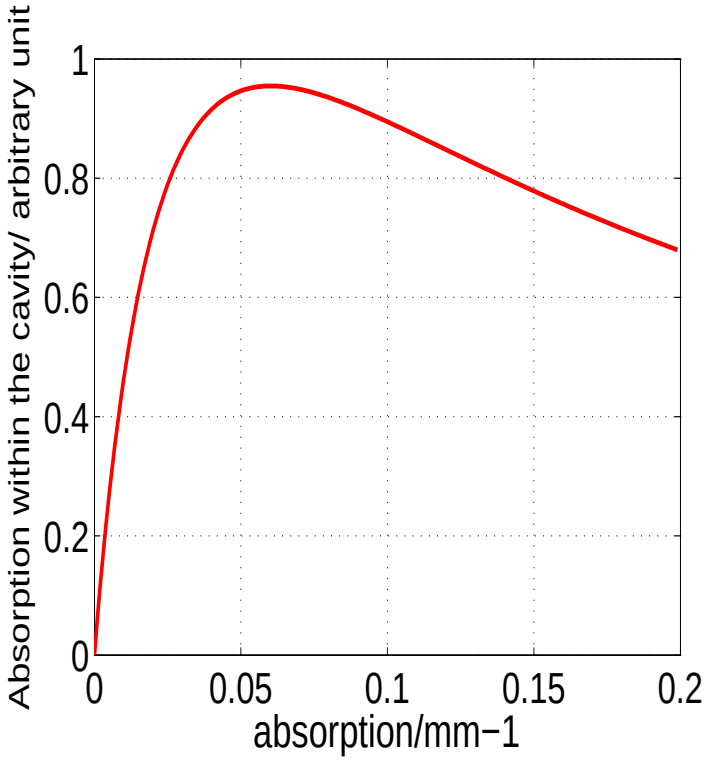

(b)

Figure 4.12: (a) Effect of the material absorption on the cavity absorption. (b) Enlarge view of material absorption changes from 0 to 0.2

4.5 Optimized cavity design base on geometrical consideration

Based on the results from section 4.4 and the cost of manufacturing, we settle for a crystal cavity with the following properties. The two mirrors have reflectivity of 80% and 99.7% and the round trip losses (absorption) of the cavity is 0.2. To achieve this round trip absorption, a Pr^{3+} doped crystal with a dopant concentration of 0.05% was used. The crystal base length of 2 mm, wedge length of 250 nm, crystal diameter of 12mm given a wedge angle of 0.00119^0.

Based on these (see figure (3.2)), the efficiency of the AFC cavity assisted memory was calculated to be 90% and together with the geometrical losses, we expect an efficiency of 80% or above. Using the parameters above, we calculated the cavity finesse to be 28, the spectral free range to be 41.7 GHz, the spectral width to be 1.5 GHz, the mode spacing in wavelength unit is 168 nm and the quality factor to be $3.29{\cdot}10^5$.

As stated above, the cavity material was made from praseodymium doped crystal (Pr^{3+}:Y_2SiO_5) with a praseodymium concentration of 0.05%. The crystal without the coating was manufacture by Scientific Material Corporation (Bozeman, Montana, USA). The crystal could not be manufacture to our specification (see figure (4.11)), as such we settled for a crystal with a higher wedge angle and less absorption in the cavity. The coating on the crystal was done by Optida (Vilnius, Lithuania) and figure (4.13) shows the theoretical coating curves for both surfaces.

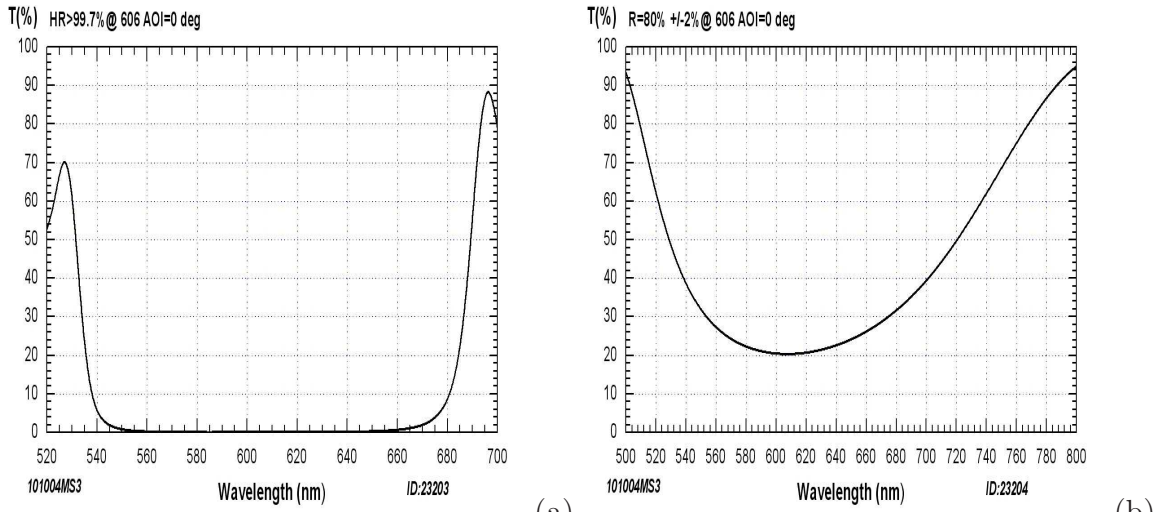

(a) (b)

Figure 4.13: Reflection and transmission coefficient plots of the real coating made by Optida. (a) High reflection coating at 605.9 nm, (b) partial reflcetion coating at same wavelength.

4.6 Summary

- With the help of the visualization window in FRED, the design of optical components have been made very easy.
- Simulations in FRED can be done either directly or with the help of a FRED script.

- Our design cavity has a cavity absorption less than 10 % at resonant and impedance matched, which is good for our purpose.

Chapter 5

Experimental realisation of the cavity assisted optical quantum memory

So far, no mention of the properties of the materials used for the quantum memories have been made mention. The quantum memories properties used to asset its performance has been mention (see section 2.2). Therefore, to realize a quantum memory, the memory material together with the storage protocol used, must be able to produce a quantum memory fulfilling the performance criteria in section 2.2. In this chapter, I present one of the materials used for quantum state storage and the properties of the material that makes its a good candidate for it. This is closely followed by a simple experiment to measure the flatness of the cavity surfaces. The preliminary test on the cavity together with results from the experiment is presented last.

5.1 Material for the optical quantum memory

The material used for the quantum state storage experiments is a rare-earth (precisely praseodymium Pr^{3+}) doped in a yttrium orthosilicate (Y_2SiO_5) crystal. Strong ion-ion interaction can be achieved with the crystal. In the periodic table, the rare-earth elements makes up the Lanthanide group, which 15 members in total [34].

Y_2SiO_5 is a monoclinic crystal with each unit cell having 16 yttrium atoms, that is 8 molecules [50]. The unit cell has dimensions $a \times b \times c$, where $a = 1.04nm^3$, $b = 0.67nm^3$ and $c = 1.25nm^3$. The b−axis is perpendicular to both a and c, while a and c are at an angle of 102.39^0 to each other [34, 50]. The crystal has two optical axes, which we called D_1 and D_2, D_1 is perpendicular to D_2 and both of them are perpendicular to the b−axis, therefore they lie in the a,c plane. This crystal is highly birefringent, thus only light that is polarized along the optical axes will maintain its polarization after going through the crystal (see figure (5.1)) [27].

The yttrium in Y_2SiO_5 has nuclear spin of 1/2 while silicon and oxygen has zero nuclear spins. Nuclear spin interaction between the Y_2SiO_5 (host crystal) and the Pr^{3+} (dopant) is minimal, thus less coherence losses due to nuclear spin interaction in the crystal.

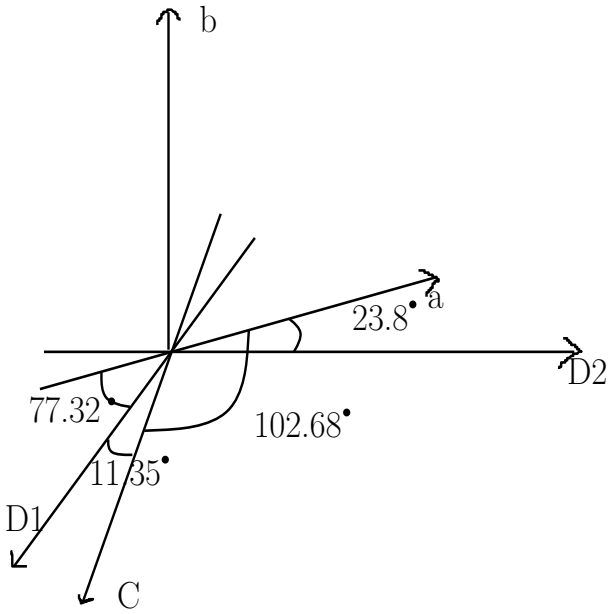

Figure 5.1: The polarization axes of the praseodynium doped crystal.

In the crystal, the yttrium occupy two non-equivalent sites and the rare-earth ions are a good substitute for it in the crystal. This is due to the fact that, it has similar 3^+ ionic radius (1.023nm) as the rare−earths ions (Pr^{3+} has 0.97nm) [34]. As such, the praseodymium has two non-equivalent sites when doped into the crystal. On doping the crystal, site 1, with a wavelength of 605.9 nm is the favorite site, as 90% of the Pr^{3+} ions will end up there, while site 2, just 2 nm away, that is, 607.9 nm will have just 10% of the ions [50].

In our experiments, site 1 will be used and has a dipole moment of $7.5 \cdot 10^{-}3$ Debye [50]. On doping the Y_2SiO_5 crystal with Pr^{3+}, the Pr^{3+} ions in the host crystal acquire a permanent electric dipole moment oriented in two equivalent direction, which are at angle of 24.8^0 apart [34, 50]. The presence of an external E−field create a transition electric dipole moment, which is oriented along the two equivalent directions of the permanent dipole moments. To achieve maximum interaction (absorption) with the Pr^{3+} ions, the doped crystal is either rotated or the polarization state of the input light field is rotated (the latter is the method we use in our experiments), until such a maximum is achieved. Below, a brief overview of some of the properties of Praseodymium (the rare earth element used to dope our yttrium crystal), useful for the quantum state storage using the AFC protocol is presented.

5.1.1 Pr^{3+} hypefine energy levels

The Lanthanides group is at the bottom of the periodic table thus given its members a strong spin−orbit coupling [34]. This results in the 4-f states splitting into manifolds. Spin-orbit coupling conserved angular momentum, J, thus the manifolds have the same total angular momentum, J, as the 4f state [34]. When doped in the Y_2SiO_5 crystal, the crystal field and the number of 4f electrons determines the number of manifolds resulting from the splitting [34]. The crystal field can be viewed as causing a small perturbation to the rare earth ions spin−orbit coupling. Below liquid helium temperature ($< 4K$), the 4f state splitting due to the interaction with the crystal field is at most $2J + 1$, where J is the angular momentum

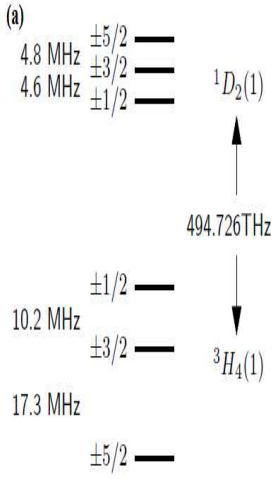

(b)

g \ e	±1/2	±3/2	±5/2
±1/2	0.56	0.38	0.06
±3/2	0.39	0.60	0.01
±5/2	0.05	0.02	0.93

Figure 5.2: The figure shows the hyperfine energy levels of the Pr^{3+} ions in a Pr^{3+}:Y_2SiO_5 crystal. (a) This shows the $^3H_4 \rightarrow ^1 D_2$ transition (site 1 transition) in Pr^{3+}:Y_2SiO_5 crystal. (b) The relative oscillator strength of the various optical transition between the $^3H_4$ and $^1D_2$ hyperfine manifolds [55].

quantum number. In the present of the host crystal field, the number of 4f electrons greatly matter, as such, the rare earth ions can be classify into two categories:

(i) Those with odd numbers of the 4f electrons resulting in a doublet energy level splitting due to an unpaired spin (large magnetic moments) called the Kramer's Doublets [34] and

(ii) Those with even numbers of 4f electrons (e.g. Pr^{3+} used in the doping for our case), called the non−Kramer's ions resulting in singlet energy level splitting. Since all the state has a net zero angular momentum, they will experience a quenching of the angular momentum [34].

Site 1 will be used for our experiment, see figure (5.2). The Pr^{3+} ions in this site, have a nuclear spin of 5/2, resulting in 6 hyperfine splitting of both the ground and excited 4f states, labeled ±1/2,±3/2 and ±5/2. In the absence of any external magnetic field, this 6 hyperfine states, are two-fold degenerate yielding 3 hyperfine states, see figure (5.2) [34, 50]. The hyperfine levels have long lifetime (at liquid helium temperature, a lifetime, T_1 of 100 s [34] has been observed and a coherence lifetime T_2 of 500μs without any external field and 860 ms with a carefully chosen field has been observed [34]), with relaxation between the levels (in particular the ground levels) very unlikely (that is, an excited state decays to the ground states and not to another excited state). This has been exploited to extend the coherence time (memory time) of the system [53]. Care must be taken, as an attempt to extend the coherence time using the hyperfine state, amount to the application of an external B-field, thus destroying the 2-fold degeneracy associated with the no field situation.

The third degenerate stated is use as a shelving state, where ions are kept temporarily during the storage process (see section (2.5.1)), and as such it's must have a very long

population lifetime.

The splitting between the hyperfine ground states in Pr^{3+}:Y_2SiO_5 has been measured to be $10.2MHz$ between the hyperfine state $+|1/2>\rightarrow +|3/2>$ and 17.3 MHz between the hyperfine state $+|3/2>\rightarrow +|5/2>$. The hyperfine splitting in the excited state has been measured to be 4.6 MHz between the hyperfine state $+|1/2>\rightarrow +|3/2>$ and 4.8 MHz between the hyperfine state $+|3/2>\rightarrow +|5/2>$, see figure (5.2).

5.1.2 Pr^{3+} homogeneous linewidth

In a solid crystal, the phonons existing in it, perturb the interaction between the electron and the orbital lattice but this perturbation is minimal in a Pr^{3+}:Y_2SiO_5 crystal, due to the shielding of the 4f electrons. Due to this effect, the transition intensity is concentrated on a very narrow zero phonon line with no phonon sideband [38]. The narrowest zero phonon line is associated with the optical transition between the ground state with the lowest energy (manifold), to the excited state with the lowest energy (manifold). Other transitions are broader due to non radiative cascade decay [38]. Individual ions in a solid crystal experience the same homogeneous broadening line-width. The coherence time between energy levels or hyperfine energy levels, T_2, is directly related to the homogeneous line-width Γ_{hom} of the individual ions in the crystal as [34]:

$$\Gamma_{hom} = \frac{1}{\pi T_2}. \tag{5.1}$$

In a Pr^{3+} doped crystal, several different mechanism contribute toward the de-phasing of Γ_{hom} and can be expressed as [34]:

$$\Gamma_{hom} = \Gamma_{pop} + \Gamma_{Pr-Pr} + \Gamma_{phonon} + \Gamma_{Pr-spin} + \Gamma_{spectral}. \tag{5.2}$$

Γ_{pop} is the linewidth associated with the excited state population life time, T_1 given by [34], $\Gamma_{pop} = \frac{1}{2\pi T_1}$. Γ_{Pr-Pr} is the line width associated with the interaction between two Pr^{3+} ions, due to the fact that, exciting one Pr^{3+} ion, changes the electric dipole moment around it. Due to this change, the resonance frequencies of ions around it, will be perturb but this effect can be decreased by reducing the dopant concentration, such that each Pr^{3+} ion has no immediate neighbor. Γ_{phonon} is associated with phonon scattering, phonon absorption and scattering in the crystal. These are temperature dependent, thus can be eliminated by working at low temperature, say below 4k [38]. $\Gamma_{Pr-spin}$ is associated with the interaction of the Pr^{3+} ion nuclear spin and that of the host material. This can be minimized by using a host material with low or zero magnetic moment and Pr^{3+}:Y_2SiO_5 possess such property. $\Gamma_{spectral}$ is associated with spectral diffusion or excitation induced broadening. This is caused by the changes in the E-field in the crystal as a result of the excitation of ions from the ground state to the excited state. This effect is small, if the number of excited ions is small [38, 50].

The upper bound of the coherence time (T_2),is twice the population life time (T_1) that is, $T_2 \leq 2T_1$, with equality only went the de-phasing in Γ_{hom} is determine only by Γ_pop [34, 50]. In Pr^{3+}:Y_2SiO_5 at liquid helium temperature ($< 2.2K$), a population life time of $164\mu s$ has been achieved [50], given an upper bound of the homogeneous line width in the kilohertz range. The optical storage time depends on the coherence time, T_2, and its can be improve upon by using superposition of the hyperfine ground state together with the application of a magnetic field [53], given a storage time of the order of milliseconds.

5.1.3 Pr^{3+} inhomogeneous linewidth

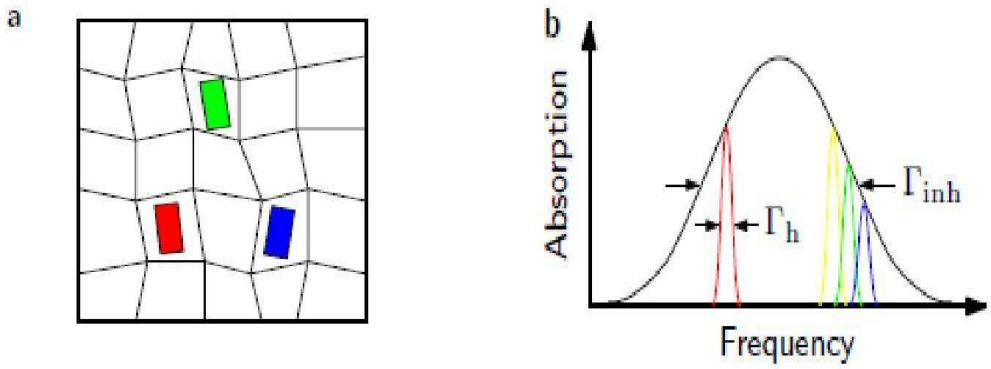

Figure 5.3: (a) The strain in the crystal lattice due to the presence of Pr^{3+} ions in the crystal. The different colorede square shows the slight different in the absorption frequencies of the doped Pr^{3+} ions due to the crystal strain. (b) An inhomogenously broaden media, which consists of homogeneous linewidths of the atoms, drawn not to scale [55].

In the preceding section, we describe some mechanism causing broadening in the absorption line, but they have the same affected on all the ions in the crystal. There are some other broadening mechanisms, which are position dependent, and will thus affect only ions closed to the position but not others further away. These effects are group under the term inhomogeneous broadening mechanism. Inhomogeneous broadening in a crystal can result from several different factors. For example, it maybe due to strain in the crystal structure as a results of crystal imperfection, point defects and dislocation in the crystal, as well as the size different between the Pr^{3+} ion and the Y^{3+} ion [34, 38, 50]. All these effects will cause the crystal to have an imperfect crystal lattice and this will create a position dependent crystal field. As such, each Pr^{3+} ion will experience a slightly different local environment, resulting in their transition frequencies been slightly different, given a frequency distribution of the transition frequencies. The width of the frequency distribution is called the inhomogeneous line width Γ_{inh}, see figure (5.3) [50].

5.2 Experimental measurement of cavity surface flatness

One of the cavity's surfaces is slightly tilted and from the FRED simulation, the lack of parallelism in the surfaces causes losses below 10% at the matched cavity resonance. Further tilting of the surfaces, that is, increasing the lack of parallelism, leads to the losses increases greatly, see figure (4.11). Therefore, to avoid further tilting of the cavity surfaces, the both cavity surfaces must be very flat and parallel. To measure the cavity surface flatness, we use interference effects in the cavity, and this is done using the setup shown in figure (5.4) .

An optical fibre, emitting a divergence laser beam is used as the light source. A converging lens, with a focal length, f, and a diameter, d, is carefully placed a distance equal to its focal length from the fibre, to ensure that the light rays after the lens are parallel. The diameter of the lens must be greater than the diameter of the cavity which is 12 mm, such that, the light beam after the lens must cover the cavity fully. Also, the focal length of the lens must be such that, by the time, the beam hits the lens, the beam diameter must be larger than the cavity diameter. The cavity is tilted a little, such that, the interference fringes from the cavity can be image unto a screen. Two measurement were done, one before the cavity was coated, see figure (5.5) a and the second one, after the cavity was coated, see figure (5.5 b. Before the coating, the fringes can be obtained either from the transmitted beam or the reflected beam. After the coating, the reflected beam is used because of its high visibility, since the first mirror has a reflectivity of 80 % while the second has 99.7 %. Both measurements were done using the reflected beam, such that they can be compared. From figure (5.5), we can see that, the flatness of the surfaces are not that good, as such, depending on where you position the laser on the cavity, you might have higher losses than at other position. For example, position A in figure (5.5) , is flatter than position B or C and as such placing the laser at position A, will give less losses as compare to positioning it at position B or C. The cavity surfaces are clearly not uniform as shown by the fringe patterns in figure (5.5) b. To see this, we use the fringes to calculate the wedge angle of the cavity at position A, B and C and use this angles in FRED to get the corresponding losses. To do this, we measure the horizontal distance between either two bright or dark fringes and uses the fact that, the changes in cavity length must be $\lambda_{material}/2$ in order to observe either two bright or dark fringes in the cavity. The change in the cavity length gives the vertical distance and as such, the angle is the arctangent of the changes in the cavity length divided by the horizontal distance between fringes, that is:

$$\Theta \approx \frac{\text{change in cavity length}}{\text{distance between fringes}}.$$

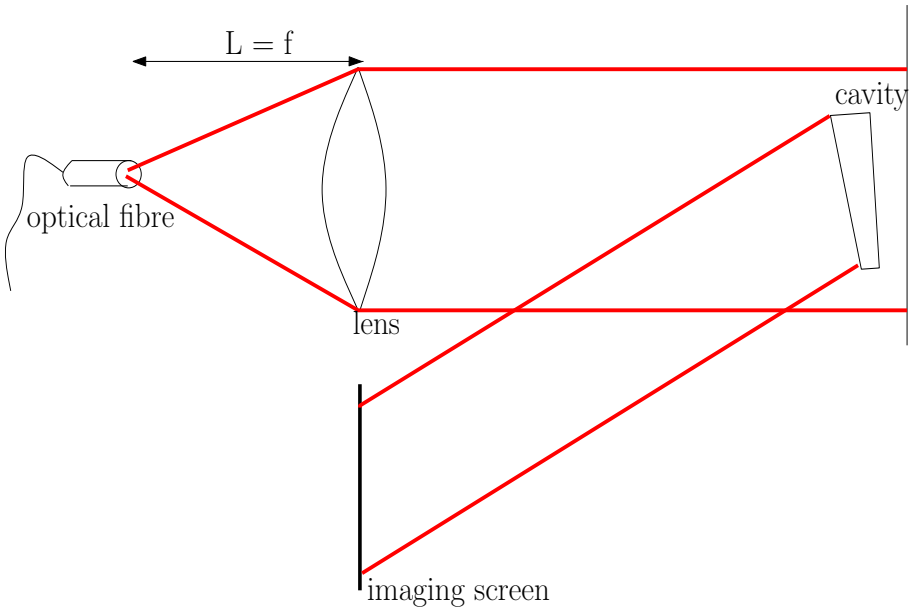

Figure 5.4: The experimental setup for measuring the cavity surface flatness.

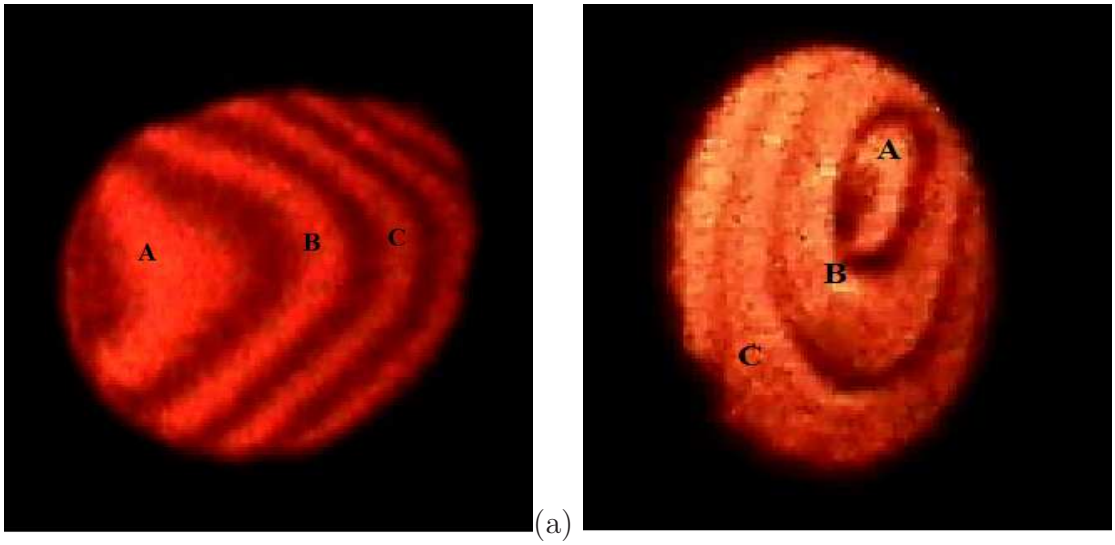

(a) (b)

Figure 5.5: Cavity flatness measurement using interference from the two cavity surfaces. (a) Before the cavity is coated, (b) After the cavity is coated.

The table below shows the calculated angles as well as the corresponding loses in the cavity calculated from FRED at the cavity resonance. This confirm our suspicion that position a will be the best spot to use, since it has less cavity losses than the others.

Angle from figure (5.5)	cavity losses from FRED
0.0019	0.09476
0.0046	0.25809
0.0055	0.30752

5.3 Experimental setup for testing the cavity

Figure (5.6) is the experimental setup used in this work. The setup consists of 3 parts: the laser frequency stabilization system, the pulse-shaping system and the experimental system.

5.3.1 Laser frequency stabilization system

The atoms used for the experiments are rare-earth atoms. The rare-earth ions have transition line-width of the order of kilohertz (kHz), corresponding to a coherence time of the order of hundred microseconds (μs). Therefore, the coherence properties of the laser system used to drive these ions should be of the same order or better. In our experiments, the laser source is the most important device, as such, its must meet the following requirements [34]:

(i) Its must produce light with a wavelength corresponding to the absorption wavelength of the rare-earth atoms used for the experiments.

(ii) The laser output power as well as its phase, must be sufficiently stable.

We will be using Pr^{3+} ions for our experiments. The transition $^3H_4 \rightarrow^1 D_2$ in Pr^{3+} ions corresponding to a wavelength of 605.9 nm will be used, therefore, our laser system should be able to excite this transition.

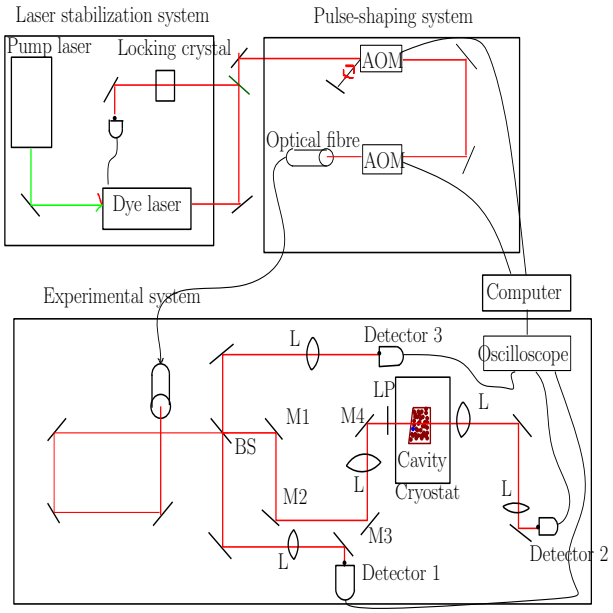

Figure 5.6: The experimental setup used for most of the experiments in the preliminary testing of the crystal cavity.

We use a dye laser in the experiments. The dye laser is pumped by a 6 W solid state Nd:YVO_4 laser (coherent Verdi V6) green laser. The dye laser is made up of a ring cavity dye laser with Rhodamine 6G dye as the active medium. The dye laser can be tuned to 605.9 nm, which is the required wavelength to drive the transition for the experiments. The temperature of the dye is kept at 8^0 by a temperature stabilization system and the pressure at 4.2 bars. The stability of the dye laser system depends on both the temperature and pressure been kept constant, for any change in them will change the dye jet flow position. The phase of the dye laser is fluctuating due to the dye jet flow.

To increase the stability of the dye laser system, an intra-cavity electro-optic crystal which is frequency locked to a very stable Fabry-Perot cavity is used [34]. Vibration and thermal changes, changes the length of the Fabry-Perot cavity, posing a problem to the stabilization. The system is further stabilized with respect to a crystal. The laser create a spectral hole in the crystal and this spectral hole is used to stabilize against [55]. Spectral holes are insensitive to vibration disturbances. Figure (5.7) is a photograph of the laser stabilization system and for details see reference [55] and references there in. The dye laser system shown in figure (5.7) has a stability of the order of kilohertz (kHz) and coherence times of the order of microseconds (μs) [55].

5.3.2 The pulse shaping system

In section 3.2.4, we came to the conclusion that, the complex hyperbolic secant (sechyp) pulses are a good pulse type to use if we need to interact with atoms of a certain frequency range. Therefore, in the real experiments, we need to be able to create this and other pulse types with high accuracy. In our system, this is done using an Acousto-Optics Modulator (AOM) [34]. A matlab scripts in a computer create these pulses shapes and send them to an arbitrary waveform generator (1GS/S Tektronix 520 Arbitrary Waveform Generator), which

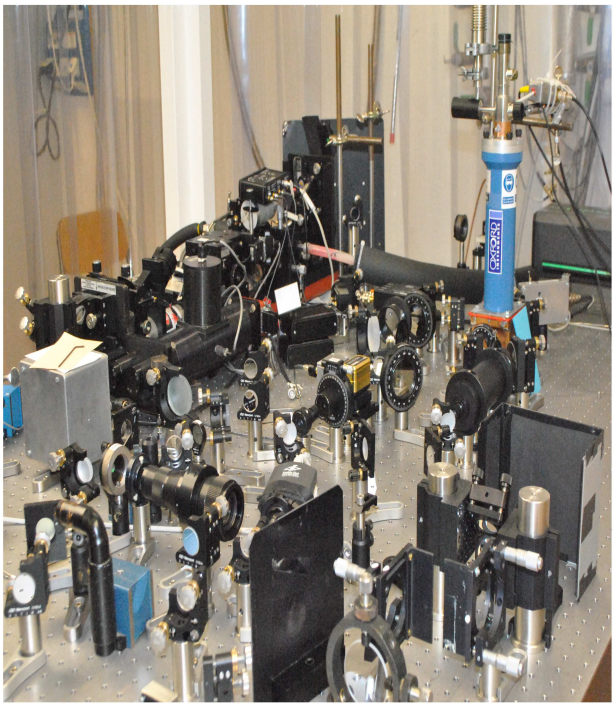

Figure 5.7: Picture of the laser frequency stabilization system.

generate the pulses and send them to the AOMs using two channels via an RF-amplifiers.

5.3.3 The experimental system

After the second AOM, the light is coupled into a single-mode optical fibre, which cleans the light (that is, cleans the spatial mode of the light). A $50-50$ beam splitter remove 50% of the light beam intensity before the cryostat, to be used as a reference beam in the experiments. The rest of the light beam, goes through a lens, a couple of mirrors and a $\lambda/2$ plate. The $\lambda/2$ plate is used to adjust the light polarization, such that its matches that of the crystal orientation. The lens is used to focus the laser beam down to $100\mu m$ diameter at the center of the sample, resulting in the strongest transition having at most a Rabi frequency of approximate 2 MHz. Our sample is a crystal cavity with a tilted surface. The mirrors after the beam splitter are meant to ensure that we have good overlap between the input beam and the zeroth order reflection beam from the crystal cavity.

The sample (crystal cavity) is attached to a nano-positioner attocube (ANPz51) for vertical movement of the sample inside the cryostat. The sample together with the attocube are both lower into the cryostat, immersed in liquid helium. The sample is kept at a temperature below 2.1K. The 3 signals, that is, the reference beam, the reflected beam and the transmitted beam were all detected using the detector Thorlabs PDB150A. The detectors all have switchable gain that can be change from 10^3 to 10^7 in 5 steps with a bandwidth of 150MHz at the lowest gain and 0.1 MHz at the highest gain [34]. A picture of the experimental system setup is shown in figure (5.8).

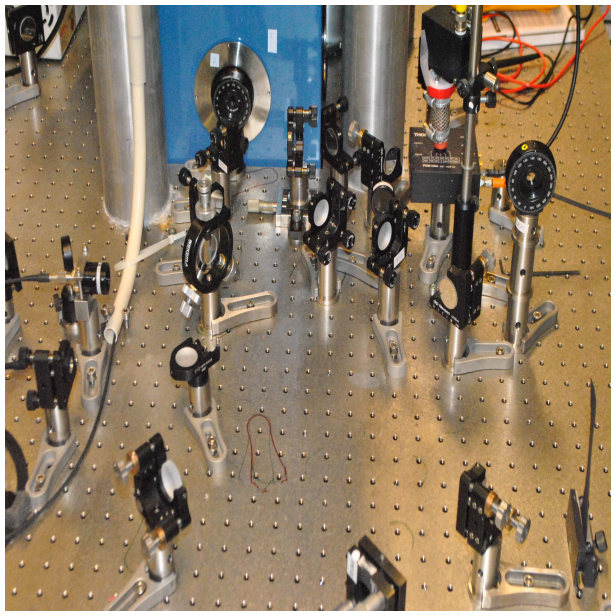

Figure 5.8: Picture of the experimental system setup used in the experiments.

5.4 Results and discussion

Note that every thing so far, has been about high efficiency quantum memories. Due to the observation of cavity resonance frequency pulling effects in the crystal cavity, as a result of spectral pit burning, all the experiments linked to quantum memory was suspended. Further investigation into the frequency pulling effects in the crystal cavity was carrierd out. Below, I present the experimental results from the preliminary tests done on the crystal cavity.

5.4.1 Cavity fringes, resonance peaks and absorption profile

On cooling down the crystal cavity from a temperatures of about 150 K to superfluid helium temperatures ($\approx 2.1K$) using liquid helium, in the presence of the laser beam, we can see the cavity fringes, see figure (5.9) a and b. At temperatures above 3.0 K, the visibility of the fringes are very good, (see figure (5.9) a) but as the temperature goes below 2.1 K, the higher order fringes disappears (see figure (5.9) b). At temperatures slightly above 2.2 K, the liquid helium in the cryostat has bubbles and the bubbles dissappers went we have superfluid helium at temperatures below 2.1 K. Figure (5.9) a was taken when the helium in the cryostat was at the liquid state with temperatures above 2.2 K and figure (5.9) b, when the helium was at superfluid state.

At temperature below 2.1K, the absorption profile is more confined but is still frequency broad. With the presence of the mirrors attached to the crystal, it is difficult to measure the crystal absorption profile directly. In order to see the cavity crystal absorption profile, the cavity effect must be destroyed somehow. Note, that the usage of the word destroy in this case, does not imply destroying the cavity mirrors but making the crystal cavity not to have any field built-up within it. To do that, we increase the input incidence angle, such that the reflected beam and the input beam no-longer overlap. This gets rid of the cavity buid-up inside the crystal. Figure (5.9) d) shows the crystal absorption profile. The profile have a FWHM of 9.4 GHz larger than the 5 GHz measured for a similar doped crystal [34]. We

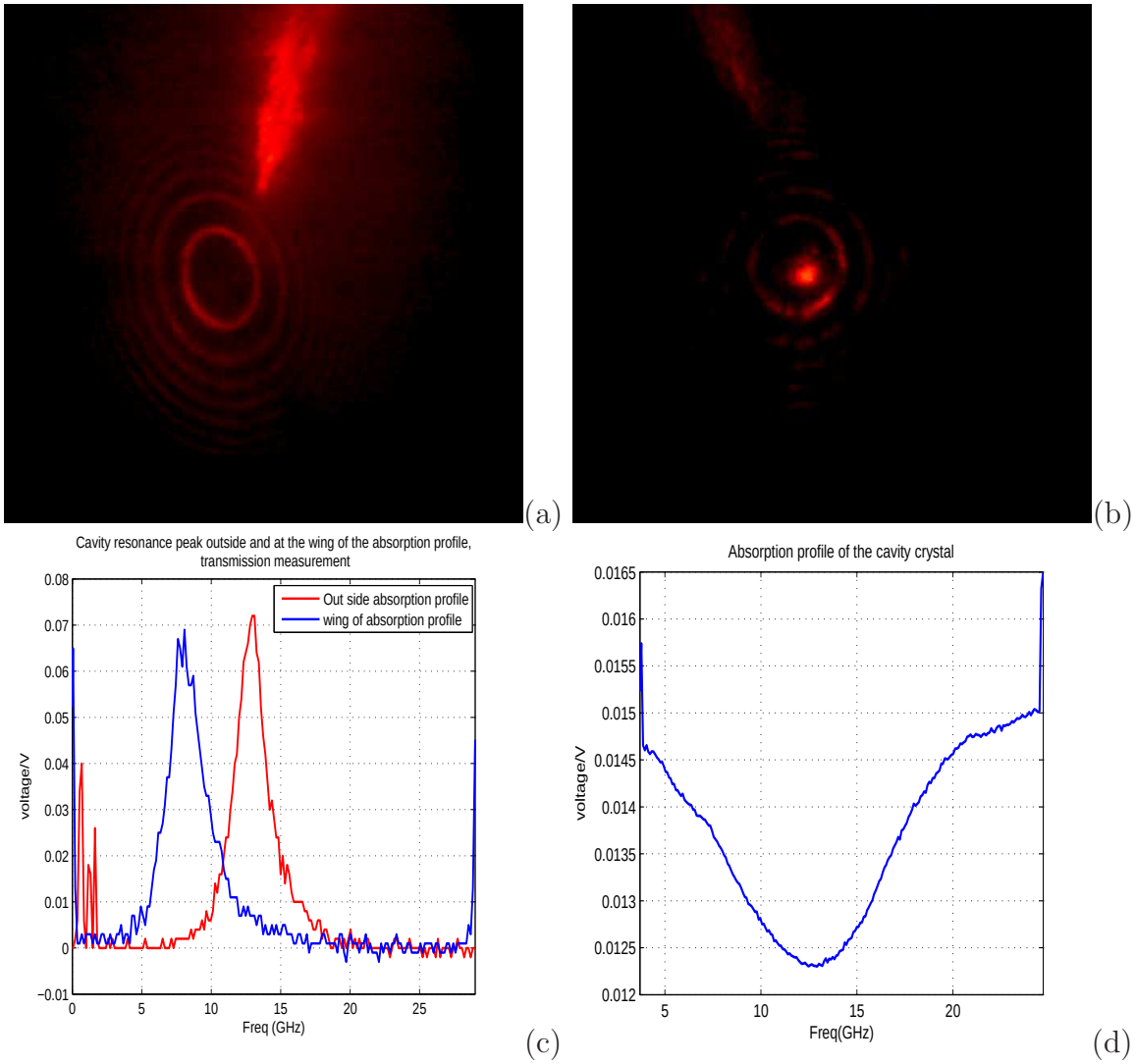

Figure 5.9: The cavity interference fringes, at high and low temperatures and its resonance peak. (a) At temperatures above 2.2 K, we have liquid helium with bubbles in the cryostat and the fringes are more visible. (b) At temperatures below 2.2 K, we have superfluid helium in the cryostat and the higher order interference fringes are been abosrbed. (c) Cavity resonance peak. The read curve is with a center frequency offset of 10GHz, to ensure we are outside the inhomogeneous absorption profile of the crystal. The blue curve is at the wings of the absorption profile, see d. Both plots had a scan of 30GHz at 7.5GHz/s. The blue curve has a FWHM of 2.7GHz while the red has 2.2GHz. Both are higher than the 1.5GHz calculated. The height of the peak without any absorption is higher than that with absorption as would aspect. (d) Crystal absorption profile obtained by destroying the cavity effect. The $\lambda/2$ plate was at 35^0 for maximum interaction with the Pr^{3+}. The total scan was 21GHz with a light intensity of 0.5mv. A FWHM of 9.4GHz was measured higher than the 5GHz measured in [34].

don't know why the absorption profile is that large.

We then return the crystal back to the overlap position, were the cavity is now active. We then try to measure the cavity resonance of the crystal cavity. To do that, we were face with 2 options: option 1, we move the crystal cavity vertically and measure the transmitted power (the transmitted power was easier to measure in this case) or option 2, keep the crystal cavity fix and scan the laser frequency.

Option 1 was a little problematic, because we had the crystal cavity attached to an attocube, with a maximum vertical movement of 2.5 mm. Our crystal cavity has a diameter of 12 mm, therefore to scan the complete diameter of the crystal cavity; we will need to lift the crystal cavity manually after each movement of the attocube. The manual lifting was a problem, as we were not sure exactly where we were on the crystal cavity after each manual lifting and also, if we are doing measurement at a new spot or the same old spot.

Option 2, was a better option since we could scan our laser frequency easily. Figure (5.9) c shows the crystal cavity resonance peaks obtained from scanning the laser frequency. We measured a FWHM of 2.2 GHz out side the inhomogeneous profile and 2.7GHz inside the profile, approximately 1GHz larger than the calculated value of 1.5 GHz (see section 4.5 or 3.1.4). The differences between the experimental value and the calculated value can be due to the the destruction of the cavity build-up by the strong absorption in the crystal or due to saturation or that we are not really on the center or outside of the absorption profile, causing the peak to broaden. The peak inside the absorption profile is broader than that out side and has less intensity dues to the absorption. This method tells us how large the crystal cavity resonance peak is (that is, in GHz), which is very good for the quantum memory protocol. In order for the cavity to be used to increase the memory material absorption, we need the FWHM of the cavity resonance peak to be large than the AFC bandwidth. The AFC protocol we will be using, have a bandwidth in the MHz range and therefore the cavity resonance peak in GHz range, can cover the AFC peaks. It doesnt say anything if the crystal cavity is impedance matched [24] or if we are on resonance with the Pr^{3+} ions. The main purpose of using the cavity for the quantum state storage is that the cavity will enhance the memory material if it is on resonance both with the ions and impedance matched.

Out AFC bandwidth is in the MHz range and our crystal cavity has a GHz resonance peak, therefore we are fine to use our cavity for quantum state storage using AFC protocol. We move the cavity both manually and using the attocube, until we get to a point in the crystal cavity were we think we are at resonance with the cavity and the Pr^{3+} ions. At this position, and at a temperature of 2.1 K, we did all the experiments in the next sections.

5.4.2 pit creation in cavity and slow light effects

(i) ***Empty spectral pit, slow light and group velocity*** : The crystal inhomogeneous profile is about 9.4 GHz and each Pr^{3+} ions has a homogeneous line width of about a kHz at liquid helium temperature ($\approx$ 2.1 K). On the absorption of a chirp laser pulse, the pr^{3+} ions are excited to the excited state. The excited Pr^{3+} ions can either relaxed to their original hyperfine ground state or to the other 2 hyperfine ground states with total seperation of 27.5 MHz. If the ions falls back to their original hyperfine state, they re-absorbed the chirp laser pulse and re-excited again. This process continues until the ions relaxed to a different hyperfine ground state. When this happens, the

intensity of the transmitted pulse at that frequency increases due to a decrease in the inhomogeneous absorption profile, thus creating a spectral hole like structure for that frequency. This process can be repeated several time, until there are no absorbing ions left at that frequency. Scanning the chirp laser frequiency, a spectral pit is created with the possibility of no absorbing ions being presence within the frequency range . The maximum spectral pit that can be created is reduced by the total splitting of the hyperfine excited state, which is 9.4 MHz, giving a maximum spectral pit of 18.1 MHz (see figure (5.10) a) [22]. The pulses and the number of times they are applied are all generated by a matlab script and send to the waveform generator. The waveform generator generates the pulses and sends to the AOM for implementation, which then send the pulses to the crystal cavity via a single mode fibre. For a detail of the list of pulses used for the spectral pit creation sequence for the 1 , 2, 4, 6, 8, 10 and 16 MHz spectral pit, see appendix B and for the 18 MHz spectral pit see the appendix in reference [22].

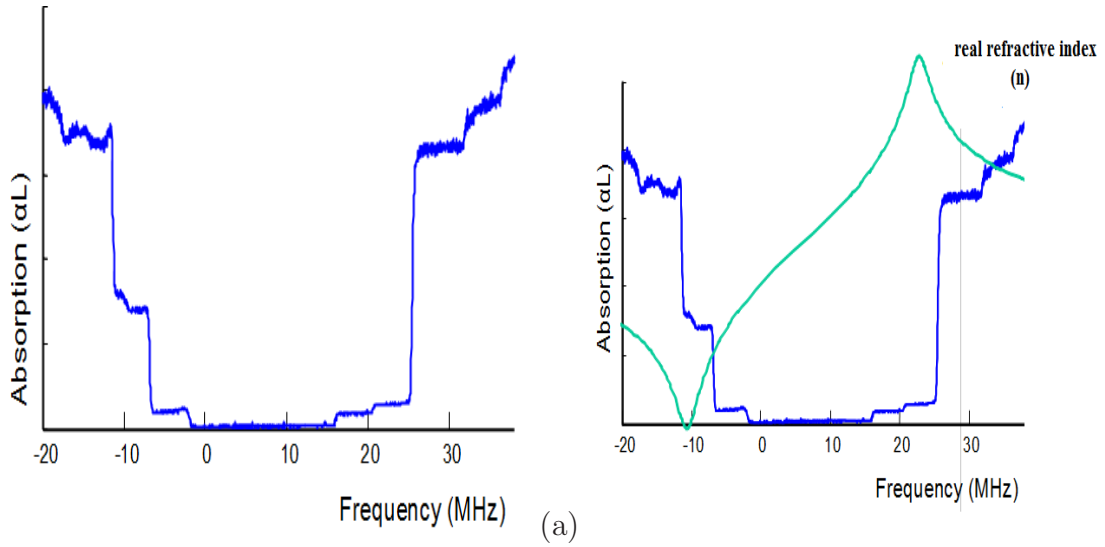

Figure 5.10: (a) An 18 MHz empty spectral pit, with scan readout from -3 MHz to 15 MHz. The pit is from -1.2 MHz to 16 MHz. (b) The 18 MHz empty spectral pit together with the changing real refractive index over the pit. The change in the real refractive index is due to the change in absorption across the pit. [22, 58]

This pulse sequence then creates the spectral pit in the crystal cavity. Figure (5.11) shows different spectral pits with different widths. Figure (5.11) a, b shows the reflection/transmission measurement of the different spectral pits. Figure (5.11) c, is the αL (decovulution) measurement using the reflected beam for a spectral pit with an 18MHz width.

We notice that, the spectral pit shapes are not visible in any of the plots, neither in the transmission nor in the reflection measurements. Also, in each of the plots, crystal cavity resonance peaks are visible contrary to what we were expecting, given that the peaks should be in GHz range (as measured in the previous section).

The spectral pit causes some changes in the absorption profile of the crystal. These changes results in a corresponding changes in the susceptibility of the crystal. The

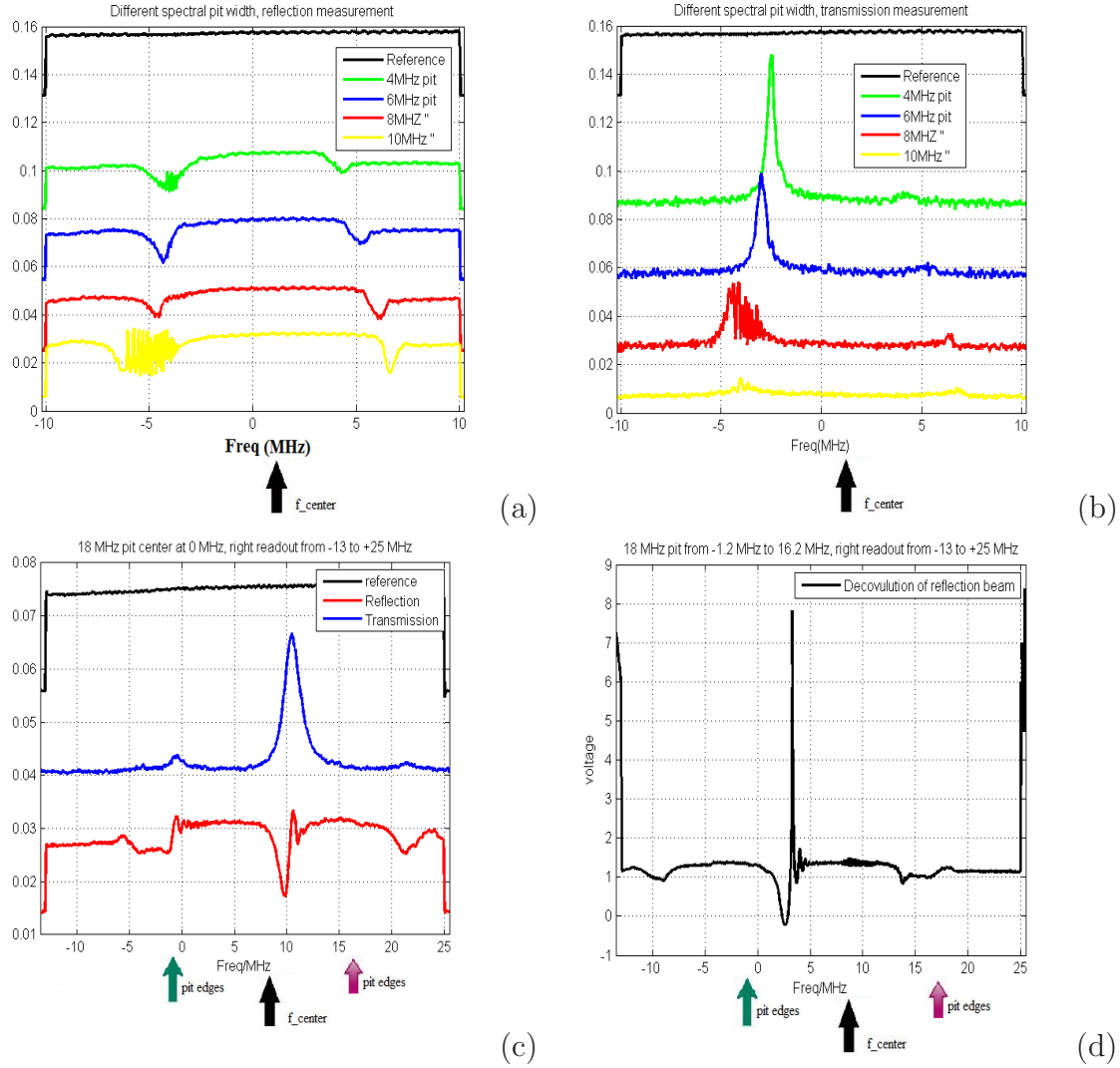

Figure 5.11: Different empty spectral pit widths. (a) Reflection beam measurement for different pit width. All the spectral pits are centered at +1MHz and a high resolution readout ($10kHz/\mu s$) was used to obtained the data. The readout scan was from -10 to +10 MHz and the detector gain was 10^5. Only two detectors instead of three, was used for this set of experiments. Therefore, one detector was moved between the transmission and the reflection beam measurements, as such a and b, were not taking simultaneously. (b) same as a but meaurements were done using the transmitted beam, that is, the detector was moved to the transmitted beam for measurement to be done. Every thing is the same as a, except the detector gain that was change to 10^7, due to the low light intensity in the transmitted beam. (c) Cavity resonance peak at center of spectral pit for an 18 MHz pit width, starting from -3 MHz to 15 MHz. Right readout (1MHz/μs), with a readout scan from -13 to +25MHz. In this measurement, all three detectors were present, that measuring the reflected beam had a gain of 10^5 and that for the transmitted 10^6. (d) αL measurement of the 18MHz pit in c. This is the decovulution of the spectral pit in c.

changes in the susceptibility causes corresponding changes in the crystal refractive index over the pit (see figure (5.10) b), that is [27]:

$$\chi^{''}(\nu) \approx \left(\frac{n_0 c_0}{2\pi\nu}\right)\alpha(\nu) \tag{5.3}$$

$$\chi^{'}(\nu) \approx 2\left(\frac{\nu-\nu_0}{\Delta\nu}\right)\chi^{''}(\nu) \tag{5.4}$$

$$n(\nu) \approx n_0 + \frac{\chi^{'}(\nu)}{2n_0} \tag{5.5}$$

Thus across the spectral pit, the pulse propagation velocity called the group velocity, is different at different position. This can either result in fast or slow light depending on the changes of the refractive index with respect to the frequency within the pit. The group velocity is [27]

$$V_g = \frac{c_0}{n_0 + \nu\frac{dn}{d\nu}} \equiv \frac{c_0}{n_g}, \tag{5.6}$$

where $n_g = n_0 + \nu\frac{dn}{d\nu}$ is the group refractive index. When $\frac{dn}{d\nu} >> n_0 > 0$, we get slow light effect and when $0 > \frac{dn}{d\nu} >> n_0$, we get fast light.

In our case with the empty pit, $\frac{dn}{d\nu} >> n_0$, and therefore, we get slow light effects in the crystal cavity. To see the slow light effects, we sent a Gaussian pulse with a FWHM less than the pit width through the pit at different position; see figure (5.12) c. The shape of the spectral pit determines how large $\frac{dn}{d\nu}$ can be, as such how much slowing down of the light we can get. Also, the output Gaussian pulses undergo broadening due to the cavity build-up effect. Since we can't see the spectral pit, we decided to keep the FWHM of the Gaussian pulse constant and change it's center frequency. Doing this, we can send the Gaussian pulse at different position of the spectral pit. Sending the Gaussian pulse at different position of the spectral pit (which we can describe as scanning the pit with the Gaussian pulse) and moving the pit and repeat the process again, we obtained figure (5.12) a,b and d. Sending the Gaussian pulse at different position of the spectral pit and moving the spectral pit, are done by changing the Gaussian pulse and spectral pit respectively, center frequencies in the matlab scripts generating them. In figure (5.12) a, the spectral pit center frequency is at -1MHz and scanning the Gaussian pulse across it, we get the slowest light (duration τ=1 μ s) with a Gaussian center frequency of -2.5 MHz. In figure (5.12) b, the spectral pit center frequency is 0 MHz and the slowest light was at -1 MHz. In figure (5.12) d, the spectral pit center frequency is +1 MHz and the slowest light was at -1 MHz. From the duration measurement, we get a group velocity of the order of km/s, given that the cavity has a thickness in the order of mm. From figure (5.12), we can see that, our pit is steeper at the left edge than at the right edge thus larger changes in the refractive index implying more slowing of the light.

The relationship between the group velocity, the spectral pit width and the material absorption is give by $v_g = \frac{\pi\Gamma}{\alpha}$, where Γ is the spectral pit width measured in hertz (Hz) and α is the round trip absorption (round trip losses in the cavity) measured in m^{-1}. In the presence of the spectral pit, the Pr^{3+} ions outside the spectral pit now interact off resonantly with the light pulse. Due to this off resonant interaction, they do not absorbed the light pulse but now contribute to the phase shift imparted to the

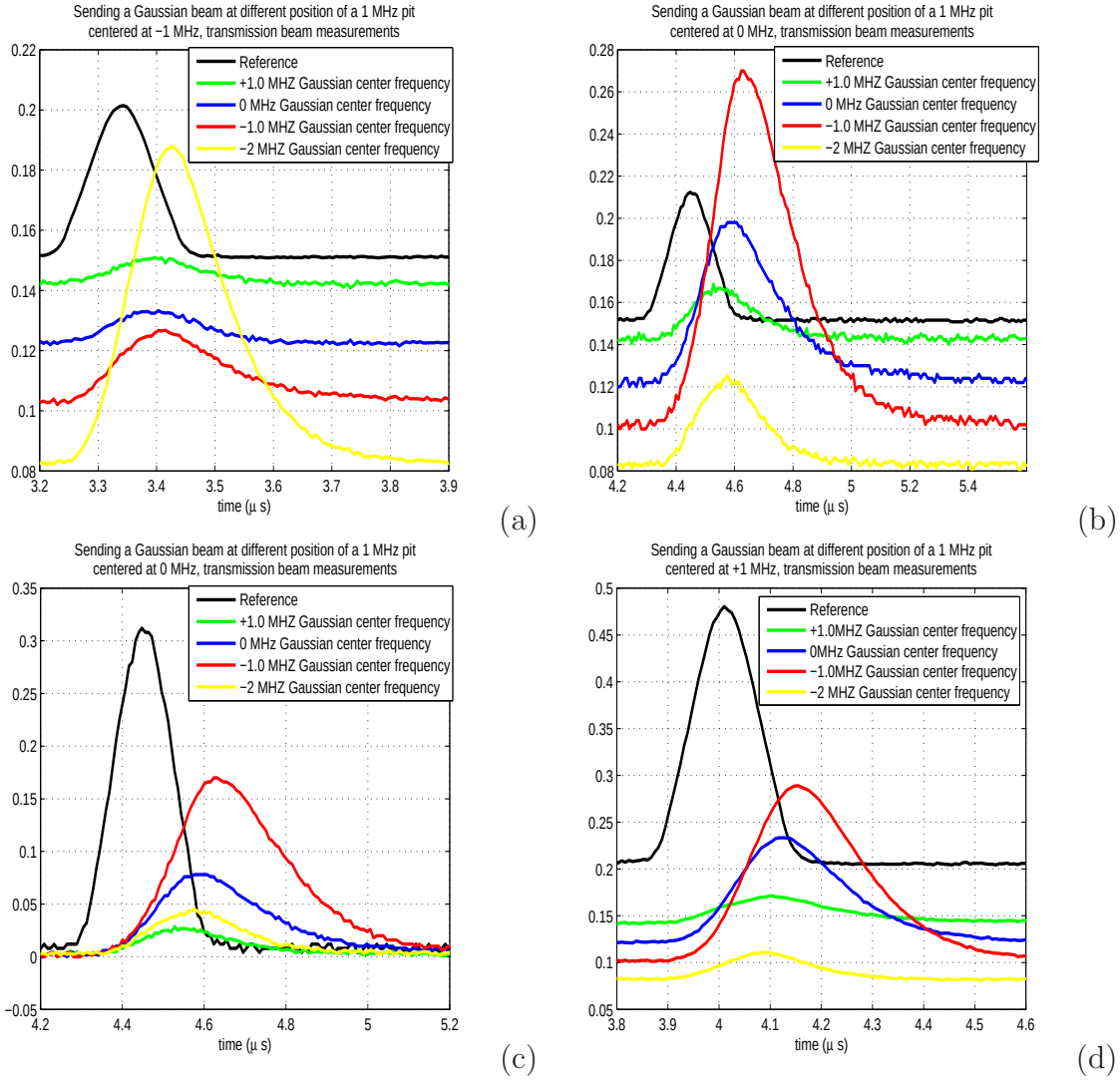

Figure 5.12: Slow light effect due to the spectral pit in the cavity. There is overlap between the inhomogeneous profile and the cavity resonance peak. The detectors had a gain of 10^6 and the temperature was 2.1k. All measurements are done in the transmitted beam. An eraser pulse, scanning -60 to +60 MHz was present to erase any structure created after every readout process. (a) Sending a Gaussian pulse with FWHM of 800 ns at different position of the spectral pit and the spectral pit has a width of 1 MHz. The spectral pit is centered at -1 MHz with the spectral pit creation sequence scaning from -1.5 MHz to -0.5 MHz. The slowest light is obtained for the Gaussian with center frequency at -2.0 MHz. (b) Sending a Gaussian pulse with FWHM of 1000 ns at different position of the spectral pit and the spectral pit has a width of 1 MHz. The spectral pit is centered at 0 MHz with the spectral pit creation sequence scaning from -0.5 MHz to + 0.5 MHz. The slowest light is obtained for a Gaussian with center frequency at -1 MHz. (c) Same as b but ploted on normal scale, that is, no water fall ploting. (d) Sending a Gaussian pulse with FWHM of 800 ns at different position of the spectral pit and the spectral pit has a width of 1 MHz. The spectral pit is centered at +1 MHz with the spectral pit creation sequence scaning from 0.5 MHz to +1.5 MHz. The slowest light is obtained for the Gaussian with center frequency at -1MHz.

light wave in a round trip which must be equal to 2π [27]. This contribution tends to pull the cavity resonance frequency closer together. We can also, look at this frequency pulling effect differently, say we need to move from one resonant peak of the cavity (cavity mode) to the another cavity mode, we need a wavelength change of $\lambda/2$ that is, $\lambda = \frac{c_0}{n\nu}$, corresponding to a very large frequency change (in this case, in GHz). Now with the spectral pit presence, the real refractive index is now frequency dependent and changing faster than the frequency (see figure (5.10) b), that is, $\lambda = \frac{c_0}{n(\nu)\nu}$, thus over a small frequency change, it is possible to change the wavelength by $\lambda/2$, moving from one cavity mode to another cavity mode. This process in laser terminology is called frequency pulling of the cold resonator modes [27]. I will borrow that terminology here to describe this effect in our cavity. Due to this pulling effects, our cavity free spectral range ν_F, now depends on the group velocity of the light beam across the pit instead of the normal speed of light in the medium, that is:

$$\nu_F = \frac{v_g}{2L} = \frac{\pi\Gamma}{2\alpha L}. \tag{5.7}$$

Suppose we have a spectral pit with a width of 10 MHz and an αL of about 1.5 in our crystal, then using equation (5.7), we get the cavity free spectral range to be 10.5 MHz (which make sense, see figure (5.11) a). The cavity free spectral range for a fix spectral pit, depends greatly on the αL we can get in the crystal cavity, the higher the values, the closer the resonance peaks of the cavity. Therefore, for us to have 2 cavity resonance peaks within the spectral pit, we need to have an αL of atleast 2 in the crystal cavity. For the 10 MHz spectral pit with an αL of 2, the free spectral range of the cavity becomes 7.9 MHz, showing clearly that, we can fit 2 peaks within the spectral pit. Thus, when the group velocity reduces by 4 orders of magnitude, we expect the free spectral range to have a corresponding reduction, that is, move from GHz to MHz. Also, with a 4 order reduction in the free spectral range, the spectral width should have the same 4 order reduction in magnitude. Figure (5.11) a clearly shows these changes, as the spectral width is in MHz range now from GHz before and the free spectral range is also in MHz range. Also, from equation (5.7), the free spectral range depends on the width of the spectral pit, thus changing the spectral pit width, changes the free spectral range as shown by figures (5.11) a, b. In figure (5.11) a, b, all the cavity resonance peaks are at the edges of the spectral pits, which implies that we have an αL $\approx$ 1.5. Figure (5.11) a, b, agrees well with this value for the αL using equation (5.7).

From figure (5.11) a, the free spectral range is in the order of MHz. This corresponds to a cold cavity of length in the order of hundreds of meters.

(ii) ***Effects of peaks in pit***: Now, on inclusion of peaks in the spectral pit, the crystal cavity resonance peaks completely changes. To understand this, we first created an empty pit and move the cavity until we have the crystal cavity resonance in the center of the pit, see figure (5.11) c and d. The cavity resonance peak shown in figure (5.11) c, has the frequency pulling effects of the empty pit presence already. Including a peak (absorption line) in the spectral pit, introduces new Pr^{3+} ions in the spectral pit. This new ions will now contribute to additional phase shift to the light wave during one round trip. This additional phase shift will cause a corresponding additional frequency pulling effects on the crystal cavity resonance peaks. This will make the crystal cavity resonance peaks more closer together and more narrow, see figure (5.13) b,c. The higher

the number of peaks in the spectral pit, the narrower and closer the crystal cavity resonance becomes. Figure (5.13) d shows the crystal cavity resonance peak together with the changes of the resonance peak due to the inclusion of a peak in the spectral pit.

Moving the attocube changes the cavity thickness and hence alters the cavity resonance frequency. For the same pit width, the frequency pulling effect will also be the same, but the cavity resonance frequency will be at different frequencies for different attocube position. Figure (5.13) a shows different cavity resonance frequency in the presence of a peak in the pit.

The presence of peaks in the spectral pit causes the free spectral range of the cavity to be in units of MHz range. This further corresponds to a cold cavity with length of the order of hundreds of meters. Thus, we can turn our cavity, with the help of a spectral pit plus peaks (absorption lines) to a cavity with a free spectral range of the order of units of MHz, corresponding to cold cavities of lengths in the order of hundreds of meters.

(iii) ***Cavity free spectral range and cavity sensitivity***:

Our cavity is a standing wave cavity, and as such we expect a built-up of the E-field within the cavity at the resonance of the cavity.

First we investigated the crystal cavity effect on the pit creation process by using different number of pulses in the spectral pit burning sequence. Figure (5.14) a, b shows the result from the measurement using both the reflected and transmitted beams. For as low as 10 pulses, we start to see the frequency pulling effects due to the formation of the spectral pit. On the application of 500 pulses, the spectral pit is completely formed and any further increase of the number of pulses, doesnt change the spectral pit structure.

We next investigated the effect of the cavity on the readout pulse by using readout pulses with very low Rabi frequencies (15 kHz); see figure (5.14) c. We then see that due to the built up within the crystal cavity, the readout pulse acquired enough intensity to create a spectral pit with then pulls the cavity resonance peaks through frequency pulling. To see if the effect is position dependent, we moved the attocube and repeat the process see figure (5.14) c. At different position of the attocube, the cavity resonance peak (due to the frequency pulling effects as a result of the presence of the spectral pit) appears at different frequency positions. All the curves moves to the left as we scan the attocube, moving the attocube from a position when the attocube is open to a position when it is fully closed. We then created the spectral pit again and use different readout pulses to read the spectral pit, see figure (5.14) d and (5.15). In figure (5.14) d, two slow readout pulses (that is, 1 MHz/μs), with one of the pulse scaning from -10 to +10 MHz (red curve) and the other from +10 to -10 MHz (blue curve). The both plots are the same. Further investigated of the readout pulses was done using a high resolution readout (10 kHz/μs) of the spectral pit, see figure (5.15) .

5.4.3 Discussion

During the experiments, we encounter several difficulties, some we could resolve immediately, and others that we couldnt.

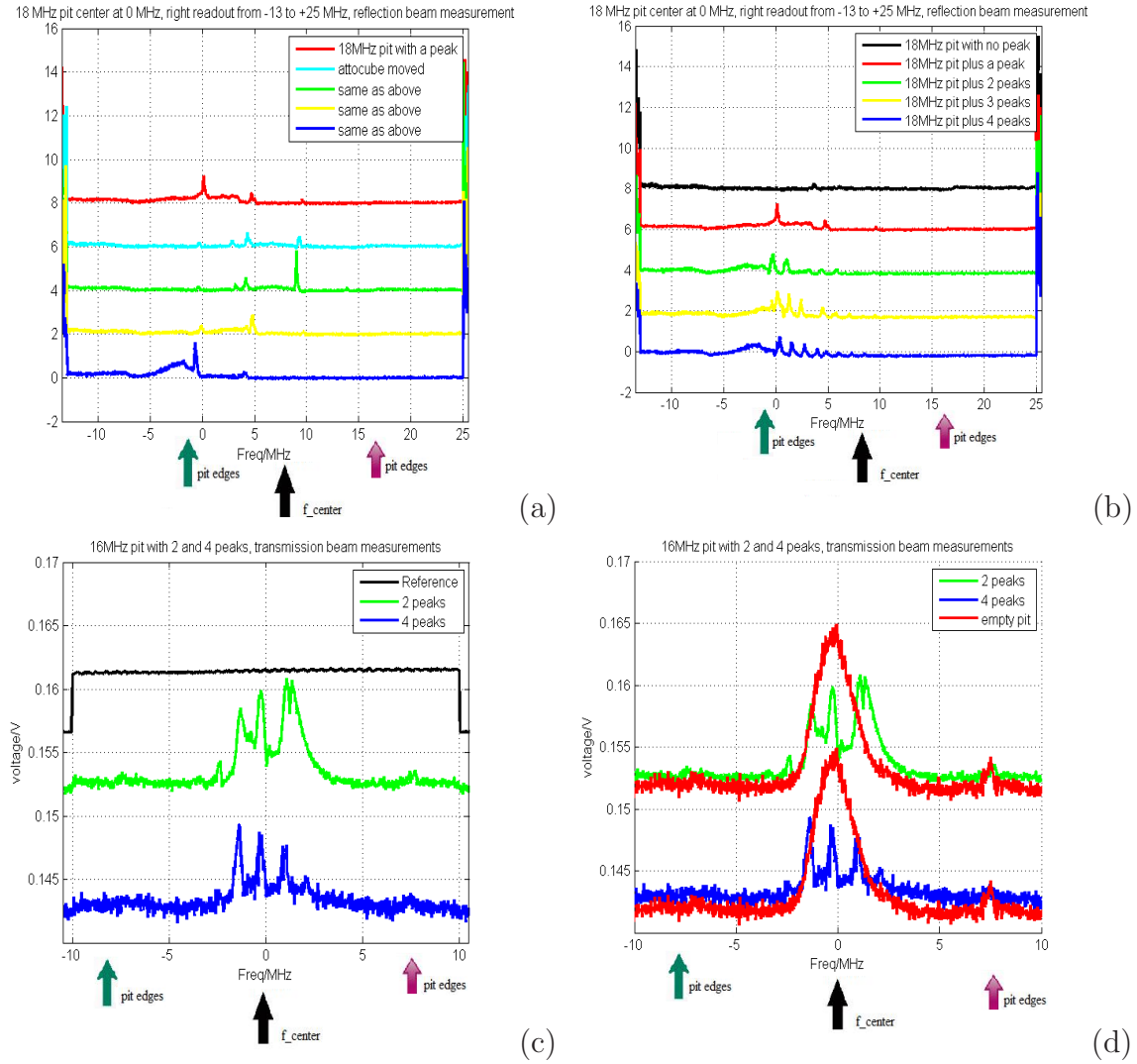

Figure 5.13: Effect of cavity resonance in the presence of a spectral pit plus peaks. (a) 18MHz spectral pit, from -1.2 to 16.2 MHz, with a peak at 0 MHz corresponding to the $1/2_g \rightarrow 1/2_e$ transition in Pr^{3+} ion. There are 2 other peaks corresponding to the $1/2_g \rightarrow 3/2_e$ and $1/2_g \rightarrow 5/2_e$ transition in Pr^{3+} ion. The peak has FWHM of 100 kHz and the readout is a right readout, from -13 to 25 MHz. The detector gain is 10^5 and measurement done using the reflected beam. The length of the cavity is changed by moving the attocube and each plot corresponds to different attocube position. We can clearly see the frequency pulling effect of the resonance peak. Moving the attocube, moves the cavity resonance peak (b) Same as a but with 1, 2, 3, 4 peaks. The peaks have a FWHM of 100kHz with a seperation of 1.2 MHz. The number of resonance peaks we see correspond to the number of peaks. The first peak is at 0 MHz, the second peak at 1.2 MHz, the third at 2.4 MHz and the fourth at 3.6 MHz. (c) 16MHz spectral pit, center at 0MHz and scan -10 MHz to +10 MHz with 2 and 4 peaks. The first peak is at 0 MHz, the second peak at 1.2 MHz, the third at 2.4 MHz and the fourth at 3.6 MHz. The pit creation sequence is made up of 500 pulses. The burn back pulses has Rabi frequency 300 kHz with a peak FWHM of 100kHz, seperation 1.2MHz. The first peak is position at 0 MHz at the center of the pit. The data acquisition was done using a high resolution readout, that is, 10 kHz/μs, with a readout scan from -10 to +10MHz in the transmission beam. All the data are average. We see the frequency pulling effects on the cavity resonance frequency, pulling them closer. (d) This is same as c but in addition, the resonance peak before the inclusion of the peaks is also included, to show how the inclusion of absorption peaks changes the cavity resonance peak.

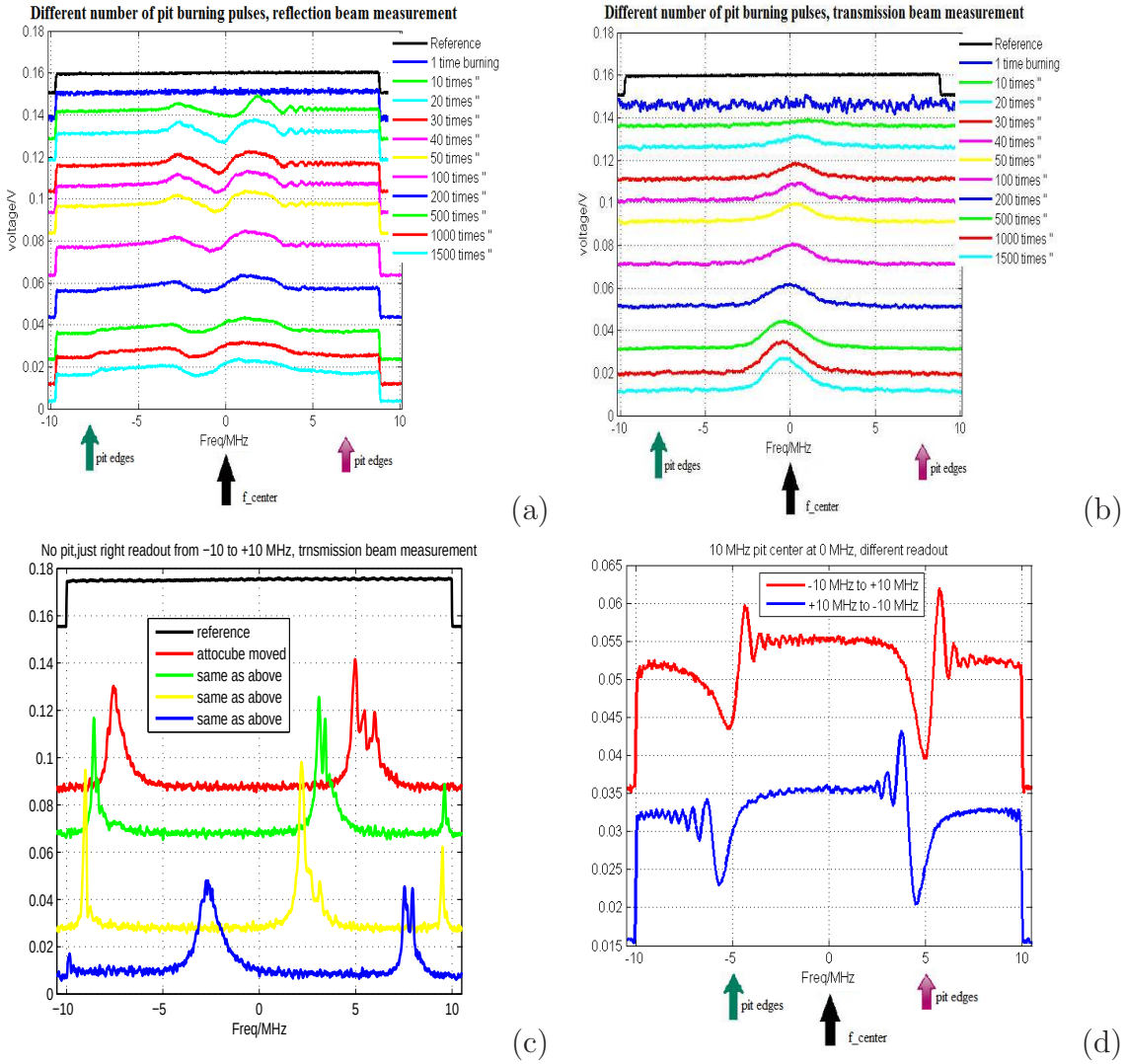

Figure 5.14: Effects of the cavity build-up on the input and readout pulses. (a) Effect of different number of pit burning pulses in reflection measurement. The number of pulses in the pit creation sequence for a 10 MHz wide pit centered at 0 MHz were changes to see the effects of the number of pulses used in the pit creation. The crystal cavity was adjusted using the attocube such that, the center of the inhomogeneous profile of the crystal coincided with the cavity resonance. An eraser pulse was included during the pit creation sequence, which range from -60 to +60 MHz. This pulse re-shuffle the ions after each pit creation before the creation of a new pit. All the plots are average with a right right used for data acquisition. A readout scan of -10 to +10 MHz was used. Already for 10 pulses present in the creation sequence, we start seeing the cavity resonance, implying we start have a formation of the spectral pit. After the application of 500 pulses in the pit creation sequence, any further increase of the pulse number doesn't result in any apparent changes in the pit shape. (b) Same as a but in transmission. (c) No pit creation, just readout. Effect of the readout pulses in transmission measurement. We see that the readout pulse in itself creates a pit in the crystal, and due to the frequency pulling effect, we can see the cavity resonance peaks. Changing the cavity length by moving the attocube the cavity resonance moves with it. The $\lambda/2$ plate was at 35^0 for maximum interaction with the ions. High resolution readout (that is, 10 kHz/μs scan rate) was used in the data acquisition process and readout every 2 ms followed by a waiting time of 200 ms. The readout pulse have a Rabi frequency of 15 kHz. (d) Effect of readout direction on 10 MHz pit centered at 0 MHz. Two slow readout pulses (that is, 1 MHz/μs), with one of the pulse scaning from -10 to +10 MHz (red curve) and the other from +10 to -10 MHz (blue curve). The two plots are the same.

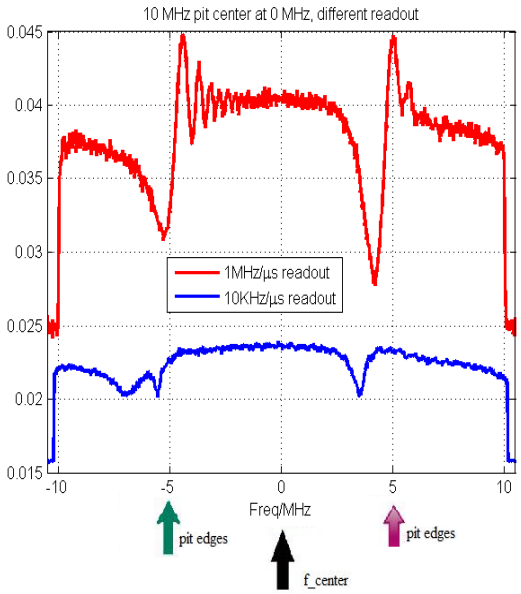

Figure 5.15: The sensitivity of the cavity. Effect of different readout pulse on a created 10 MHz pit centered at 0MHz. The high resolution readout, that is, 10 kHz/μs, has less ringing as compared to the fast readout that is, 1 MHz/μs.

The FWHM of the cavity resonance peak far away from the inhomogeneous ion absorption peak, was obtained by scanning the laser frequency. If we are to use the cavity for quantum state storage, in addition to the cavity resonance peaks FWHM, we will need the position in the crystal cavity were the cavity is matched to the ion absorption in the crystal, see figure (3.2). To obtain the position were the cavity is impedance matched accurately; we will need to scan the cavity full diameter. One suggestion will be to use an attocube with a larger movement range, say 6 mm. the cavity has two resonance peaks within its diameter, with one in the upper half of the cavity and the other in the lower half. Therefore, if we can scan either the lower or upper half of the cavity, we will be sure to find a resonance peak present. Also, due to the frequency pulling effects on the cavity resonance, extral care must be taken to make sure, the FWHM of the cavity resonance peak will be larger than the AFC bandwidth. Even if this is achieved, inclusion of peaks within the spectral pit destroy the resonance peak and as of now, we are not sure of the exact effect of this on the memory efficiency.

During the experiments, there were too many parameters to control and optimized all at once. For example, we needed the cavity resonance to be within the crystal absorption profile and at the same time, the cavity needs to be impedance matched to the ions absorption. We couldnt control, for example the cavity FWHM of its resonance peaks, which is very important for the quantum state storage experiments.

In the sets of experiments presented above, it was important that we are able to interact with the Pr^{3+} ions in the crystal maximally. To achieved this, we had to rotate the $\lambda/2$ plate to 35^0, thus changing the light polarization. Due to the fact that, our crystal is a birefringence crystal, the polarization of the light that interacts maximally with the ions does not interact maximally with the cavity. Maximum interaction with the cavity was obtained at 0^0 of

the $\lambda/2$ plate. Therefore, there was always a trade-off between interacting maximally with the cavity or with the Pr^{3+} in the crystal. Since our main goal was quantum state storage using the Pr^{3+} ions, we therefore chose to interact maximally with the ions and not the cavity.

In all, the time I spend in the lab, was very educating and I wish I could do it more often and even permanently.

5.4.4 Suggestion

My first suggestion would be that a detail mathematical model should be developed, that can simulate the cavity resonance peaks changes in the presence of the spectral pit plus peaks (absorption lines). This will help in the control and optimization problems encounter in the lab during the experiments. A mathematical model has been developed by another diploma student in the group to study the effect on the cavity resonance due to the presence of a spectral pit in the cavity.

Also, more experiments needs to be done, to investigate the frequency pulling effect in the cavity. Quantum state storage experiments needs to be performed using the AFC protocol to see if the idea of using a cavity to enhance the absorption of a memory material with low absorption works with the AFC protocol or not.

The option of using a different memory protocol (e.g. CRIB protocol) with the cavity should be considered.

5.5 Summary

- Praseodynium doped in Y_2SiO_5 crystal is a very good candidate for quantum state storage. The hyperfine energy levels, the homogeneous and inhomogeneous line widths are some of its good properties making it a good candidate for AFC protocol.
- Cavity surface flatness can be measured using inference effects from the cavity.
- A spectral pit in a crystal cavity, changes th cavity resonance frequencies due to frequency pulling effects.

Conclusion

It is possible to use a cavity to enhance the absorption of a material used for quantum state storage, as long as the cavity resonance peak FWHM is larger than the memory material absorption profile FWHM. If the AFC protocol is used to realized the quantum memory, care must be taken as the creation of the spectral pit, brings in the frequency effect and every thing becomes messy.

On creation of a spectral pit in a crystal cavity, frequency pulling effects pulls the cavity resonance peaks closer. Due to the changing absorption in the crystal caused by the spectral pit creation, there will always be slow light in the cavity. The presence of absorption peaks within the spectral pit, will causes further frequency pulling effects on the cavity resonance peaks, pulling them even closer together.

Appendix A

```
'dimension structures and data array
Dim ent As T_ENTITY, op As T_OPERATION, idl As Long, id As String
Dim data() As Double, datas() As Double, samynew As String

'find node numbers of source, etalon crystal, etalon material and Analysis surface
ida&=FindName("Analysis 3")
idas&=FindName("Analysis 4")
idl&=FindName("wedge etalon crystal")
idm&=FindMaterial("etalon")
ids&=FindName("Source 1")
'SetTextFile samynew.txt, fileOnly


Set excelApp = CreateObject("Excel.Application")
Set excelWB = excelApp.Workbooks.Add
Set excelRange = excelWB.ActiveSheet.Cells(1,1)

'=====================================================
'Make Excel visible
'=====================================================
excelApp.Visible = True

'=====================================================
'Name the worksheet
'=====================================================

sheetName = "angle_0.0031"
excelWB.Worksheets("Sheet1").Name = sheetName

'=====================================================
'write column headers
'=====================================================

RowCount = 1
xName = "distance"
yName1 = "losses from first mirror"
yName2 = "losses from second mirror"
yName3 = "total losses from cavity"
```

```
excelRange.Cells(RowCount,1).Value = xName
excelRange.Cells(RowCount,2).Value = yName1
excelRange.Cells(RowCount,3).Value = yName2
excelRange.Cells(RowCount,4).Value = yName3


'Imported from 'C:\Documents and Settings\photonecho\Desktop\fred\test_script.frs   fr


'set file name string and clear output window
fname$=GetDocDir() & "\temp.fgd"
fnames$=GetDocDir() & "\temps.fgd"
ClearOutputWindow

'print header for two column data printing
Print "offset", Chr(9), "R"


'computation of Fabry-Perot transmission resonance thickness
M&=11883                              'integer
wv#=GetSourceIthWavelength(ids,0)   'wavelength
mindx#=RefractiveIndex(idm,wv)      'etalon index
thk#=M*(wv*1e-3)/(2*mindx)   'transmission resonance thickness

GetOperation idl,2,op
op.val2= 0    : startval=op.val2
SetOperation idl,2,op
Update

nstep&=1223
'nstep&=2337
'nstep&=Int(7*Abs(startval +1))*100
Print nstep
EnableTextPrinting(False)

'cavity thickness change increment
'ink#=wv*1e-3   '0.0005*wv*1e-3
ink=1'0.0005
testv=10'0.065

'loop over cavity thicknesses
For i=0 To nstep

'get and set etalon crystal thickness
'GetCustomPrism idl,id,ent,lnz
'lnz.param2=thk+i*ink
'SetCustomPrism idl,ent,lnz

SetMaterialAbsorb idm, wv, testv
```

```
'GetOperation idl,2,op
 'If i=0 Then
  'op.val2=op.val2
' Else
  'op.val2=op.val2+ink
 'End If
SetOperation idl,2,op
Update

'trace ray with no draw
TraceCreate

'compute irradiance on Analysis Surface
cnt&=IrradianceToFileAS(ida,fname)

'load data into Analysis Results Node and compute total integrated power
idarn&=ARNCreateFromFile(fname,"temp")
ARNGetDataAsDoubleArray idarn,data
px#=ARNGetAAxisValueAt(idarn,0)-ARNGetAAxisValueAt(idarn,1)
py#=ARNGetBAxisValueAt(idarn,0)-ARNGetBAxisValueAt(idarn,1)
ARNDelete idarn
ptot#=0
For j=0 To UBound(data,1)
 For k=0 To UBound(data,2)
  ptot=ptot+data(j,k)*px*py
 Next k
Next j

cnts&=IrradianceToFileAS(idas,fnames)
idarns&=ARNCreateFromFile(fnames,"temps")
ARNGetDataAsDoubleArray idarns,datas
pxs#=ARNGetAAxisValueAt(idarns,0)-ARNGetAAxisValueAt(idarns,1)
pys#=ARNGetBAxisValueAt(idarns,0)-ARNGetBAxisValueAt(idarns,1)
ARNDelete idarns


ptots#=0
For j=0 To UBound(datas,1)
 For k=0 To UBound(datas,2)
  ptots=ptots+datas(j,k)*pxs*pys
 Next k
Next j


'================================================
'move pointer to next row
'================================================
RowCount = 2
```

```
'fileOnly (True)
    excelRange.Cells(RowCount+i,1).Value = testv
     'excelRange.Cells(RowCount+i,1).Value =  op.val2
excelRange.Cells(RowCount+i,2).Value = ptot
excelRange.Cells(RowCount+i,3).Value = ptots
excelRange.Cells(RowCount+i,4).Value = ptot + ptots
excelWB.Worksheets(sheetName).Columns("A:E").Autofit


'print result to output window

'EnableTextPrinting(True)
'Print Chr(9), testv, Chr(9), ptot, Chr(9), ptots, Chr(9), ptot+ptots

'Print op.val2, Chr(9), ptot, Chr(9), ptots, Chr(9), ptot+ptots
EnableTextPrinting(False)

'end loop
testv=testv-ink
Next i


EnableTextPrinting(True)

'reset cavity thickess to initial value
'GetCustomPrism idl,id,ent,lnz
'lnz.param2=thk
'SetCustomPrism idl,ent,lnz

GetOperation idl,2,op
op.val2=startval
SetOperation idl,2,op
Update

Print "done"
Set excelRange=Nothing
Set excelWB=Nothing
Set excelApp=Nothing
```

Appendix B

2 MHz pit				
pulses	ν_{start} (MHz)	ν_{center} (MHz)	ν_{end} (MHz)	Ω_{rel}
burnpit13	-0.5	0	+0.5	$3/2_g \rightarrow 1/2_e$
burnpit14	+0.5	0	-0.5	$3/2_g \rightarrow 1/2_e$
4 MHz pit				
burnpit13	-2	0	+2	$3/2_g \rightarrow 1/2_e$
burnpit14	+2	0	-2	$3/2_g \rightarrow 1/2_e$
6 MHz pit				
burnpit13	-3	0	+3	$3/2_g \rightarrow 1/2_e$
burnpit14	+3	0	-3	$3/2_g \rightarrow 1/2_e$
8 MHz pit				
burnpit13	-4	0	+4	$3/2_g \rightarrow 1/2_e$
burnpit14	+4	0	-4	$3/2_g \rightarrow 1/2_e$
10 MHz pit				
burnpit13	-5	0	+5	$3/2_g \rightarrow 1/2_e$
burnpit14	+5	0	-5	$3/2_g \rightarrow 1/2_e$
16 MHz pit				
pulses	ν_{start} (MHz)	ν_{center} (MHz)	ν_{end} (MHz)	Ω_{rel}
burnpit13	-8	0	+8	$3/2_g \rightarrow 1/2_e$
burnpit14	+8	0	-8	$3/2_g \rightarrow 1/2_e$

The table above shows the list of pulses used for the spectral pit creation sequences, with the start, center, end and Rabi frequencies. The Rabi frequency shows which transition will be targeted by the pulse and hence what intensity the light pulse should have, in order for it to matched the oscillator strength. Burnpit13 was first applied followed by burnpit14 and they where each repeated 500 times. For the 18 MHz pit, the pit burning sequence was as shown in [22]

Bibliography

[1] Jonathan P. Dowling, and Gerard J. Milburn, *"Quantum technology: the second quantum revolution"*, Phil. Trans. R. soc. Lond. A 361, 1655 (2003).

[2] Michael A. Nielsen and Isaac L. Chuang, *"Quantum computation and quantum information"*, Cambridge University Press, 2000 .

[3] David McMahon, *"Quantum computing explained"*, John Wiley and son, 2008 .

[4] Artur K. Ekert, *"Quantum cryptography based on bell's theorem"*, Phys. Rev. Lett. 67, 661 (1991).

[5] Nicolas Gisin, Grégoire Ribordy, Wolfgang Tittel,and Hugo Zbinden, *"Quantum cryptography"*, Rev. Mod. Phys. 74, 145 (2002).

[6] Nicolas Sangouard, Christoph Simon, Hugues de Riedmatten, and Nicolas Gisin, *"Quantum repeaters based on atomic ensembles and linear optics"*, arxiv:0906.2699.

[7] Dick Bouwmeester, Jian/Wei Pan, Klaus Mattle, Manfred Eibl, Harald Weinfurter, and Anton Zeilinger, *"Experimental quantum teleportation"*, nature 390, 579 (1997).

[8] M. Riebe, H. Häffner, C. F. Roos, W. Hänsel, J. Benhelm, G. P. T. Lancaster, T. W. Körber, C. Becher, F. Schmidt-Kaler, D. F. V. James, and R. Blatt, *"Deterministic quantum teleportation with atoms"*, nature 429, 737 (2004).

[9] Brian Julsgaard, Jacob Sherson, J. Ignacio Cirac, Jaromir Fiurasek, and Eugen S. Polzik, *"Experimental demonstration of quantum memory for light"*, nature 432, 486 (2004).

[10] Alexander I. Lvovsky, Barry C. Sanders, and Wolfgang Tittel, *"Optical quantum memory"*, nature photonics 3, 714 (2009).

[11] C. Simon, M. Afzelius, J. Appel, A. B. de la Giroday, S. J. Dewhurst, N. Gisin, C. Hu, F. Jelezko, S. Kröll, J. H. Müller, J. Nunn, E. Polzik, J. Rarity, H. de Riedmatten, W. Rosenfeld, A. J. Shields, N. Sköld, R. M. Stevenson, R. Thew, I. Walmsley, M. Weber, H. Weinfurter, J. Wrachtrup and R. J. Young, *"Quantum memories "*, arxiv:1003.1107.

[12] Jian-Wei Pan, Christoph Simon, Caslar Brukner , and Anton Zeilinger, *"Entanglement purification for quantum communication"*, nature 410, 1070 (2001).

[13] Jian-Wei Pan, Sara Gasparoni, Rupert Ursin, Gregor Weihs, and anton Zeilinger, *"Experimental entanglement purification of arbitrary unknown states"*, nature 423, 422 (2003).

[14] Jian-Wei Pan, Dick Bouwmeester, Harald Weinfurter, and Anton Zeilinger, *"Experimental entanglement swapping: Entangling photons that never interact"*, Phys. Lett. 80, 3894 (1998).

[15] *http : //quantumrepeaters.eu.*

[16] Mattias Nilsson, and S. Kröll, *"Solid state quantum memory using complete absorption and re-emission of photons by tailored and externally controlled inhomogeneous absorption profiles"*, Optics Comm. 247, 403 (2005).

[17] Nicolas Sangouard, Christoph Simon, Mikeal Afzelius, and Nicolas Gisin, *"Analysis of a quantum memory for photons based on controlled reversible inhomogeneous broadening"*, Phys. Rev. A 75, 032327 (2007).

[18] Mikeal Afzelius,Christoph Simon, Hugues de Riedmatten, and Nicolas Gisin, *"Multimode quantum memory based on atomic frequency combs"*, Phys. Rev. A 79, 052329 (2009).

[19] G. Hétet, J. J. Longdell, A. L. Alexander, P. K. Lam, and M. J. Sellars, *"Gradient echo quantum memory for light using two-level atoms"*, arxiv:quant-ph/0612169v2.

[20] G. Hétet, J. J. Longdell, A. L. Alexander, P. K. Lam, and M. J. Sellars, *"Electro-optics quantum memory for light using two-level atoms"*, Phys. Rev. Lett. 100, 023601 (2008).

[21] Morgan P. Hedges, Jeron J. Longdell, Yongmin Li, and Mathew J. Sellars, *"Efficient quantum memory for light"*, nature 465, 1056 (2010).

[22] A. Amari, A. Walther, M. Sabooni, M. Huang, S. Kröll, M. Afzelius, I Usmani, B. Lauritzen, N. Sangouard, H. de Riedmatten, and N. Gisin, *"Towards an efficient atomic frequency comb quantum memory"*, J. Lumin. 130, 1585 (2010).

[23] M. Sabooni, F. Beaudoin, A. Walther, Lin Nan, A. Amari, M. Huang, and S. Kröll, *"Storage and recall of a weak coherent optical pulses with an efficiency of 25 %"*, Phys. Rev. Lett. 105, 060501 (2010).

[24] Mikeal Afzelius, and Christoph Simon, *"Impedance-matched cavity quantum memory"*, Phys. Rev. A 82, 022310 (2010).

[25] Sergey A. Moiseev, Sergey N. Andrianov, and Firdus F. Gubaidullin, *"Efficient multimode quantum memory based on photon echo in an optimal QED cavity"*, Phys. Rev. A 82, 022311 (2010).

[26] Anthony E. Siegman, *Lasers*, University Science Books 1986.

[27] B. E. A. Saleh, and M. C. Teich, *"Fundamentals of Photonics"*, John Wiley and Sons Inc. 2007.

[28] L. M. Duan, M. D. Lukin, J. I. Cirac and P. Zoller, *"Long-distance quantum communication with atomic ensembles and linear optics"*, nature 414, 418 (2001).

[29] M. Bonarota, J-L Le Gouët, and T. Chaneliére, *"Highly multimode memory in a crystal"*, New Journal of Physics 13, 01301 (2011).

[30] Y. O. Dudin, A. G. Radnaev, R. Zhao, J. Z. Blumoff, T. A. B. Kennedy, and A. Kuzmich, *"Entanglement of light-shift compensated atomic spin waves with telecom light"*, Phys. Rev. Lett. 105, 260502 (2010).

[31] Björn Lauritzen, J. Minář, H. de Riedmatten, M. Afzelius, N. Sangouard, C. Simon, and N. Gisin, *"Telecommunication-wavelength solid-state memory at the single photon level"*, Phys. Rev. Lett. 104, 080502 (2010).

[32] A. E. Kozhekin, K. M⊘lmer, and E. Polzik, *"Quantum memory for light"*, Phys. Rev. A 62, 033809 (2000).

[33] Marlan O. Scully, and M. Suhail Zubairy, *Quantum optics*, Cambridge University press 1997.

[34] Atia Amari, *"Towards efficient quantum memories in rare/earth/ion doped solids"*, Doctorate thesis, department of Physics, Lund university 2010.

[35] Christoph Simon, Hugues de Riedmatten, Mikeal Afzelius, Nicolas Sangouard,Hugo Zbinden, and Nicolas Gisin, *"Quantum repeaters with photon pair sources and multimode memories"*, Phys. Rev. Lett. 78, 190503 (2007).

[36] L. Rippe, B. Julsgaard, A. Walther, Yan Ying, and S. Kröll, *"Experimental quantum-state tomography of a solid state qubit"*, Phys. Rev. A 77, 022307 (2008).

[37] J. J. Longdell, and M. J. Sellars, *"Experimental demonstration of quantum-state tomography and qubit-qubit interactions for rare-earth-metal-ions-based solid-state qubits"*, Phys. Rev. A 69, 032307 (2004).

[38] W. Tittel, M. Afzelius, T. Chanelieère, R. L. Cone, S. Kröll, S. A. Moiseev and M. Sellars *"Photon-echo quantum memory in solid state systems"*, Laser and photon. Rev. 1-24 (2009)/DOI 10.1002/lpor.200810056.

[39] Hugues de Riedmatten, Mikeal Afzelius,Matthias U. Staudt, Christoph Simon, and Nicolas Gisin, *"A solid-state light-matter interface at the single-photon level"*, nature 456, 773 (2008).

[40] Y. Sun, C. W. Thiel, R. L. Cone, R. W. Equall, and R. L. Hutcheson, *"Recent progress in developing a new rare earth materials for hole burning and coherent transient applications"*, Journal of Luminescence 98, 281 (2002).

[41] M. D. Lukin, *"Colloquium:Trapping and manipulating photon states in atomic ensembles"*, Rev. Mod. Phys. 75, 457 (2003).

[42] Christopher J. Foot, *"Atomic Physics"*, Oxford University Press, 2005 .

[43] R. W. Equall, R. L. Cone, and R. M. Macfarlane, *"Homogeneous broadening and hyperfine structure of optical transition in Pr^{3+}:Y_2SiO_5"*, Phys. Rev. B 52, 3963 (1995).

[44] Mattias Nilsson, Lars Rippe, Stefan Kröll, Robert Klieber, and Dieter Suter *"Hole-burning techniques for isolation and study of individual hyperfine transition in inhomogeneous broadened solids demonstrated in Pr^{3+}:Y_2SiO_5"*, Phys. Rev. B 70, 214116 (2004).

[45] B. A. Maksimov, V. V. Ilyukhin, Yu. A. Kharitonov, and N. V. Belov, *"Crystal structure of yttrium oxyorthosilicate $Y_2O_3.SiO_2 = Y_2SiO_5$ dual function of yttrium"*, Soviet Physics-Crystallography 15, 806 (1971).

[46] Stephen Harris, *"Electromagnetically Induced Transparency"*, Physics Today 50, 36 (1997).

[47] C. Liu, Z. Dutton, C. H. Behroozi, and L. V. Hau, *"Observation of coherent optical information storage in an atomic medium using halted light pulses"*, nature 409, 490 (2001).

[48] M. Fleischhauer, and M. D. Lukin, *"Dark-state polaritons in Electromagnetically Induced Transparency"*, Phys. Rev. Lett. 84, 5094 (2000).

[49] M. Mitsunaga, *"Time-domain optical data storage by photon echo"*, Optical and Quantum Electronics 24, 1137 (1992).

[50] Andreas Walther, *"Coherent processes in rare-earth-ion-doped solids"*, Doctorate thesis, department of Physics, Lund university 2009.

[51] Lars Rippe, Mattias Nilsson, and Stefan Kröll, *"Experimental demonstration of efficient and selective population transfer and qubit distillation in a rare-earth-metal-ion-doped crystal"*, Phys. Rev. A 71, 062328 (2005).

[52] M. Bonarota, J. Ruggiero, J-L Le Gouët, and T. Chaneliére, *"Efficient optimization for atomic frequency comb storage"*, Phys. Rev. A 81, 033803 (2010).

[53] M. Afzelius, Imam Usmani, A. Amari, B. Lauritzen, A. Walther, C. Simon, N. Sangouard, J. Minář, H. de Riedmatten, N. Gisin, and S. Kröll, *"Demonstration of atomic frequency comb memory for light with spin-wave storage"*, Phys. Rev. Lett. 104, 040503 (2010).

[54] M. Berta, M. Christandl, R. Colbeck, J. M. Renes, and R. Renner, *"The uncertainty principle in the presence of quantum memory"*, nature doi:10.1038/NPHYS1734.

[55] Lars Rippe, *"Quantum Computing with Naturally Trapped Sub-Nanometre-Spaced Ions"*, Doctorate thesis, department of Physics, Lund university 2006.

[56] Alexy V. Gorshkov, Axel André, Mikhail D. Lukin, and Anders S. S⊘rensen, *"Photon storage in* Γ*-type optically dense atomic media.I. Cavity model"*, Phys. Rev. A 76, 033804 (2007).

[57] $http://www.photonengr.com/software/$

[58] Simulation done by Axel Thuresson on the various quantum memory protocols for his diploma work, on going in the quantum information group, Lund University.